Disorder and Magnetism in Two Dimensional Quantum Systems

A thesis submitted to

Tata Institute of Fundamental Research, Mumbai, India

for the degree of

Doctor of Philosophy

in

Physics

By

Kusum Dhochak

Department of Theoretical Physics

Tata Institute of Fundamental Research

Mumbai - 400 005, India

May 2013

Declaration

This thesis is a presentation of my original research work. Wherever contributions of others are involved, every effort is made to indicate this clearly, with due reference to the literature, and acknowledgement of collaborative research and discussions.

The work was done under the guidance of Professor Vikram Tripathi, at the Tata Institute of Fundamental Research, Mumbai.

(Kusum Dhochak)

In my capacity as the supervisor of the candidate's thesis, I certify that the above statements are true to the best of my knowledge.

(Vikram Tripathi)

Acknowledgments

Firstly, I would like to thank my advisor Vikram Tripathi for his guidance, support and encouragement in last five years. He is a very patient teacher and I have learnt a lot from him. I also thank Kedar Damle, Deepak Dhar and Mustansir Barma for their great courses and discussions which make the condensed matter group a pleasure to work in. I also thank other faculty members of the department for the physics I have learned through their courses and discussions.

I thank my friends at TIFR, specially in Theoretical Physics students room for making my years at TIFR enjoyable. A special thanks to Sayantan, Satya, Loganaygam, Arnab, Argha, Tridib, Kabir, Debasish, Samarth and Prerna.

This thesis would not have been possible without the support and hard work of my parents who gave foremost importance to providing the best opportunities to their children. I also thank my sister and brother for their constant love and care. Lastly, my warmest appreciations to Prithvi for all his love and support.

Collaborators

This thesis is based on work done in collaboration with several people and most parts of it have appeared in print before. The work presented in Chapter 2 is based on work done with Vikram Tripathi. Chapter 3 is based on work done with Vikram Tripathi and R. Shankar. Chapter 4 is based on work done in collaboration with Vikram Tripathi, K. Kugel, B. A. Aronzon, V. V. Rylkov, A. B. Davydov, B. Raquet and M. Goiran.

To

My Family

Contents

Synopsis **iii**

Publications **xxiii**

1 Introduction **1**

References **10**

2 Kondo Lattice Scenario in Semiconductor Heterostructures **11**

2.1 Introduction 11

2.2 Two dimensional Kondo model 17

2.2.1 One impurity spin 21

2.2.2 Two impurity spins 23

2.2.3 Lattice of impurity spins 25

2.3 Summary 30

References **34**

3 Magnetic impurities in the honeycomb Kitaev model **35**

3.1 Introduction 35

3.1.1 Kitaev model 36

3.2 Kondo effect in Kitaev model 38

3.2.1 Stability of strong coupling point 45

3.2.2 Topological transition 48

3.3 RKKY interactions 50

3.4 Summary 54

References **56**

4 Charge transport in magnetic semiconductor heterostructures 57
4.1 Introduction 57
4.2 Model of nanoscale inhomogeneities 63
4.3 Resistivity 71
4.4 Summary 76

References 81

5 Conclusion 81

Synopsis

Introduction

Disorder in some form is almost always present in condensed matter systems. It could arise from missing atoms, external impurities or disordered distribution of dopants giving rise to a random scattering potential. Studying the effects of disorder is therefore necessary to have a good understanding of the properties of these systems. Disorder/impurities can also give rise to new and interesting features in the host systems. Kondo effect and heavy fermions [1], spin fractionalization in frustrated magnets [2], weak localization in two-dimensions [3, 4] are some examples of these effects. External impurities are also often used as probes to study the electronic state of host system, nature of order parameter and phase transitions [5] etc. All these properties make it interesting to study disorder effects in condensed matter systems.

In low dimensions, the quantum effects are enhanced and studying them provides an opportunity to understand and observe the effects of quantum fluctuations. Moreover, low dimensional systems can be easily created in semiconductor heterostructures which are useful for technological applications. These semiconductor heterostructures provide the advantage of tunability of various parameters like carrier density, disorder in the system, which allows exploring different phases of the system. Strong correlations, where the interactions between particles dominate over their kinetic energy, are another important feature of many condensed matter systems giving rise to various novel effects like high Tc superconductivity, fractional quantum hall effect and spin liquid states [6, 7, 8]. Disorder, low dimensionality and strong correlations are main components of the three systems we studied in this thesis work. Following is a brief description of our work. More details of the immediate context, motivations etc are discussed in individual sections.

Our first work concerns Kondo lattice scenarios in semiconductor heterostruc-

tures. We have studied Nuclear Magnetic Resonance (NMR) to probe the nature of the electronic state in two dimensional electron gas (2DEG) in the heterostructures [9]. In Kondo systems, a free electron gas interacts with localized spins and the system can show a transition to a Fermi liquid state at low temperatures where the localized spins are screened by the conduction electrons. Magnetic interactions between the localized impurities, which are mediated by conduction electrons (Ruderman Kittel Kasuya Yosida (RKKY) interactions [10]), compete with the Kondo coupling and the system shows a rich phase diagram, including a quantum critical point and heavy fermion superconductivity, arising out of this competition [11]. Semiconductor heterostructures can be used to explore this phase diagram if the formation of a Kondo lattice in these structures is confirmed. We showed that nuclear relaxation rate shows distinguishable features for a Kondo lattice and a disordered arrangement of localized spins and can thus can be used to confirm the formation of Kondo lattice in these structures. NMR can also distinguish a Kondo interaction dominated regime from RKKY interaction dominated regime.

In second part of this thesis, we have analyzed the effects of coupling external magnetic impurities to spin-1/2 Kitaev model [12] which is a quantum spin-1/2 model on honeycomb lattice with very anisotropic interactions [13]. The model can be exactly solved and has a spin liquid ground state with very short ranged spin correlations. The exact solvability of this model might be utilized to understand quantum spin liquid states better. The model also allows non-abelian anyonic excitations which make it interesting for quantum computation. We studied the effects of spin-S impurities coupled to the Kitaev model in its gapless spin liquid phase. We found that there is an interesting Kondo effect in the Kitaev model which is independent of the sign of the Kondo coupling (ferromagnetic or antiferromagnetic) and it is accompanied by a change of topology of the ground state. The ground state has finite fluxes at the impurity sites in strong coupling regime. These fluxes are associated with localized zero energy Majorana fermionic modes and have non-abelian statistics. We also calculated the inter-impurity interactions mediated by the gapless excitations of Kitaev model and found interesting non-dipolar interactions.

In our final study of the effects of disorder and magnetism, we have analyzed the transport properties of magnetic semiconductor heterostructures [14]. These heterostructures have a thin layer of Mn atoms separated from the transport channel and show ferromagnetism at low temperatures. The ferromagnetism also affects the transport properties of these heterostructures. These systems are of relevance for spintronic devices and understanding the transport properties is thus an important

question. Also, the mechanism of ferromagnetism in bulk magnetic semiconductors and semiconductor heterostructures is not very well understood. Due to the potential fluctuation caused by the disorder in Mn layer, charge carriers in the quantum well accumulate in potential wells forming charge droplets at low carrier densities. We incorporated the effects of ferromagnetism of Mn atoms in the hopping probabilities of charge carriers which could explain the observed anomaly (peak/shoulder) in the resistivity of these structures. In bulk magnetic systems, the position of this anomaly is generally used to infer the Curie temperature, but we showed that in two dimensional systems, the anomaly can appear much below the Curie temperature.

Kondo Lattice Scenario in Disordered Semiconductor Heterostructures

Semiconductor heterostructures are layered structures of two or more semiconductors of different band gaps that can give rise to quantum well structures and the density of charge carriers in the quantum well can be controlled by gate voltages (Fig. 4a). These structures can be $\delta-$doped with an atomic layer of dopants spatially separated from the quantum well, to further control the carrier densities in the quantum well with minimal effect on their mobility. Semiconductor heterostructures have played a key role in the discovery and exploration of important phenomena in condensed matter systems, like Fractional quantum Hall effect [15], due to their reduced dimensionality, high mobilities and enhanced quantum effects. In our work, we analyzed these systems in context of possibility of formation of a Kondo lattice in Si $\delta-$doped GaAs/AlGaAs heterostructures. Such a realization, if confirmed, can be very useful to study properties of Kondo lattice systems in various regimes of parameters. The main advantage of these structures is their tunability which is not possible in actual Kondo lattice (heavy fermion) materials. These can be used to study the complex phase diagram of Kondo lattice systems which arises from the competition of the magnetic ordering tendency of the localized electrons and the screening tendency (Kondo effect) of the conduction electrons and to explore the nature of this quantum critical point [16, 11].

An electron gas is formed at the junction of GaAs and AlGaAs due to band bending and mismatch of band gaps. The Si layer is partially ionized and provides carriers in the quantum well region. These ionized Si atoms would like to arrange in a triangular lattice to minimize the Coulomb energy. Generally disorder in the arrangement of Si atoms is known to be significant. The possibility of spatial ordering of charged donors, or Wigner crystallization, in $\delta-$ doped heterostructures,

when the degree of ionization is around 1/3 or lower has been theoretically predicted [17, 18]. These ions cause a spatially varying Coulomb potential at the junction of GaAs and AlGaAs where two dimensional electron gas (2DEG) is formed. The potential profile depends on the arrangement of ions in the delta layer and could be disordered or ordered. The potential wells can bind electrons and can give rise to local moments in the 2DEG. This forms a Kondo system with these local moments interacting with the free electrons. If the ions form a crystalline structure, there is an interesting possibility of forming a Kondo lattice. There are two competing interactions in the system, the Kondo coupling which tries to screen the impurity spins and give rise to Kondo effect at low temperatures, and the inter-impurity spin interaction mediated by the free electrons (RKKY interaction) which tends to build correlations between the impurity spins.

In transport measurements, which are generally used to study these systems, the enhanced density of states at the Fermi energy due to the Kondo resonance gives rise to a peak in zero bias tunneling conductance in the Kondo-coupling dominated regime which splits in the RKKY dominated regime. These were observed in the experiments ([19]) done in these heterostructures. However, we argued that the transport measurements are unable to give information about the spatial order of localized spins and can not be used to confirm the formation of an artificial Kondo lattice in semiconductor heterostructures. A zero bias conductance anomaly can appear as long as each impurity is Kondo screened and it can split when pairwise magnetic interactions become strong.

Although their small sizes make it difficult to employ standard bulk methods such as neutron diffraction, suitably adapted NMR methods have been proposed by which nuclear polarization may be generated locally in such devices and its relaxation can be feasibly detected through two-terminal conductance measurements [21]. The behavior of the nuclear relaxation rate conveys important information about the electronic state in the device. We studied NMR for these systems in different regimes and showed that nuclear relaxation rate shows distinct features for a lattice of localized spins and a disordered distribution as well as for different interaction regimes.

We consider the Hamiltonian for $S = 1/2$ magnetic impurities in a 2-dimensional electron gas:

$$H = \sum_k \xi_k c^\dagger_{k\sigma} c_{k\sigma} + J \sum_i \boldsymbol{\sigma}_i \cdot \mathbf{S}_i. \tag{1}$$

Here $\mathbf{S}_i$ is the localized spin and $\boldsymbol{\sigma}_i$ is the conduction electron spin density at $\mathbf{r}_i$. J is the antiferromagnetic Kondo coupling between localized spins and free electron density. The second term also gives rise to inter-impurity RKKY interaction which in two-dimensions is $J_{\mathrm{RKKY}}(R_{ij}) \sim \frac{J^2\rho(\epsilon_F)}{R_{ij}^2}\cos(2k_F R_{ij})$; where, $\rho(\epsilon_F)$ is the electron density of states at the Fermi energy and k_F is the Fermi momentum.

Nuclear spin relaxation takes place by coupling to various degrees of freedom of the system. In our system, the nuclear polarization couples to both the localized spin $\mathbf{S}$ and conduction electrons $\boldsymbol{\sigma}$. The nuclear spins see an effective local magnetic field $\mathbf{h}_{\mathrm{loc}} = \frac{1}{\gamma_n}(A_d\mathbf{S} + A_s\boldsymbol{\sigma})$, where A_d and A_s are the hyperfine coupling with the localized spin and conduction electrons respectively and γ_n is nuclear gyromagnetic ratio. Nuclear relaxation rate is given by the transverse fluctuation of the local effective field.

In the vicinity of localized spins, the relaxation through interaction with local moments is dominant [20] and the relaxation rate can be written in terms of localized moments susceptibility (χ_i) as

$$T_1^{-1} = \frac{A_d^2 k_B T}{\hbar^2 (g_s\mu_B)^2}\mathrm{Im}\left(\frac{\chi_i^{+-}(\omega)}{2\omega}\right)_{\omega\to 0}. \tag{2}$$

We calculated the susceptibility χ_i for different possible physical scenarios of the system, *i.e.*, few impurities case, a lattice of impurities in Kondo dominated and RKKY dominated regimes and showed that it has unambiguously distinguishable temperature dependences for these scenarios [9].

In the Kondo interaction dominated regime we fermionize the localized spins, S_i, in terms of a spin-less fermion f_i and a Majorana fermion χ_i [22] as $S_i^+ = f_i^\dagger\chi_i/\sqrt{2}$, $S_i^- = \chi_i f_i/\sqrt{2}$, and $S_i^z = f_i^\dagger f_i - 1/2$, where $\{\chi_i, \chi_j\} = 2\delta_{ij}$. We factorize the quartic terms in Hamiltonian by using Hubbard-Stratonovich factorization and do a mean field analysis. For a single localized spin coupled to the 2DEG, we calculate the Kondo energy scale (ω_K) and the spin susceptibility at low frequencies using imaginary time Green's functions. The mean field analysis gives $\omega_K == D\exp(-4/3\rho J)$ and at low temperatures $T \ll \omega_K$,

$$\frac{\chi_i^{+-}(\omega_m)}{(g_s\mu_B)^2} \approx \frac{1}{\pi}\frac{1}{(|\omega_m| + \omega_{Ki})}. \tag{3}$$

where $\omega_m = 2\pi m k_B T$ are bosonic Matsubara frequencies. This gives the localized spin contribution to nuclear relaxation rate $T_{1i}^{-1} = \frac{A_d^2 k_B T}{\pi\hbar\omega_K^2}$ at low temperatures from the screened impurity while at high temperatures, the unscreened local moment

gives a constant T_{1i}^{-1} as $\chi \sim 1/T$

Thus, a few non-interacting local spins give a linear-T relaxation rate. If the localized spins are nearby, RKKY interactions compete with the Kondo screening. To get the effect of this competition, we considered two nearby localized spins. RKKY interaction between nearby spins is much larger than the hyperfine coupling and the nuclear spins couple to an RKKY pair instead of individual spins at low temperatures. Therefore, spin-spin correlations also affect the relaxation rate. Taking these into account, at low temperatures $T \ll \omega_K$, the relaxation rate is given by

$$T_1^{-1} = \frac{2}{\pi}\frac{A_d^2 k_B T}{\omega_K^2 \hbar}\left(1 - \frac{1}{\pi}\frac{J_{\mathrm{RKKY}}(R_{12})}{\omega_K}\right). \tag{4}$$

Although, in this case too, the relaxation rate is linear in T, it decreases as $J_{\mathrm{RKKY}}(R_{12})$ increases for antiferromagnetic couplings. Thus, in the RKKY dominated regime with disordered local spin arrangement, nuclear relaxation rate becomes very small as nearest spins form spin- singlets for $J_{\mathrm{RKKY}}(R_{12}) > \pi\ \omega_K$ and do not exchange spin with nucleus. In contrast, for a lattice of spins, the nuclear relaxation rate is finite even in the RKKY dominated regime. The main physical difference from the two-impurity case is the existence of low energy magnetic excitations (magnons) in the lattice for any value of the ratio $J_{\mathrm{RKKY}}/\omega_K$. As a result, significant nuclear relaxation still occurs for large anti-ferromagnetic inter-impurity couplings unlike the two-impurity case where it vanishes.

For the Kondo lattice, in weak RKKY interaction limit ($J_{\mathrm{RKKY}} \ll \omega_K$), we treat the RKKY interaction as a perturbation in Random phase approximation (RPA) scheme for calculating the dynamical susceptibility:

$$\chi_q^{+-}(\omega, T) = \frac{\chi_i^{+-}(\omega, T)}{1 - \chi_i^{+-}(\omega, T)(n_{\mathrm{imp}} J_{\mathrm{RKKY}}(q)/(g_s\mu_B)^2)}. \tag{5}$$

Here, n_{imp} is the density of localized spins. If $J_{\mathrm{RKKY}}(q)$ (or more generally, exchange interaction J_{ex} which includes RKKY interactions) has maximum value at wave-vector $\mathbf{Q}$, we can write $J_{\mathrm{RKKY}}(\mathbf{Q}+\mathbf{q}) = J_{\mathrm{RKKY}}(\mathbf{Q}) - (D_s/n_{\mathrm{imp}})a^2q^2$ and with $\chi_i^{+-}(0,T) \simeq \frac{(g_s\mu_B)^2}{\pi\omega_K}(1 - Ck_B^2T^2/\omega_K^2)$, ($C$ is a constant of order 1), we get

$$\left(\frac{\chi''(\omega)}{\omega}\right)_{\omega\to 0} = \frac{a^2}{4\pi^2 D_s \omega_{sf}\,(T)}, \tag{6}$$

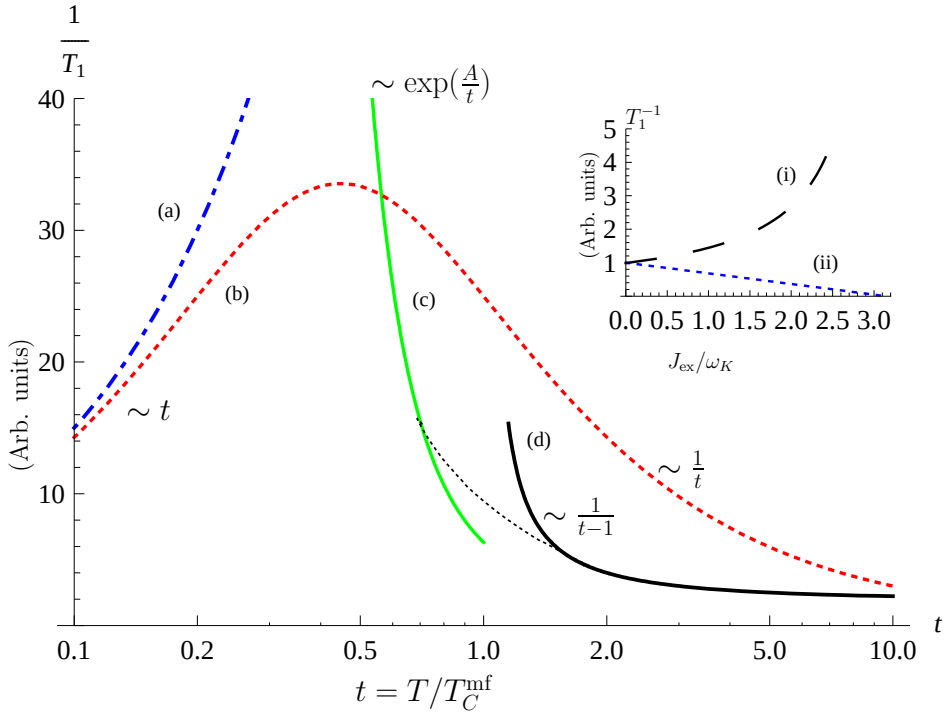

Figure 1: Plots showing the qualitative differences in the temperature and (AFM) inter-impurity exchange interaction $J_{\rm ex}$ dependencies of the nuclear relaxation rates T_1^{-1} for a two impurity system and Kondo lattice. Main plot: $T_1^{-1}(T)$ for (a) a two impurity system; (b) a Kondo interaction dominated lattice ($J_{\rm ex}/\omega_K < 1$); (c,d) a Kondo lattice where $J_{\rm ex}/\omega_K > 1$ and $T < (>) T_C^{\rm mf}$, where $T_C^{\rm mf}$ is the mean-field transition temperature. Dotted curve interpolates between these two temperature regimes (there is no phase transition). Inset: T_1^{-1} as a function of $J_{\rm ex}/\omega_K$ for (i) Kondo lattice (ii) two impurities - the T_1^{-1} vanishes for $J_{\rm ex}/\omega_K > \pi$.

where a is the lattice constant and D_s is spin stiffness of the Kondo lattice and

$$\omega_{sf}\left(T\right) \simeq \omega_{sf}(0)\left(1+\frac{CT^2}{\omega_k \omega_{sf}(0)}\right) . \tag{7}$$

$\omega_{sf}(0) = \omega_K - J_{\rm ex}(Q) n_{\rm imp}/\pi$ is the energy scale that represents the competition of Kondo and inter-impurity exchange interactions. Although the temperature dependence that follows from this for the Kondo lattice is linear in temperature, similar to the two impurity case; there is the crucial difference that even when $J_{\rm RKKY} \sim \pi\, \omega_K$, there is a finite relaxation rate which vanishes for the two impurities case.

In the RKKY-dominated regime, we neglect the Kondo effect in the lowest order

and the conduction electrons provide magnon decay. Within RPA approach, we can write the dynamical susceptibility near mean field transition point $T_C^{\rm mf}$ in terms of magnetic correlation length ξ as

$$\chi^{+-}_{\mathbf{Q}+\mathbf{q}}(\omega) \;=\; \frac{(g_s\mu_B)^2}{4k_BT_C^{\rm mf}\left\{\alpha^2/\xi^2+\alpha^2q^2-i\gamma_{\mathbf{Q}+\mathbf{q}}(\omega)\right\}}. \tag{8}$$

Here, $\gamma(\mathbf{Q}+\mathbf{q}) \sim \pi(J\rho)^2\hbar\omega/4J_{\rm ex}(\mathbf{Q})k_Fq$ is the imaginary part of exchange interaction and $\mathbf{Q}$ is the ordering wave vector. For a ferromagnet (FM), $\mathbf{Q}=0$ and for anti-ferromagnet(AFM), $\mathbf{Q}=(\pi/a,\pi/a)$. The temperature dependence of the nuclear relaxation rate is then given by

$$T_1^{-1}(T) = \frac{A_d^2(J\rho)^2J_{\rm ex}(Q)n_{\rm imp}^2}{64\hbar D_s^2k_FQ}\frac{T}{T_C^{\rm mf}}\,\frac{\xi(T)^2}{a^2}. \tag{9}$$

for AFM and similarly for FM, $T_1^{-1}(T) \sim T\xi(T)^3$

In a two dimensional isotropic Heisenberg model, their is no phase transition but magnetic correlation length increases exponentially fast at low temperatures ($\xi(T) \sim \exp(T_0/T)$). Thus the temperature dependence of nuclear relaxation rate T_1^{-1} is exponential at low temperatures in RKKY dominated regime for a Kondo lattice. This gives a clear distinguishable feature for a lattice as T_1^{-1} is linear for a disordered set of localized spins. Also, the behaviour is very different from Kondo interaction dominated regime and is thus able to distinguish between them. These results are shown in Fig. 1.

Magnetic impurities in the honeycomb Kitaev model

We studied the behavior of spin-S impurities in the gapless spin liquid regime of the Kitaev model on the honeycomb lattice [12]. The $S=1/2$ Kitaev model [13] is a honeycomb lattice of spins with direction-dependent nearest neighbor exchange interactions,

$$H_0 = -J_x\sum_{x\text{-links}}\sigma_j^x\sigma_k^x - J_y\sum_{y\text{-links}}\sigma_j^y\sigma_k^y - J_z\sum_{z\text{-links}}\sigma_j^z\sigma_k^z, \tag{10}$$

where the three bonds at each site (Fig.2) are labeled as x, y and z.

This is an exactly solvable interacting quantum two-dimensional model which makes it very interesting to explore its various properties. The ground state is a quantum spin liquid with both gapless and gapped excitations in different regimes

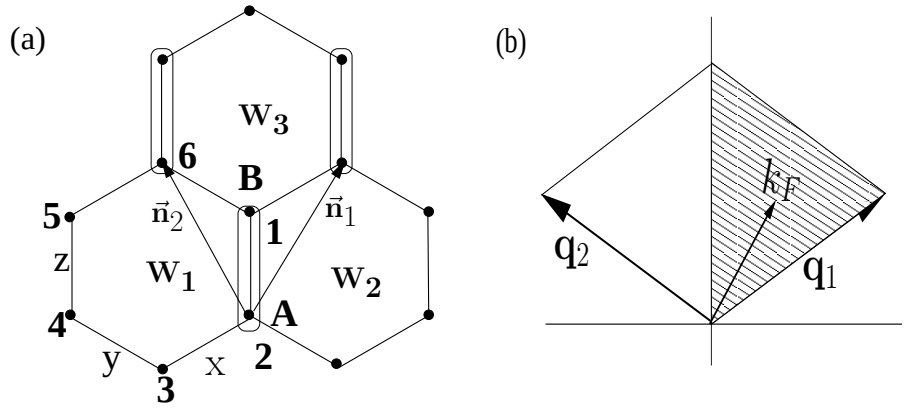

Figure 2: (a) Schematic of the Kitaev lattice showing the A and B sublattice sites and the x, y and z types of bonds. (b) Brillouin zone. The Dirac point for the massless Majorana fermions is denoted by k_F and momentum summations are over the (shaded) half Brillouin zone.

of parameter space. Impurities provide a very useful way to probe correlations in the quantum spin liquid states where a simple observable order parameter is usually not available. Non-magnetic impurities in quantum spin liquids have been extensively studied theoretically [23, 24] and experimentally [25, 26] to build an understanding of different types of ground states and excitations in these systems. The model has non-abelian anyonic excitations in its gapless phase which makes it possibly useful for quantum computing. Topological nature of states defined by the plaquette fluxes and gapless Majorana fermionic excitations in the ground state are other interesting features of the model. We studied spin-S impurities in the Kitaev model to probe the nature of the spin liquid ground state and to study the possibility of novel impurity effects due to fractionalization of spin into dispersing and localized Majorana fermions.

The model can be solved [13] by writing the spins in terms of Majorana fermions c, b^x, b^y, b^z as $\sigma_i^\alpha = ib_i^\alpha c_i$ and using the conservation of plaquette operators (fluxes) $W_p = \sigma_1^x\sigma_2^y\sigma_3^z\sigma_4^x\sigma_5^y\sigma_6^z = \pm 1$. Also, on each $\alpha-$type bond, $u_{ij}^\alpha = ib_i^\alpha b_j^\alpha$ is conserved which converts the Hamiltonian to a hopping Hamiltonian for $c-$Majorana fermions with gauge fixing condition $D_i = ib_i^x b_i^y b_i^z c_i = 1$ to take care of the extra degrees of freedom introduced by this representation. The ground state corresponds to a flux free state with all $W_p = 1$ for which we choose all $u_{ij} = 1$. The ground state is a spin liquid with very short ranged spin-spin correlations and has gapless excitation in large area of parameter space where the coupling constants J_x, J_y, J_z satisfy the triangle inequality. The excitations have a massless linear Dirac cone dispersion

which can give rise to a Kondo-like screening of the impurity spins. We studied the nature of this Kondo effect and the RKKY-like long range interaction between two distant impurities mediated by the gapless excitations.

We couple an external spin-S to the Kitaev model at one site (at origin) through the Kondo coupling term $V_K = \sum_\alpha K^\alpha S^\alpha \sigma^\alpha(0)$. To understand the behaviour of system at low energies (low temperatures), we did a Poor man's scaling analysis of the impurity coupling K by integrating out the high energy modes of the dispersing Majorana fermions. To obtain corrections to K, we considered the Lippmann-Schwinger expansion for the $T-$matrix element, scattering of a $c-$Majorana fermion to a $b-$Majorana, $T = V + VG_0V + VG_0VG_0V + \cdots$, in increasing powers of K.

The first correction to the bare $T-$matrix comes from *third* order terms s.t., $T^{(3)} \sim -K^\beta S^\beta \frac{\rho(D)\delta D}{JD} \sum_{\tilde{\beta}} (K^{\tilde{\beta}})^2 (S^{\tilde{\beta}})^2$. Here $\rho(\epsilon) = (1/2\pi v_F^2)|\epsilon| \equiv C|\epsilon|$ is the density of states and D is the band edge energy. If the Kondo interaction is rotationally symmetric or if the impurity is a $S = \frac{1}{2}$ spin, this contribution renormalizes the Kondo coupling constant.

Just as for the Kondo effect in graphene [27], there is a correction to the Kondo coupling due to the change in the density of states with decrease in bandwidth as the density of states vanishes at Fermi energy. This gives a contribution $K \to K(D'/D)^r, \quad (D' = D - |\delta D|)$ and the total contribution is

$$\delta K = -K \frac{\delta D}{D} \left(2K^2 a^2 CDS(S+1)/J - 1 \right). \tag{11}$$

Interesting features of the scaling equation are that there is an unstable fixed point at $K_c = \sqrt{J/[2a^2\rho(D)S(S+1)]} \sim J/S$ and that the direction of coupling constant flow is independent of its nature (ferromagnetic or anti-ferromagnetic). For $K > K_c$, the coupling scales to infinity while for $K < K_c$, the coupling flows to zero and impurity spin is not screened. Also, we found that the strong coupling fixed point $K \to \infty$ is stable for anti-ferromagnetic coupling.

Another remarkable property of the Kondo effect in Kitaev model is that the unstable fixed point is associated with a topological transition from the zero flux state to a finite flux state. The strong coupling (antiferromagnetic) limit amounts to studying the Kitaev model with a missing site or cutting the three bonds linking this site to its neighbors. Kitaev has shown [13] that such states with an odd number of cuts are associated with a finite flux, and also that these vortices are associated with unpaired Majorana fermions and have non-abelian statistics under exchange. It has also been shown numerically [28] that the ground state of Kitaev model with

one spin missing has a finite flux pinned to the defect site. We argued the existence of a localized zero energy Majorana mode from degeneracy of the ground state in presence of impurity spin and elucidated on the nature of this zero mode.

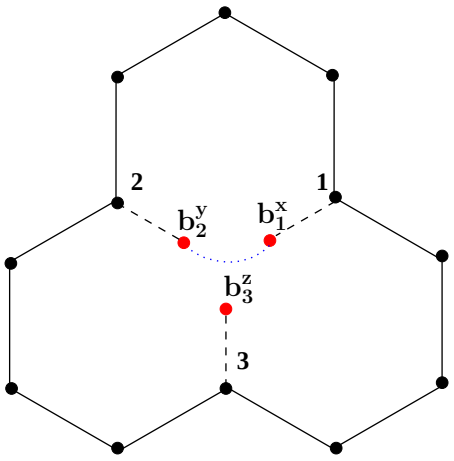

Figure 3: Schematic of the three unpaired bMajorana fermions formed as a result of cutting the links to the Kitaev spin at the origin. Any two of the three can be given an expectation value (dotted bond).

We define new operators involving the impurity spin and Kitaev spins, $\tau^x = W_2W_3S^x$, $\tau^y = W_3W_1S^y$ and $\tau^z = W_1W_2S^z$, which are conserved and form an SU(2) algebra $[\tau^\alpha, \tau^\beta] = 2i\epsilon_{\alpha\beta\gamma}\tau^\gamma$. This $SU(2)$ symmetry is exact for all couplings and is realized in the spin-1/2 representation $\left((\tau^\alpha)^2 = 1\right)$ and all eigenstates, including the ground state are doubly degenerate. In the strong (antiferromagnetic) coupling limit $J_K \to \infty$, low energy states are the ones in which the spin at origin forms a singlet $|0\rangle$ with the impurity spin. The double degeneracy in this case comes from rest of the Kitaev system with spin at origin removed. This implies that there is a zero-energy mode in the single particle spectrum and the two degenerate states correspond to the zero mode being occupied or unoccupied. There are three free $b-$Majorana fermions on the neighboring sites on the cut bonds (Fig 3). Any two of them can be given an expectation value by using the gauge freedom and one localized, zero energy, $b-$fermion remains at the defect site. Since a full zero energy mode is made of two Majorana fermions, there has to be a zero energy Majorana mode in the dispersing $c-$sector. This has also been shown explicitly by considering the Kitaev's model with one site missing [29]. Thus, in strong coupling limit, we can create localized fluxes in the Kitaev model with zero energy Majorana mode at their core, similar to the half vortices in p-wave superconductors which have non-abelian

statistics [30].

The gapless $c-$Majorana excitations can also mediate long range RKKY-type interactions between far away impurities. An impurity in Kitaev model couples to one localized Majorana fermion and one massless dispersing fermion. For long range interaction, we need to contract the localized $b-$Majorana fermion locally by considering a second order term in Kondo coupling. This generates a term involving only dispersing $c-$Majorana fermions only if the impurity spin locally couples to a bond (two nearest neighbour spins) of Kitaev model. Therefore no long range interaction is mediated between two distant spins if each one couples to only one Kitaev spin. When the external spin is coupled to an $\alpha_{ij}-$bond, the second order term is of the form $(K^\alpha S^\alpha)^2 c_i c_j/J$. The interaction with an impurity spin coupled to $\beta_{i'j'}-$bond is then given by terms of the type $\frac{1}{J^2}\langle (K^\alpha)^2 (S_1^\alpha)^2 (K^\beta)^2 (S_2^\beta)^2 c_i c_j c_{i'} c_{j'}\rangle$. The fermionic averaging gives the long range interaction between the impurity spins to be

$$J_{12}^{ij,i'j'} \sim -(K^\alpha)^2 (S_1^\alpha)^2 (K^\beta)^2 (S_2^\beta)^2 \ \frac{1}{J^2} \ \frac{1+\cos(2\tilde{\alpha}(\mathbf{k}_F)) - 2\cos(2\mathbf{k}_F\cdot\mathbf{R}_{12})}{R_{12}^3}. \quad (12)$$

$\tilde{\alpha}(\mathbf{k}_F)$ is a constant related to the position of Fermi point k_F and is $\pi/2$ for symmetric Kitaev coupling. Note that for spin-1/2 impurities, $(S^\alpha)^2 = 1/4$, no long-ranged interaction is generated. Similarly if the impurities couple to all the bonds of a hexagon symmetrically where $\sum_{\text{bond pairs}} (S_1^{\alpha_{ij}})^2 (S_2^{\beta_{i'j'}})^2 = \text{const.}$, again the interaction term is not generated. The interaction is non-dipolar (non $\mathbf{S}_i \cdot \mathbf{S}_j$) unlike the usual RKKY interaction in metals and has $1/R_{12}^3$ decay in 2-dimensions due to vanishing density of states at Fermi energy which is also the case for graphene. The RKKY interaction also reflects the bond-bond correlations in the Kitaev model's ground state.

Charge inhomogeneities and transport in magnetic semiconductor heterostructures

We studied the effects of disorder and magnetism on transport in $\delta-$doped magnetic semiconductor heterostructures [14]. In these heterostructures, a $\delta-$layer of Mn atoms is deposited slightly away from the quantum well (where charge transport takes place) separated by a spacer layer of GaAs. The Mn atoms get partially ionized acting as acceptors and provide holes in the quantum well. A schematic of the heterostructure is shown in figure 4a. The Carbon $\delta-$layer is introduced to

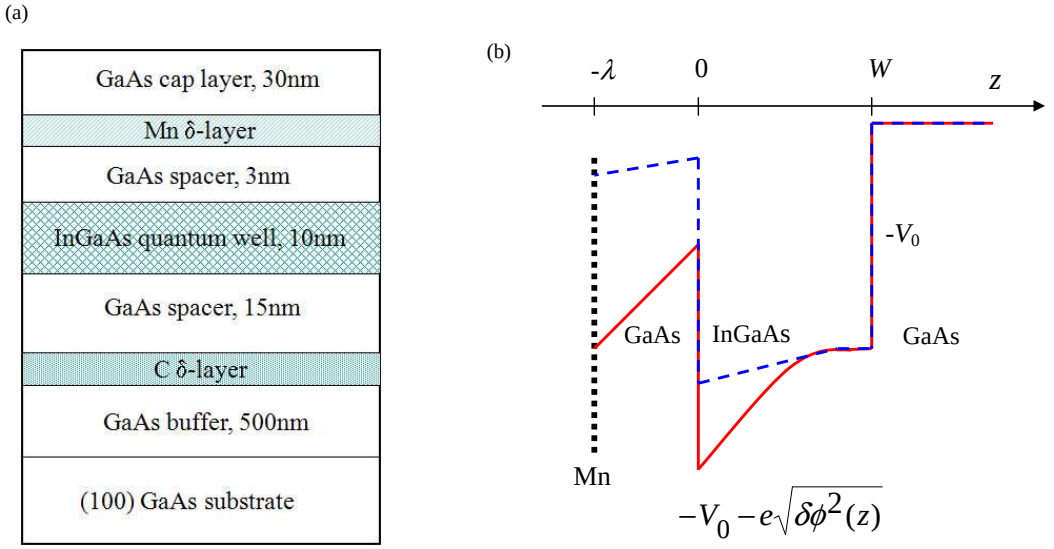

Figure 4: (a) Schematic layout of the heterostructure δ-doped by Mn. (b) Schematic of the quantum well potential (shown inverted). Dashed (blue) line represents the quantum well potential in the absence of fluctuations and the solid (red) line shows the potential well with an attractive fluctuation potential.

provide further carriers. The Mn atoms have finite magnetic moment in the semiconductor host and the system shows ferromagnetism [31]. Semiconductors with bulk doping of Mn atoms also show ferromagnetism at fairly high temperatures and the mechanism of the ferromagnetism has not been understood fully [32]. Research interest for studying these magnetic semiconductor heterostructures mainly arises from their possible use in spintronic devices [33] to generate and manipulate spin polarized currents. Studying the nature of magnetism and its effect on transport is therefore important. Also these systems could provide opportunities to explore the physics of ferromagnetism in doped semiconductors. Both the bulk magnetic semiconductors and heterostructures show a resistance anomaly (a peak/shoulder like feature in temperature dependence of resistance) which arises due to onset of ferromagnetic order of Mn atoms (Fig. 5a). For bulk systems this anomaly appears near the ferromagnetic transition temperature and is often used to get an estimate of the Curie temperature [32]. We studied the resistance anomaly in heterostructures where both the magnetic layer and the transport channel are two dimensional. We found that the resistance anomaly can appear at temperatures much lower than the Curie temperature of the Mn layer and there are significant magnetic correlations in the $\delta-$layer well above the peak temperature. Also a phase transition is not

necessary for the peak to appear (as is the case for 2-dimensional magnetic system).

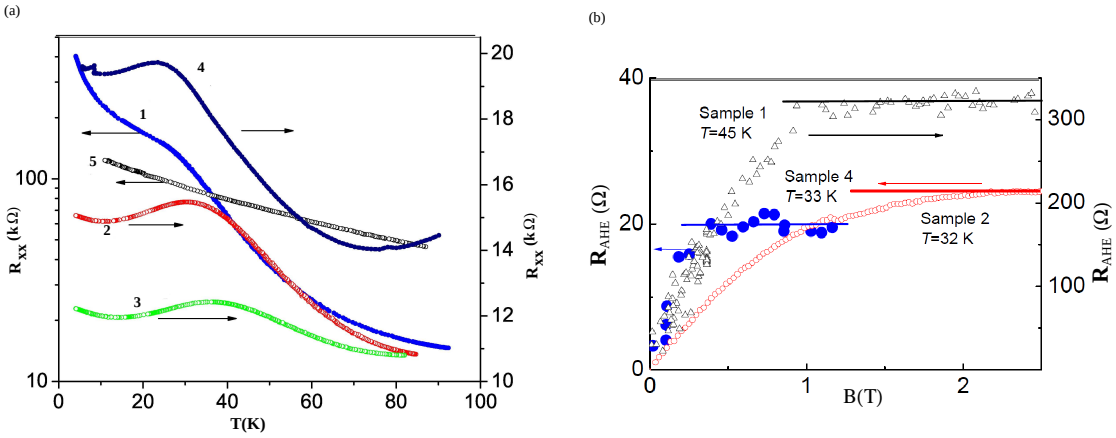

Figure 5: (a) Resistance data for the Mn δ-doped heterostructures (1, 2, 3, and 4) for different carrier and doping densities and a carbon δ-doped heterostructure (5). Resistance anomaly is absent in the carbon δ-doped sample, while the Mn δ-doped samples exhibit an anomaly (hump or shoulder), which is likely due to the magnetic ordering. (b) Anomalous Hall effect data for these samples. The Anomalous Hall effect saturates at temperatures well above the peak in the resistivity for insulating samples 1 and 4 while closer to the peak temperature for more metallic sample 2

As discussed for Si doping of semiconductor heterostructures above, the ionized Mn atoms produce a fluctuating potential for charge carriers in the quantum well (Fig 4b). We estimated the size of these potential fluctuations and typical radius of the potential wells where the holes accumulate to form charge droplets. These estimates give us the nature of the samples (insulating/metallic) as the samples with spatially distant droplets are insulating while closely placed droplets with significant tunneling give a more metallic sample. The disorder in Mn layer is assumed to be Gaussian white noise with $\delta-$function spatial correlations. Holes in the quantum well screen the potential fluctuations. The screening length $R_c = \sqrt{n'_a/\pi}/p$ is the radius beyond which the potential fluctuations get screened *i.e.* the holes in this area balance the total charge fluctuation in region of radius R_c in Mn $\delta-$layer. n'_a is the density of ionized dopants and p is the hole density in quantum well. The r.m.s. value of this potential fluctuation for the case when $2d >> R_c, \lambda$ is ([34]),

$$V_{\text{fluc}} = \sqrt{\langle \delta\phi^2 \rangle} \approx \left(\frac{n'_a e^2}{16\pi\kappa^2\epsilon_0^2} \ln\left[1 + \left(\frac{R_c}{\lambda + z_0} \right)^2 \right] \right)^{1/2}. \tag{13}$$

Sample	R_c(nm)	$z_{0,1}$(nm)	$z_{0,2}$(nm)	$R_{p,1}$(nm)	$R_{p,2}$(nm)	D_1(nm)	D_2(nm)	ξ(nm)
1	24.28	1.79	3.62	8.96	0	11.58	–	1.82
2	15.45	1.57	0.78	8.79	0	5.72	–	3.50
3	15.67	1.71	2.30	8.90	0	5.82	–	3.70
4	18.02	1.71	1.34	8.90	0	7.53	–	3.46

Table 1: Calculated values for the screening length R_c, droplet sizes $R_{p,n}$, droplet separations D_n corresponding to $R_{p,n}$, hole localization position $z_{0,n}$, and the localization length ξ at 77K. The calculations are for an effective $n_a' = 0.1 n_d$ (total Mn density). In the last three samples, the separation of the droplets is comparable with the localization length, implying proximity to the "metallic" phase. At 77K, only one sub-band is occupied and thus $R_{p,2}$ and D_2 are nor defined.

Here λ is the spacing between hole gas and Mn layer, (z_0) is the position of localization of hole gas in quantum well and d is the distance of metallic gate from Mn layer. We estimate z_0 by solving the Schroedinger equation along $z-$direction

$$\left[-\frac{\hbar^2}{2m^*}\frac{d^2}{dz^2} + V(z)\right]\psi_n = E_n\psi_n, \tag{14}$$

where $V(z)$ includes both the quantum well and fluctuation potentials. The holes form puddles filling the potential wells. One or more sub-bands (bands arising from confinement in z-direction) can be occupied. Sizes of the puddles depend on the hole density and dopant density. Using various parameters of the structures (*e.g.* for Sample 1, Mn density $n_d = 6.0 \times 10^{14}\text{cm}^{-2}$, hole density $p = 0.3 \times 10^{12}\text{cm}^{-2}$, quantum well depth $V_0 \approx -85$meV at 5K), we estimated puddle sizes, distance between puddles, localization length of holes and mean level separation in these droplets, etc. These estimates are shown in Table 1. The measured resistivities of these heterostructures are shown in Fig 5. The comparison of hole localization lengths and droplets separations qualitatively matches the experimental observation that sample one is insulating while 2, 3 and 4 are more metallic at 77K as localization lengths are comparable to droplet separations. Similar estimates at 5K give all the samples to be insulating.

We analyze the resistivity behavior for insulating samples. The transport in these samples takes place by hopping between puddles. The temperature dependence of resistivity is expected to be of variable-range hopping type $[\exp(T_0/T)^{1/3}]$ at very low temperatures and of Arrhenius type at higher temperatures. In the Arrhenius regime, resistivity would behave as $\rho(T) \sim e^{E_A/T}$ where E_A is an activation energy of the order of the mean level spacing Δ in a droplet or the classical thermal exci-

tation over the barrier separating neighboring droplets. In the ferromagnetic phase, we incorporate the effects of ferromagnetic correlations in hopping probability amplitude. When the Mn layer becomes magnetic, the droplets also get polarized in the direction of local magnetization in Mn layer. If magnetic polarization of neighbouring droplets is not aligned, the hopping is suppressed. Extra energy cost to hopping is $\sim J(1-\cos\theta_{ij})$ if θ_{ij} is the angle between magnetization of two neighbouring droplets. J can be related to both the magnetic exchange interaction in Mn $\delta-$layer and exchange interaction in the droplets. Since the droplet magnetization is approximately aligned with the local magnetization in Mn layer, $\langle\cos\theta_{ij}\rangle = e^{-D_1/\xi_M(T)}$, for a two dimensional ferromagnet, where D_1 is the droplet separation and ξ_M is the magnetic correlation length in Mn layer. With, ferromagnetism taken into account the resistivity behaves as

$$\rho(T) \approx Ae^{E_A/T+J(1-\langle\cos\theta_{ij}\rangle)/T}, \tag{15}$$

where we have approximated $\langle e^{-\cos\theta_{ij}/T}\rangle \approx e^{-\langle\cos\theta_{ij}\rangle/T}$. For two-dimensional ferromagnet [35, 36, 37]

$$\xi_M(T) = \begin{cases} a/\sqrt{1-T_C/T}, & T \gg T_C \\ a\exp[\pi T_C/2T], & T \ll T_C \end{cases}. \tag{16}$$

Here $a \sim 1/\sqrt{n_d}$ is a length scale of the order of inter-atomic separation of the Mn dopants and T_C is the Curie temperature, below which the ferromagnetic correlations increase rapidly.

We fit the model to measured resistivity data of sample 1 and 4 by adjusting the parameters. The fits and the corresponding values of parameters are shown in Fig. 6. An important point to be observed is that the peak/shoulder in resistivity appears at much lower temperature than the mean field T_C. This can be explained in our hopping transport picture. T_C corresponds to the temperature below which magnetic correlation length (ξ_M) start increasing rapidly in Mn layer. But since the droplet separation is much larger than the Mn separation, the onset of ferromagnetism in Mn layer does not affect transport significantly at temperatures near T_C. At lower temperature, when ξ_M becomes comparable to droplet separation D_1, inter-droplet tunneling probability increases rapidly which gives a decrease in the resistivity. This gives rise to a dip in the resistivity which results in the peak/shoulder feature. As the temperature further decreases, the magnetic part saturates and the activated behaviour starts dominating which at further lower temperatures becomes

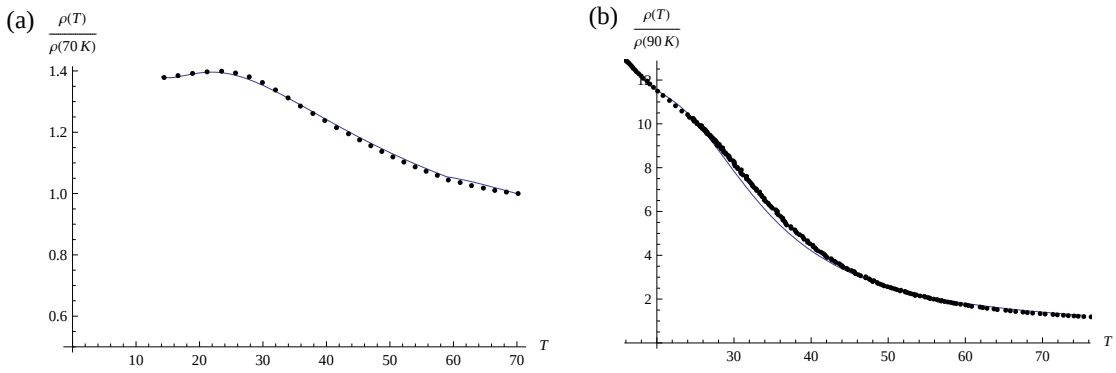

Figure 6: Observed temperature dependence of resistance for (a) Sample 4, in units of the resistance at 70 K, and (b) Sample 1, in units of the resistance at 90 K (points), and theoretical fits (solid lines). Sample 4 is near the percolation threshold and Sample 1 is well-insulating. Parameters such as the activation energy E_A and the droplet separation D_1 were chosen close to the values obtained from the droplet model and the magnetic parameters J and T_C were varied to obtain the above fits. In both cases, the best fit value of T_C was significantly larger than the temperature, at which the resistance anomaly (hump or shoulder) was observed. At lower temperatures, the resistivity becomes variable-range hopping type (not taken into account in our model). For Sample 4 in panel (a), the values used for the fit are $D_1 = 2$ nm, $E_A = 9$ K, $J = 39$ K, and $T_C = 30$ K; for Sample 1 in panel (b), the parameters are $D_1 = 9.4$ nm, $E_A = 51$ K, $J = 56$ K, and $T_C = 49$ K.

variable range hopping. In metallic samples, as the droplet separation is lower, the peak lies closer to T_C. These results clearly show that, unlike the bulk magnetic semiconductors, the peak position should not be used as as estimate for T_C of the Mn layer in these heterostructures, specially for non-metallic samples. Our analysis is also supported by the anomalous Hall effect measurements in these samples (Fig 5) which show saturation at temperatures much above the peak temperature [38]. This shows that there is significant ferromagnetism in Mn layer much before the peak appearance in resistivity. The values of fitted parameters are shown in figure 6. Another important observation is that a phase transition is not needed to have an anomaly in the resistivity and presence of significant magnetic correlations is sufficient.

References

[1] A. C. Hewson, *The Kondo Problem to Heavy Fermions*, Cambridge Univ. Press, Cambridge, (1993).

[2] A. Sen,K. Damle, R. Moessner, Phys. Rev. Lett. **106**, 127203 (2011).

[3] E. Abrahams, P. W. Anderson, D. Licciardello, and T. V. Ramakrishnan, Phys. Rev. Lett. **42**, 673 (1979).

[4] L. P. Gorkov, A. I. Larkin, D. E. Khmelnitskii, JETP Lett. 30, 228 (1979).

[5] H. Alloul, J. Bobroff, M. Gabay and P. J. Hirschfeld, Rev. Mod. Phys. **81**, 45 (2009).

[6] Patrick A. Lee, Rep. Prog. Phys. **71**, 012501 (2008).

[7] Leon Balents, Nature **464**, 199 (2010).

[8] J. K. Jain, *Composite Fermions*, Cambridge Univ. Press, Cambridge, (2007).

[9] K. Dhochak, V. Tripathi, Phys. Rev. Lett. **103**, 067203 (2009).

[10] M.A. Ruderman and C. Kittel, Phys. Rev. **96**, 99 (1954); T. Kasuya, Prog. Theor. Phys. **16**, 45 (1956); K. Yosida, Phys. Rev. **106**, 893 (1957).

[11] P. Gegenwart *et al.*, Nature Phys. **4**, 186 (2008).

[12] K. Dhochak, R. Shankar and V. Tripathi, Phys. Rev. Lett. **105**, 117201 (2010).

[13] A. Yu. Kitaev, Ann. Phys. (Berlin) **303**, 2 (2003); **321**, 2 (2006).

[14] V. Tripathi *et. al.*, Phys. Rev. B **84**, 075305 (2011).

[15] D. C. Tsui, H. L. Stormer, and A. C. Gossard, Phys. Rev. Lett. **48**, 15591562 (1982).

[16] P. Coleman and A. J. Schofield, Nature **433**, 226 (2005).

[17] M. S. Bello *et al.*, Sov. Phys. JETP **53**, 822 (1981).

[18] R. Grill and G. H. Dohler, Phys. Rev. B **59**, 10769 (1999).

[19] C. Siegert *et al.*, Nature Phys. **3**, 315 (2007).

[20] V. Tripathi and N. R. Cooper, J. Phys. Cond. Mat. **20**, 164215 (2008).

[21] D. C. Dixon *et al.*, Phys. Rev. B **56**, 4743 (1997); T. Machida *et al.*, Phys. Rev. B **65**, 233304 (2002); V. Tripathi *et al.*, Europhys. Lett. **81**, 68001 (2008).

[22] D. C. Mattis, *The Theory of Magnetism*, Harper and Row, New York (1965).

[23] A. Kolezhuk *et al.*, Phys. Rev. B **74**, 165114 (2006).

[24] S. Florens, L. Fritz, M. Vojta, Phys. Rev. Lett. **96**, 036601 (2006).

[25] S. H. Pan *et al.*, Nature (London) **403**, 746 (2000).

[26] J. Bobroff *et al.*, Phys. Rev. Lett. 86, 41164119 (2001)

[27] D. Withoff and E. Fradkin, Phys. Rev. Lett. **64**, 1835 (1990).

[28] A. J. Willans, J. T. Chalker, R. Moessner, Phys. Rev. Lett. **104**, 237203 (2010).

[29] G. Santhosh *et. al.*, Phys. Rev. B **85**, 054204 (2012).

[30] D. A. Ivanov, *Non-Abelian Statistics of Half-Quantum Vortices in p-Wave Superconductors*, Phys. Rev. Lett. **86**, 268 (2001).

[31] A. M. Nazmul, S. Sugahara and M. Tanaka, Phys. Rev. B **67**, 241308(R) (2003).

[32] T. Jungwirth *et.al.*, Rev. Mod. Phys. 78, 809864 (2006).

[33] I. Žutić, J. Fabian, and S. Das Sarma, Rev. Mod. Phys. **76**, 323 (2004).

[34] V. Tripathi and M.P. Kennett, Phys. Rev. B **74**, 195334 (2006).

[35] D. P. Arovas and A. Auerbach, Phys. Rev. B **38**, 316 (1988).

[36] M. Takahashi, Prog. Theor. Phys. **83**, 815 (1990).

[37] D. A. Yablonskiy, Phys. Rev. B **44**, 4467 (1991).

[38] B. A. Aronzon *et. al.*, J. Phys.: Condensed Matter **20**, 145207 (2008).

Publications

Papers relevant to the thesis work:

- K. Dhochak, V. Tripathi, *"Kondo Lattice Scenario in Disordered Semiconductor Heterostructures"*, Phys. Rev. Lett. **103**, 067203 (2009).
- K. Dhochak, R. Shankar and V. Tripathi, *"Magnetic impurities in the honeycomb Kitaev model"*, Phys. Rev. Lett. **105**, 117201 (2010).
- V. Tripathi, K. Dhochak, B.A. Aronzon, V.V. Rylkov, A.B. Davydov, B. Raquet, M. Goiran, K.I. Kugel, *"Charge inhomogeneities and transport in semiconductor heterostructures with a manganese delta-layer"*, Phys. Rev. B **84**, 075305 (2011).

Other papers:

- V. Tripathi, K. Dhochak, B. A. Aronzon, B. Raquet, V. V. Tugushev, K. I. Kugel, *"Noise studies of magnetization dynamics in dilute magnetic semiconductor heterostructures"*, Phys. Rev. B **85**, 214401 (2012).

Chapter 1

Introduction

Disorder plays a very important role in condensed matter systems as it changes their properties non-trivially and is generally unavoidable. Disorder in condensed matter systems can be in the form of missing atoms, external impurities or disordered distribution of dopants giving rise to a random scattering potential. Disorder effects are studied in various areas of solid state/condensed matter physics, for example, semiconductors, spin systems, superconductors and other quantum correlated systems, both theoretically and experimentally. Defects are also an important part of material research as these affect various properties like material strength, their electrical properties, behaviour of the material under extreme conditions etc.

Impurities and doping effects are a major area of work in semiconductor research. Doping of semiconductor materials is often used to change their properties and making them technologically more useful. Er doping of Si makes it an optical amplifier, N doped GaP is useful for light emitting diodes, Mn/Gd doped GaAs is a magnetic semiconductor and can be used for spintronic applications. These are a few examples of the vast number of such possibilities. How a particular impurity behaves in a material depends on both the host and the impurity properties and the way these impurities sit in the host material. Density and nature of dopants affects their transport properties also significantly. Thus, understanding the effects of doping disorder and other defects in semiconductors is an important question in this field.

Disorder studies form an important part in quantum condensed matter research as these can be often used as tools to probe the nature of their state in different regimes of parameter space. These can be used to study the properties of quantum critical points [8] and deconfined criticality [9], to study the strongly correlated state

in high temperature superconductors [10] etc. We studied effects of disorder in a few two-dimensional quantum systems in this thesis. Below we describe the main ideas that are studied in the thesis briefly.

In a part of our work, we analyzed effects of impurities in spin-1/2 Kitaev model on honeycomb lattice in its gapless quantum spin liquid phase. Quantum spin liquid (QSL) systems are interacting spin systems which do not show ordering to lowest temperatures. The absence of ordering could be due to geometric frustration [1], resonating ground states [2] etc. There can be both gapped and gapless quantum spin liquids. In gapped spin liquids, the spin-spin correlations are exponentially decaying while in gapless QSLs, spins/their higher order correlators have power law correlations. These systems can have non-trivial collective excitations and long range correlations. In these systems, a simple measurable order parameter is generally not available. Studying the effects of vacancies or external impurities is one main method that is used to explore the nature of their ground states, quasi-particle excitations and transitions between different phases [3, 4, 5]. In the gapped phase, the vacancies are found to bind a magnetic moment showing a $1/T$ impurity susceptibility. In gapless phase, the gapless excitations of the spin liquid can screen the vacancy moment partially [5] or completely [6] depending upon the nature of the excitations in the spin liquid. In this context we studied effects of external magnetic impurities in the Kitaev model (an exactly solvable quantum spin-1/2 model). We studied the nature of Kondo screening of the impurity spin due to the coupling to gapless fermionic excitations of the model. We found that the Kondo coupling flows to infinity for couplings above a critical value which shows that there is a non-trivial screening of the impurity spin. This is also hinted from the vacancy susceptibility calculations (which is similar to our strong antiferromagnetic Kondo coupling case) in Ref. [6], where a vacancy in gapless phase shows screened $ln(1/T)$ behaviour. The inter-impurity spin interactions can also shed light on the nature of the quasi-particle excitations. In presence of a finite Fermi wave-vector in the host system, the inter-impurity interactions show oscillations at $2k_FR$ length scale (as is the case for our study of impurities in Kitaev model also) while, if the Fermi point lies at zero momentum, the long range interactions do not show these oscillations, *e.g.* for impurities on the surface of Topological insulators, the interaction does not oscillate in sign when the Fermi surface lies at $k = 0$ [7].

A major area of research that emerged out of disorder effects is the Kondo systems and heavy fermion physics. Study of Kondo effect and related physics forms a large part of the thesis work. Kondo effect was first observed in metals

with magnetic impurities. The signatures of the Kondo effect were seen in the low temperature resistivity measurements where the resistivity showed a minimum feature rather than the saturation behaviour expected for metals. It has been studied extensively since then in dilute as well as dense Kondo systems and various novel phenomena have been discovered. The idea has also been extended to screening of magnetic moments by gapless quasi-particle excitations of different kinds [11, 3, 4].

The first question in this puzzle was to understand the existence of a magnetic moment inside a metal. This was understood using Anderson's model with large onsite Coulomb repulsion (U) on the localized atom:

$$H = \sum_{\mathbf{k},\sigma} \epsilon_{\mathbf{k}} c^{\dagger}_{\mathbf{k}\sigma} c_{\mathbf{k}\sigma} + \epsilon_d \sum_{\sigma} d^{\dagger}_{\sigma} d_{\sigma} + U n_{d\uparrow} n_{d\downarrow} + \sum_{\mathbf{k},\sigma} \left(V_{\mathbf{k}} c^{\dagger}_{\mathbf{k}\sigma} d_{\sigma} + h.c. \right)$$

Here $c^{\dagger}_{\mathbf{k}\sigma}$ are conduction electron creation operators, and $d^{\dagger}_{\sigma}$ for the creation operator for an electron in d-level of the impurity. The large coulomb potential suppresses double occupancy and helps in formation of the local moment on the impurity. In this regime, where charge fluctuations are suppressed ($|\epsilon_d + U - \epsilon_F|, |\epsilon_F - \epsilon_d| \gg \Delta$, where Δ is the $d-$level broadening), the effective spin Hamiltonian can be obtained by Schrieffer Wolf transformation to be

$$H_K = \sum_{\mathbf{k},\sigma} \epsilon_{\mathbf{k}} c^{\dagger}_{\mathbf{k}\sigma} c_{\mathbf{k}\sigma} + J \mathbf{S}.\sigma(0)$$

where $\sigma(0)$ is the local spin density of conduction electrons at the impurity site. This is called the Kondo Hamiltonian which has been studied to understand the behaviour of dilute Kondo systems. The resistivity increase at low temperatures (below the minimum feature) was shown to be arising from singular spin flip scattering of conduction electrons at low temperatures by J. Kondo [12, 13]. This was not immediately clear as the lowest order scattering term doesn't give this singular behaviour and next order terms were needed to explain the resistivity behaviour. To see this, one can calculate the electron scattering rate (τ^{-1}_{tr}) from $T-$matrix ($T = (I - G_0 V)^{-1}$) considerations such that

$$\tau^{-1}_{\mathbf{k}\mathbf{k}'} \sim \int \delta(\epsilon_{\mathbf{k}} - \epsilon_{\mathbf{k}'}) |T_{\mathbf{k}\mathbf{k}'}|^2 (1 - \cos\theta') d\mathbf{k}',$$

where θ' is the angle between $\mathbf{k}$ and $\mathbf{k}'$. In the lowest order in J, $T_{\mathbf{k}\mathbf{k}'}$ is constant and $1/\tau(k_F) \sim J^2 S(S+1)/\epsilon_F$ again predicting a constant resistivity at low temperatures. To get the singular corrections, we need to calculate the second order terms in J also.

$$T^{(2)}_{\mathbf{k}\mathbf{k}'} = (V G_0 V)_{\mathbf{k}\mathbf{k}'}$$

Total of these terms then gives

$$\frac{1}{\tau(k)} \sim \frac{J^2 S(S+1)}{\epsilon_F}(1 - 2J(g(\epsilon_{\mathbf{k}}) + g^*(\epsilon_{\mathbf{k}}))); \text{ where } g(\epsilon) \sim \sum_{\mathbf{k}} \frac{f(\epsilon_{\mathbf{k}})}{\epsilon_{\mathbf{k}} - \epsilon - is}.$$

Here $f(\epsilon_{\mathbf{k}})$ is the Fermi distribution. It is the $g(\epsilon)$ sum that gives the singular corrections to the resistivity at low temperatures such that the spin part of resistance is [13]:

$$R_{imp}^{\text{spin}} \sim \frac{J^2 S(S+1)}{\epsilon_F}\left(1 - 4J\rho_0(\epsilon_F)\ln\left(\frac{k_B T}{D}\right)\right).$$

where D is the conduction band width.

Another way to analyze the Kondo problem is to do a scaling analysis for the Kondo coupling and see if it flows to the strong coupling fixed point and becomes relevant at low temperatures. For magnetic impurities in metals, a Poor man's scaling analysis can be performed [14]. To study the system properties at low temperatures, we find out the effective Hamiltonian in a reduced bandwidth for the fermionic excitations ($-D + \delta D$ to $D - \delta D$) by integrating out the excitations in the band edges (($-D$ to $-D + \delta D$) and (D to $D - \delta D$)). This process is repeated successively to get a scaling law for the coupling constant. For the Kondo problem, the scaling equation comes out to be

$$\frac{dJ}{d\ln D} = -2\rho_0 J^2,$$

which shows that the coupling flows to larger values for antiferromagnetic coupling while to zero for ferromagnetic case and gives the Kondo scale $k_B T_K \sim \mathrm{e}^{-1/2J\rho_0}$ for antiferromagnetic case. The impurity spin is screened at low temperatures and impurity susceptibility does not show $1/T$ divergence, rather saturates to a constant value. The screening can be understood qualitatively by imagining the conduction electrons forming singlet with the impurity spin at low temperatures.

The above perturbation theory for resistivity breaks down at $T < T_K$ and the resistivity actually saturates at low temperatures in the unitarity limit for scattering. These properties hold for dilute Kondo systems and have been understood well.

In dense Kondo systems, where the localized spins are close by, magnetic RKKY (Ruderman Kittel Kasuya Yosida) interactions mediated by conduction electrons [15] are large and compete with the Kondo screening. The RKKY interaction in metals is given by

$$H_{RKKY} = -J^2\chi(\mathbf{r} - \mathbf{r}')\mathbf{S}(\mathbf{r}) \cdot \mathbf{S}(\mathbf{r}') = J_{RKKY}(\mathbf{r} - \mathbf{r}')\mathbf{S}(\mathbf{r}) \cdot \mathbf{S}(\mathbf{r}'),$$

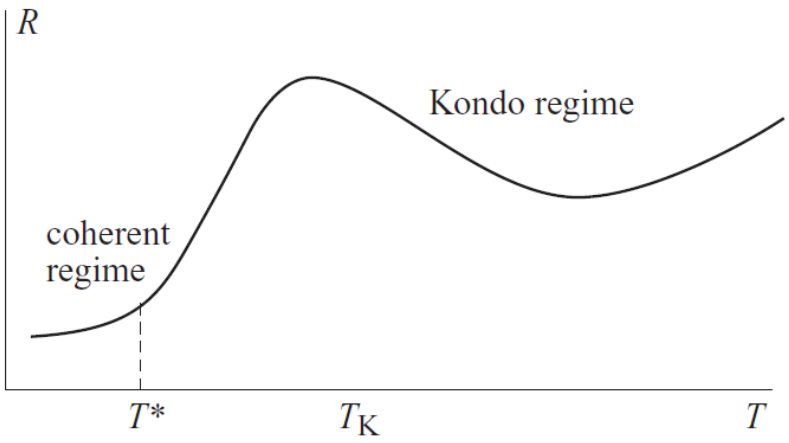

Figure 1.1: Typical behaviour of resistivity at low temperatures for a heavy fermion system [16].

where $\chi(r)$ is the conduction electron spin correlation function and can be evaluated to be

$$\chi(\mathbf{q}) = 2\sum_{k} \frac{f(\epsilon_{\mathbf{k}}) - f(\epsilon_{\mathbf{k+q}})}{\epsilon_{\mathbf{k+q}} - \epsilon_{\mathbf{k}}}$$

which gives

$$J_{RKKY}(r) \sim -J^2\rho_0 \frac{\cos(2k_F r)}{r^3}.$$

The RKKY interaction competes with Kondo effect and for large J, Kondo screening wins while in relatively small J systems, RKKY interaction is larger.

Main examples of dense Kondo systems are rare earth metallic compounds (*e.g.* $CeCu_6$, $CeAl_3$, $CePd_2Si_2$ etc.) which are Kondo lattice systems. These systems show an even richer set of interesting properties. For Kondo lattice systems also, the resistivity shows a minimum similar to dilute systems but at even lower temperatures, a new coherent regime is formed [16] (Fig. 1.1). Ground state of the system then becomes a Fermi liquid but with very large effective mass ($m^* \simeq 10^2 - 10^3 m$) and the resistivity again shows $\rho(T) \sim AT^2$ with a large A. These systems can be tuned from Kondo regime to RKKY regime by applying pressure, magnetic field etc and signatures of quantum critical behaviour can be found at the transition [17]. Some of these systems also develop superconductivity in the proximity of this point [18, 17]. We studied nuclear magnetic resonance methods as probes to study two-dimensional Kondo lattice systems in semiconductor heterostructures in both the

Kondo dominated and RKKY dominated regimes.

In a part of our work, we also studied transport properties of magnetic semiconductor heterostructures. Semiconductor heterostructures, where quantum well structures can be formed by sandwiching a layer of a semiconductor material between layers of different band gap material, play a very important role in current research as a variety of low dimensional systems can be created and studied in these systems. Their reduced dimensionality, high mobilities and enhanced quantum effects make them interesting systems to explore. Discovery of quantum Hall effect [19], Anderson localization in two dimensions [20, 21], various aspects of Kondo effect in quantum dot systems [22], spintronics applications [23] etc. are some examples of these. The density of the two dimensional electron/hole gas in the quantum well can be tuned by various gate voltages and metallic, insulating and transition transport regimes can be studied. An important class of these structures is $\delta-$doped magnetic heterostructures which have a $\delta-$doping of magnetic atoms (Mn) separated from the quantum well (to keep their carrier mobilities high). The ferromagnetism in the $\delta-$layer can produce magnetic polarization of the charge carriers and are thus interesting for spintronic applications. The magnetism and disorder of magnetic layer also affects the resistivity of these systems and is an important question to be understood. The studies of magnetic semiconductor heterostructures could also give information about the mechanism of ferromagnetism in bulk magnetic semiconductors.

Below, we give an outline with brief description of our work discussed in this thesis.

Outline

In chapter 2, we discuss the study of Kondo lattice scenarios in semiconductor heterostructures. We studied nuclear magnetic resonance (NMR) to probe the nature of the electronic state in two dimensional electron gas (2DEG) in the heterostructures [24]. In these Kondo systems, the free electron gas interacts with localized spins and the system can show a transition to a Kondo screened state at low temperatures where the localized spins are screened by the conduction electrons. Magnetic RKKY interactions between the localized impurities compete with the Kondo coupling. Semiconductor heterostructures could be used to explore the phase diagram arising out of this competition if the formation of a Kondo lattice in these structures is confirmed. We showed that nuclear relaxation rate shows distinguishable

features for a Kondo lattice and a disordered arrangement of localized spins and thus can be used to confirm the formation of Kondo lattice in these structures. NMR can also distinguish a Kondo interaction dominated regime from RKKY interaction dominated regime.

In chapter 3, we discuss the properties of external magnetic impurities coupled to spin-1/2 Kitaev model [25]. It is a quantum spin-1/2 model on honeycomb lattice with very anisotropic interactions [26]. The model can be exactly solved and has a spin liquid ground state with very short ranged spin correlations. We studied the effects of spin-S impurities coupled to the Kitaev model in its gapless spin liquid phase. We found that there is an interesting Kondo effect in the Kitaev model which is independent of the sign of the Kondo coupling (ferromagnetic or antiferromagnetic) and it is accompanied by a change of topology of the ground state. The ground state has finite fluxes at the impurity sites in strong antiferromagnetic coupling regime. These fluxes are associated with localized zero energy Majorana fermionic modes and are likely to have non-abelian statistics as is the case for the vortices with Majorana fermion at its core described in Refs. [26, 27]. We also calculated the inter-impurity interactions mediated by the gapless excitations of Kitaev model and found interesting non-dipolar interactions.

In chapter 4, we describe the effects of disorder and magnetism on transport properties of magnetic semiconductor heterostructures [28]. These heterostructures have a $\delta-$layer of Mn atoms separated from the transport channel and show ferromagnetism at low temperatures. The ferromagnetism also affects transport properties of these heterostructures. The mechanism of ferromagnetism in bulk magnetic semiconductors and semiconductor heterostructures is not very well understood and studying these systems could provide useful information about these. Due to the potential fluctuation caused by the disorder in Mn layer, charge carriers in the quantum well accumulate in potential wells forming charge droplets at low carrier densities. We incorporated the effects of ferromagnetism in hopping probabilities which could explain the observed anomaly (peak/shoulder) in the resistivity of these structures. In bulk magnetic systems, the position of this anomaly is generally used to estimate the Curie temperature, but we showed that in two dimensional systems, the anomaly can appear much below the Curie temperature.

In Chapter 5, we present a concluding summary of the thesis.

References

[1] Leon Balents, *Spin liquids in frustrated magnets*, Nature **464**, 199 (2010).

[2] F. Mila, *Quantum spin liquids*, Eur. J. Phys. **21**, 499 (2009).

[3] A. Kolezhuk, S. Sachdev, R. R. Biswas, and P. Chen, *Theory of quantum impurities in spin liquids*, Phys. Rev. B **74**, 165114 (2006).

[4] S. Florens, L. Fritz, M. Vojta, *Kondo Effect in Bosonic Spin Liquids*, Phys. Rev. Lett. **96**, 036601 (2006).

[5] A. Sen, K. Damle, R. Moessner, *Fractional Spin Textures in the Frustrated Magnet* $SrCr_{9p}Ga_{12-9p}O_{19}$, Phys. Rev. Lett. **106**, 127203 (2011).

[6] A. J. Willans, J. T. Chalker, R. Moessner, *Disorder in a Quantum Spin Liquid: Flux Binding and Local Moment Formation*, Phys. Rev. Lett. **104**, 237203 (2010); *Site dilution in the Kitaev honeycomb model*, Phys. Rev. B **84**, 115146 (2011).

[7] Rudro R. Biswas and A. V. Balatsky, *Impurity-induced states on the surface of three-dimensional topological insulators*, Phys. Rev. B **81**, 233405 (2010).

[8] S. Sachdev, C. Buragohain, Matthias Vojta, *Quantum Impurity in a Nearly Critical Two-Dimensional Antiferromagnet*, Science **286**, 2479 (1999).

[9] A. Banerjee, K. Damle and F. Alet, *Impurity spin texture at a deconfined quantum critical point*, Phys. Rev. B **82**, 155139 (2010).

[10] H. Alloul, J. Bobroff, M. Gabay and P. J. Hirschfeld, *Defects in correlated metals and superconductors*, Rev. Mod. Phys. **81**, 45 (2009).

[11] G. Khaliullin, R. Kilian, S. Krivenko, P. Fulde, *Impurity-induced moments in underdoped cuprates*, Phys. Rev B **56**, 11882 (1997).

[12] J. Kondo, *Resistance Minimum in Dilute Magnetic Alloys*, Prog. Theor. Phys. **32**, No. 1, 37 (1964).

[13] A. C. Hewson, *The Kondo Problem to Heavy Fermions*, Cambridge Univ. Press, Cambridge, (1993).

[14] P. W. Anderson, *A poor man's derivation of scaling laws for the Kondo problem*, J. Phys. C: Solid State Phys. **3**, 2436 (1970).

[15] M. A. Ruderman and C. Kittel, *Indirect Exchange Coupling of Nuclear Magnetic Moments by Conduction Electrons*, Phys. Rev. **96**, 99 (1954); T. Kasuya, *A Theory of Metallic Ferro and Antiferromagnetism on Zener's Model*, Prog. Theor. Phys. **16**, 45 (1956); K. Yosida, *Magnetic Properties of Cu-Mn Alloys*, Phys. Rev. **106**, 893 (1957).

[16] D. I. Khomskii, *Basic Aspects of Quantum Theory of Solids*, Cambridge Univ. Press, Cambridge, (2010).

[17] P. Gegenwart, Q. Si and F. Steglich, *Quantum criticality in heavy-fermion metals*, Nature Phys. **4**, 186 (2008).

[18] N. D. Mathur, F. M. Grosche, S. R. Julian, I. R. Walker, D. M. Freye, R. K. W. Haselwimmer and G. G. Lonzarich, *Magnetically mediated superconductivity in heavy fermion compounds*, Nature **394**, 39 (1998).

[19] D. C. Tsui, H. L. Stormer, and A. C. Gossard, *Two-Dimensional Magnetotransport in the Extreme Quantum Limit*, Phys. Rev. Lett. **48**, 15591562 (1982).

[20] P. W. Anderson, *Absence of Diffusion in Certain Random Lattices*, Phys. Rev. **109**, 1492 (1958).

[21] E. Abrahams, P. W. Anderson, D. Licciardello, and T. V. Ramakrishnan, *Scaling Theory of Localization: Absence of Quantum Diffusion in Two Dimensions*, Phys. Rev. Lett. **42**, 673 (1979).

[22] M. Pustilnik and L. Glazman, *Kondo effect in quantum dots*, J. Phys.: Condens. Matter 16 R513 (2004).

[23] T. Jungwirth, J. Sinova, J. Mašek, J. Kučera, and A. H. MacDonald, *Theory of ferromagnetic (III,Mn)V semiconductors*, Rev. Mod. Phys. **78**, 809 (2006).

[24] K. Dhochak, V. Tripathi, *Kondo Lattice Scenario in Disordered Semiconductor Heterostructures*, Phys. Rev. Lett. **103**, 067203 (2009).

[25] K. Dhochak, R. Shankar and V. Tripathi, *Magnetic impurities in the honeycomb Kitaev model*, Phys. Rev. Lett. **105**, 117201 (2010).

[26] A. Yu. Kitaev, *Anyons in an exactly solved model and beyond*, Ann. Phys. (Berlin) **321**, 2 (2006).

[27] D. A. Ivanov, *Non-Abelian Statistics of Half-Quantum Vortices in p-Wave Superconductors*, Phys. Rev. Lett. **86**, 268 (2001).

[28] V. Tripathi, K. Dhochak, B. A. Aronzon, V. V. Rylkov, A. B. Davydov, B. Raquet, M. Goiran, K. I. Kugel, *Charge inhomogeneities and transport in semiconductor heterostructures with a manganese delta-layer*, Phys. Rev. B **84**, 075305 (2011).

Chapter 2

Kondo Lattice Scenario in Semiconductor Heterostructures

2.1 Introduction

Kondo systems have been studied extensively for last few decades. These systems show various interesting features like enlarged Fermi surface, heavy fermions, superconductivity, magnetic ordering and signatures of quantum critical behaviour. A Kondo system generally consists of localized magnetic moments interacting with a continuum of excitations via spin exchange processes.

Kondo effect was originally observed and studied in metallic systems with magnetic impurities. In dilute Kondo systems, at low temperatures, resonant spin flip scattering processes give a large contribution to the resistivity leading to minima like feature in resistivities of these systems (Fig. 2.1). Other properties of the Kondo transition/crossover include an enhanced density of states at Fermi energy due to resonant states formed at Fermi level. The impurity spins are screened and the susceptibility saturates at low temperatures. These dilute Kondo systems show Fermi liquid properties at low temperatures well below the Kondo temperature (T_K) and have been well understood via both numerical and analytical tools including exact Bethe ansatz solution [1].

Dense Kondo systems are the systems where the magnetic moments are closely spaced (inter-impurity separation $r_{\rm imp} < \xi_K \sim 1/T_K$) and the spin-spin interactions mediated by conduction electrons (RKKY interactions) are large. Magnetic ordering tendencies due to large magnetic interactions compete with the Kondo screening. These systems show even richer variety of phases with heavy fermionic excitations,

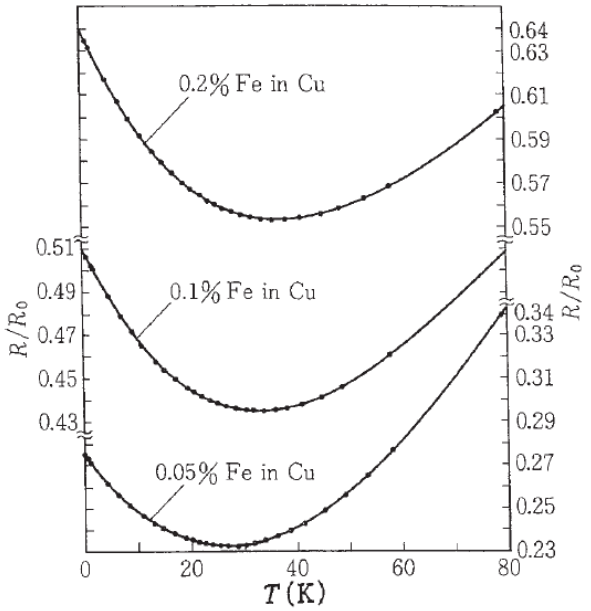

Figure 2.1: Resistivity measurements for Cu with Iron impurities showing the minima [2].

superconductivity and quantum critical behaviour arising out of this competition [3, 4]. These Kondo lattice systems are usually formed in rare earth compounds (*e.g.* $CeCu_6$, $YbRh_2Si_2$, $LaRu_2Si_2$) where the strongly localized f-electrons give rise to magnetic moments. These systems can be tuned by application of pressure and magnetic fields or by doping to study the competition of magnetic and Kondo interactions. Recent experimental studies have shown that these systems are strong candidates for finding quantum critical points [5, 6, 7]. The quantum criticality appears at the transition between Kondo and magnetic regimes. The magnetic fluctuations try to decrease the effective Kondo coupling in Kondo regime and vice-versa such that at the transition, both scales vanish and the system properties are dominated by quantum fluctuations. There is a large area of phase space where the system has non Fermi liquid behavior and the resistivity is quasi-linear in temperature (Fig. 2.2) unlike the quadratic behaviour of Fermi-liquids. These systems also show superconductivity around the critical point (Fig. 2.3) [8]. The phase diagram has similarities to the high-T_C superconductors and the Iron based superconductors as several of these systems also show co-existence of magnetism and superconductivity. These systems provide opportunities to study the physics

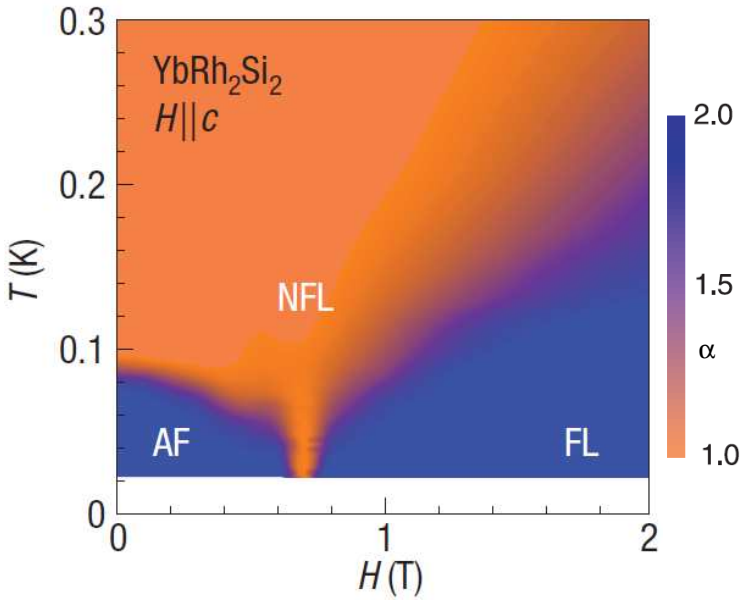

Figure 2.2: Suppression of magnetic ordering in $YbRh_2Si_2$ by application of magnetic field and the evolution of the resistivity exponent ($\Delta\rho = \rho(T) - \rho(0) \propto T^{\alpha}$) from 2 in the Fermi liquid (FL) phase to 1 in the non-Fermi liquid (NFL) phase [7].

of quantum critical points as well as could provide insights into an understanding of high-T_C superconductivity. These have given a new direction to the research work in this field. To explore and understand the complex phase diagram of Kondo lattice systems and drive it across the quantum critical point, one need to tune the parameters of the system which is usually a difficult task in solid state systems.

Tunability is a key feature of semiconductor heterostructures where the charge carrier density and other parameters can be varied easily. There have been experimental proposals of creating a Kondo lattice systems in these heterostructures [9]. Semiconductor heterostructures are layered structures of two or more semiconductors of different band gaps that can give rise to quantum well structures and the density of charge carriers in the quantum well can be controlled by gate voltages (Fig. 2.4). These structures can be $\delta-$doped with an atomic layer of dopants spatially separated from the quantum well, to further control the carrier densities in the quantum well with minimal effect on their mobility. The electron gas is formed at the junction of GaAs and AlGaAs due to band bending and mismatch of band gaps. The Si $\delta-$layer is partially ionized and provides carriers in the quantum well region. These ionized Si atoms would like to arrange in a triangular lattice to min-

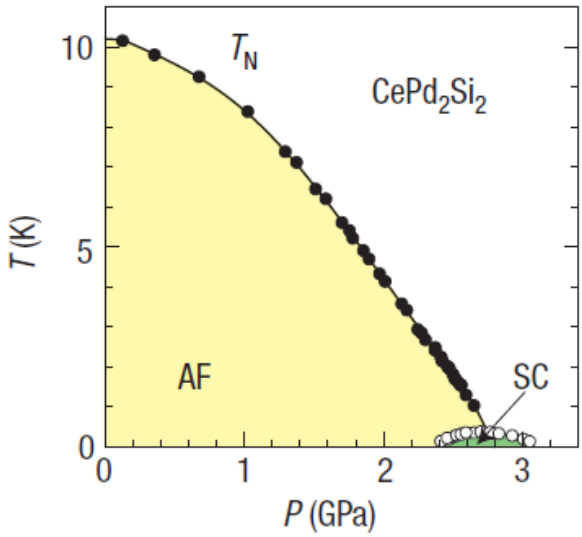

Figure 2.3: Temperature-pressure phase diagram of $CePd_2Si_2$, showing the emergence of a superconducting phase around the quantum critical point. Open circles show the superconducting ordering temperature [8, 3].

imize the Coulomb energy. Generally disorder in the arrangement of Si atoms is known to be significant. The possibility of spatial ordering of charged donors, or Wigner crystallization, in $\delta-$ doped heterostructures, when the degree of ionization is around 1/3 or lower has been theoretically predicted [10, 11]. These ions cause a spatially varying Coulomb potential at the junction of GaAs and AlGaAs where two dimensional electron gas (2DEG) is formed. The potential profile depends on the arrangement of ions in the delta layer and could be disordered or ordered. The potential wells can bind electrons and give rise to local moments in the 2DEG. This forms a Kondo system with these local moments interacting with rest of the free electrons in the quantum well. If the ions form a crystalline structure, there is an interesting possibility of formation of a Kondo lattice. Such a realization, if confirmed, can be very useful to study properties of Kondo lattice systems in various regimes of parameters.

In transport measurements, which are generally used to study these systems, the enhanced density of states at the Fermi energy due to the Kondo resonance gives rise to a peak in zero bias tunneling conductance in the Kondo-coupling dominated regime which splits in the RKKY dominated regime. These were observed in the experiments ([9]) done in these heterostructures. In Ref. [9] it was observed that

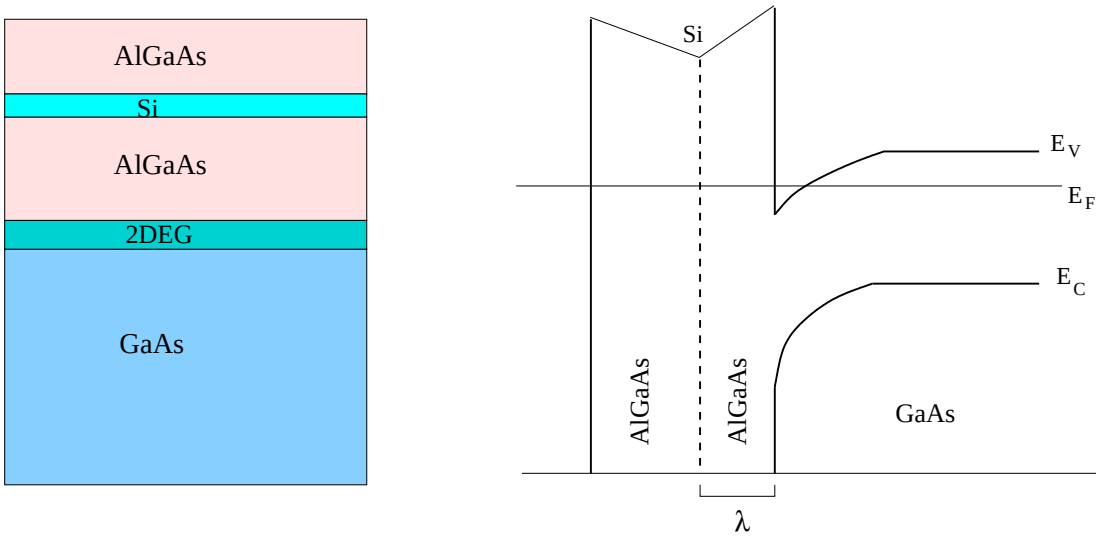

Figure 2.4: A schematic of the $\delta-$doped semiconductor heterostructure and the band bending at the AlGaAs-GaAs junction. The position of Fermi level and density of 2DEG can be varied by changing the gate voltage and Si doping etc.

the 2DEG conductance showed an alternating splitting and merging of a zero bias anomaly (ZBA) upon varying the gate voltage V_g which happens because varying the gate voltage affects the 2DEG density, which, in turn, controls the sign of the RKKY exchange interaction, $J_{RKKY}(R_{ij}) \sim (J^2\rho/R_{ij}^2)\cos(2k_F R_{ij})$, of the localized spins. Here J is the Kondo coupling of the localized spins with the conduction electrons, and ρ is the density of states at the Fermi energy. However, the transport measurements are unable to give information about the spatial order of localized spins and can not be used to confirm the formation of an artificial Kondo lattice in semiconductor heterostructures. A zero bias conductance anomaly can appear as long as each impurity is Kondo screened and it can split when pairwise magnetic interactions become strong. This is also evident from similar observation of zero bias conductance peak in coupled double quantum dot systems and its splitting when inter-dot coupling is large [12]. We studied nuclear relaxation rate as a probe to distinguish a disordered system from a Kondo lattice.

NMR for semiconductor devices

Nuclear magnetic resonance (NMR) methods usually measure the relaxation rates of the nuclear polarization or the Zeeman splitting of the nuclear levels. Both of these reflect the nature of the electronic state of the systems as the nuclear

dipolar couplings are much smaller than the nuclear couplings to electronic degrees of freedom. The relaxation rates (T_1^{-1}, T_2^{-1}) for the nuclear polarization $\mathbf{M}(t)$ are defined as

$$\frac{dM_z}{dt} = \frac{M_z(t) - M_z^0}{T_1}; \;\; \frac{dM_{x/y}}{dt} = \frac{M_{x/y}(t) - M_{x/y}^0}{T_2}. \tag{2.1}$$

NMR methods have been widely used to study strongly correlated electron phenomena in bulk systems as local probes for the magnetic state of the system, for example, to study the magnetization patterns created by magnetic/non-magnetic impurities in Cuprate superconductors [13] and quantum spin liquids, to explore bulk Kondo systems for magnetism [14] etc. The utility of NMR probes for probing strongly correlated electron phenomena in meso and nano scale devices has been hampered, in comparison with bulk systems, by the small size of the active regions in the devices. Recently, suitably adapted NMR methods have been proposed by which nuclear polarization may be generated locally in such devices and its relaxation can be feasibly detected through two-terminal conductance measurements [15]. One such detection proposal is based on the idea that electron transport through the device is sensitive to the Overhauser shift; and, by measuring the relaxation rate of the conductance at different values of temperature and other parameters, it is possible to extract the dependence of nuclear relaxation rate T_1^{-1} on those parameters. The behavior of the nuclear relaxation rate conveys useful information about the electronic state in the device.

The magnetic coupling of a nuclear moment with its external environment can be expressed as

$$\mathcal{H}_{\rm nuc} = -\hbar\gamma_n \mathbf{I} \cdot (\mathbf{H} + \mathbf{H}_{\rm loc}), \tag{2.2}$$

where $\mathbf{H}$ is the external magnetic field and $\mathbf{H}_{\rm loc}$ is the local field due to the electrons, and γ_n is the nuclear gyromagnetic ratio. The nuclear relaxation rate then depends on $H_{\rm loc}^{\pm}$, the (transverse) local field fluctuations at the site of a nucleus[16]:

$$T_1^{-1} = \frac{\gamma_n^2}{2} \int_{-\infty}^{\infty} dt \, e^{i\omega_n t} \langle \{ H_{\rm loc}^{+}(t), H_{\rm loc}^{-}(0) \} \rangle. \tag{2.3}$$

where ω_n is the nuclear Zeeman frequency which is very small and in fast electronic relaxation limit, we take $\omega_n = 0$. Nuclear relaxation takes place through coupling to localized spins $\mathbf{S}$ as well as conduction electrons $\boldsymbol{\sigma}$:

$$\mathcal{H}_{\rm loc} = A_d \mathbf{I}\cdot\mathbf{S} + A_s \mathbf{I}\cdot\boldsymbol{\sigma}. \tag{2.4}$$

Here A_d and A_s are the hyperfine coupling with the localized spin and conduction electrons respectively. T_1^{-1} is thus related to the local transverse spin susceptibility of the electrons. The relaxation contribution from localized (electron) spins is usually much larger in devices similar to those considered here [17]. Therefore, taking only localized spin part,

$$\begin{aligned} T_1^{-1} &= \frac{A_d^2\gamma_n^2}{2}\int_{-\infty}^{\infty} dt\,\langle\{S^+(t), S^-(0)\}\rangle. \\ &= \frac{A_d^2\,\gamma_n^2\,k_B\,T}{\hbar^2\,\gamma_e^2}\,\mathrm{Im}\left(\frac{\chi_i^{+-}(\omega)}{\omega}\right)_{\omega\to 0}. \end{aligned} \tag{2.5}$$

We calculated the susceptibility χ_i in different possible scenarios of the system, *i.e.*, few impurities case, lattice of impurities in Kondo dominated and RKKY dominated regimes and showed that it has unambiguously distinguishable temperature dependences for these scenarios [18]. The difference is more significant when the RKKY interaction dominates the Kondo effect.

2.2 Two dimensional Kondo model

We consider the Kondo model Hamiltonian for $S = 1/2$ magnetic impurities in a 2-dimensional electron gas:

$$H = \sum_k \xi_k c_{k\sigma}^\dagger c_{k\sigma} + J\sum_i \boldsymbol{\sigma}_i\cdot\mathbf{S}_i. \tag{2.6}$$

Here $\mathbf{S}_i$ denotes the localized spin and $\boldsymbol{\sigma}_i$ the conduction electron spin density at $\mathbf{r}_i$. J is the antiferromagnetic Kondo coupling between localized spins and free electron density. We need to calculate the susceptibility χ_i in different possible scenarios of the system.

We use the "drone-fermion" representation for the localized spins [19, 20]:

$$S_i^+ = \frac{1}{\sqrt{2}} f_i^\dagger \chi_i, \qquad S_i^- = \frac{1}{\sqrt{2}}\chi_i f_i, \qquad S_i^z = f_i^\dagger f_i - \frac{1}{2}, \tag{2.7}$$

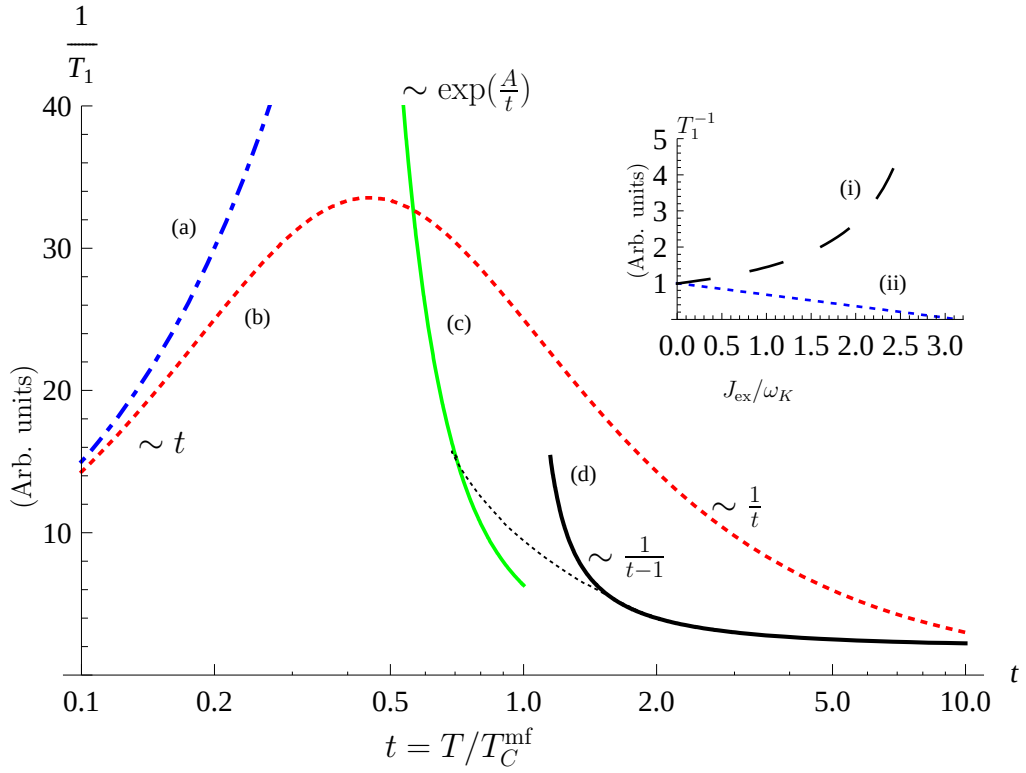

Figure 2.5: Plots showing the qualitative differences in the temperature and (AFM) inter-impurity exchange interaction $J_{\rm ex}$ dependencies of the nuclear relaxation rates T_1^{-1} for a two impurity system and Kondo lattice. Main plot: $T_1^{-1}(T)$ for (a) a two impurity system; (b) a Kondo interaction dominated lattice ($J_{\rm ex}/\omega_K < 1$); (c,d) a Kondo lattice where $J_{\rm ex}/\omega_K > 1$ and $T < (>) T_C^{\rm mf}$, where $T_C^{\rm mf}$ is the mean-field transition temperature. Dotted curve interpolates between these two temperature regimes (there is no phase transition). Inset: T_1^{-1} as a function of $J_{\rm ex}/\omega_K$ for (i) Kondo lattice (ii) two impurities - the T_1^{-1} vanishes for $J_{\rm ex}/\omega_K > \pi$.

where f_i and $f_i^\dagger$ are Fermionic operators and χ_i are real Majorana fermions defined by $\{\chi_i, \chi_j\} = 2\delta_{ij}$. The commutation relations for the impurity spins are automatically satisfied in this representation, obviating the need to impose local constraints on the fermion number as would have been the case, for example, with the Abrikosov pseudo-fermion representation. The increased number of degrees of freedom also does not need a projection procedure because it just generates two independent copies of the spin system. For a single impurity, there is no natural representation of the Majorana fermion but it can be seen if we write χ as $g+g^\dagger$, where g is a complex fermion. Now the impurity Hilbert space is 4-dimensional. It can be seen that it separates into two independent subsets $|0\rangle,\ f^\dagger g^\dagger|0\rangle$ and $g^\dagger|0\rangle,\ f^\dagger|0\rangle$. The spin operators do not connect these two sets. Thus all spin averages can be computed without needing a projection. For even number of impurity spins, it can be alternatively seen by forming fermionic operators $h = \chi_1 + i\chi_2$ ($\chi_1,\ \chi_2$ are the Majorana fermions of two neighbouring impurities). Now the 8-dimensional Hilbert space again forms two independent copies $|0\rangle,\ {f_1}^\dagger h^\dagger|0\rangle,\ h^\dagger {f_2}^\dagger|0\rangle,\ {f_1}^\dagger {f_2}^\dagger|0\rangle$ and $h^\dagger|0\rangle,\ {f_1}^\dagger|0\rangle,\ {f_2}^\dagger|0\rangle,\ {f_1}^\dagger h^\dagger {f_2}^\dagger|0\rangle$.

Introducing the Bosonic operators,

$$a_i = \frac{1}{\sqrt{2}}\left(f_i^\dagger c_{i\uparrow} + \frac{\chi_i c_{i\downarrow}}{\sqrt{2}}\right), \qquad b_i = \frac{1}{\sqrt{2}}\left(f_i^\dagger c_{i\downarrow}^\dagger - \frac{\chi_i c_{i\uparrow}^\dagger}{\sqrt{2}}\right); \tag{2.8}$$

the interaction part of the Hamiltonian (up to constants) can be written as

$$H_{int} = -J\sum_i \left(a_i^\dagger a_i + b_i^\dagger b_i\right) - \frac{J}{2} f_i^\dagger f_i + \frac{J}{8}\left(c_{i\uparrow}^\dagger c_{i\uparrow} - c_{i\downarrow}^\dagger c_{i\downarrow}\right). \tag{2.9}$$

The a_i and b_i operators resemble pairings in the exciton and Cooper channels respectively. The last term in Eq. 2.9 gives different but small shifts $J \ll \epsilon_F$ to up and down spin electrons while the second term is a constant shift of the impurity energy; we neglect these terms in further analysis (Ref. [20]) and use the interaction Hamiltonian

$$H_{int} = -J\sum_i \left(a_i^\dagger a_i + b_i^\dagger b_i\right). \tag{2.10}$$

The quartic part H_{int} can be factorized using Hubbard Stratonovich transformation. Introducing fields Δ_1^i and Δ_2^i, the partition function can be written in path integral form as

$$Q = \int D(c, f, \chi, \Delta)\ \exp\left(-\int_0^{\frac{1}{T}} d\tau\, [S_0(\tau) + S_{int}(\tau)]\right), \tag{2.11}$$

where

$$S_0 = \sum_{k\sigma} c^\dagger_{k\sigma} \left(\partial_\tau + \xi_k\right) c_{k\sigma} + \sum_i \left(f^\dagger_i \partial_\tau f_i \; + \; \frac{1}{2}\chi_i \partial_\tau \chi_i + \frac{1}{J}\left(|\Delta^i_1|^2 + |\Delta^i_2|^2\right)\right), \quad (2.12)$$

$$S_{int} = \sum_i \left(\Delta^i_1 a^*_i + \Delta^i_2 b^*_i\right) + h.c. \quad (2.13)$$

$$\Delta^i_{1,2} = |\Delta^i_{1,2}| e^{i\phi^i_{1,2}}$$

For a single impurity in the 2D electron gas, upon making the following global transformations (under which S_0 is invariant),

$$f \to f e^{i(\phi_2 - \phi_1)}, \quad c_\uparrow(r) \to c_\uparrow(r) e^{i\phi_2}, \quad c_\downarrow(r) \to c_\downarrow(r) e^{i\phi_1}; \quad (2.14)$$

S_{int} takes the form

$$\begin{aligned} S_{int} =& |\Delta^i_1| \left(a_i + a^\dagger_i\right) + |\Delta^i_2| \left(b_i + b^\dagger_i\right) + \frac{\dot{\phi_+}}{2} \sum_{k,\sigma} c^\dagger_{k\sigma} c_{k\sigma} \\ &+ \dot{\phi_-} \left\{ \sum_k \frac{1}{2} (c^\dagger_{k\uparrow} c_{k\uparrow} - c^\dagger_{k\downarrow} c_{k\downarrow}) + f^\dagger_i f_i \right\}. \end{aligned} \quad (2.15)$$

Here $\phi_\pm = \phi_1 \pm \phi_2$. The $\dot{\phi}_+$ term couples to total electron density n and $\dot{\phi}_-$ couples to $z-$component of the total spin $(\sigma_z + S_z + 1/2)$ which are both constants. Thus the $\dot{\phi}$ terms become zero (on doing integration by parts) and S_{int} is given by

$$S_{int} = |\Delta^i_1| \left(a_i + a^\dagger_i\right) + |\Delta^i_2| \left(b_i + b^\dagger_i\right) \quad (2.16)$$

We do a mean field analysis neglecting the fluctuations of $|\Delta|$'s. The saddle point solution for Δ's is $|\Delta_{1,2}|^* = r_0$, where

$$r_0 = \frac{J}{2} \mathrm{Re} \left\langle a_i + b_i \right\rangle. \quad (2.17)$$

For multiple impurities or a lattice of impurities in the 2D electron gas, the above transformations can be made with ϕ^0_1, ϕ^0_2, the average values of ϕ^i_1, ϕ^i_2 respectively, if there is a $U(1)$ symmetry breaking. S_{int} will then have extra terms containing fluctuations of $\phi^i_{1/2}$. These fluctuations are gapless and their effects on nuclear relaxation rate need to be studied in more detail. In our work, we have used the single impurity approach and have not studied the effects of ϕ fluctuations.

2.2.1 One impurity spin

We first consider a single impurity at $\mathbf{r}_i$ interacting with the conduction electrons. This scenario will also be valid for a very dilute Kondo system where the inter-impurity interactions are negligible. Up to leading order in J,

$$\langle a_i \rangle = \langle b_i \rangle \quad \text{and} \quad \langle \chi_i c_{i\downarrow} \rangle = \frac{1}{\sqrt{2}} \langle f_i^\dagger c_{i\uparrow} \rangle. \tag{2.18}$$

The mean field solution for r_0 in Eq. 2.17 is,

$$r_0 = \frac{3J}{2\sqrt{2}} \langle f_i^\dagger c_{i\uparrow} \rangle \text{ with } \langle f_i^\dagger c_{i\uparrow} \rangle = -\frac{r_0}{\sqrt{2}} k_B T \sum_{\nu_n} F_{\nu_n} G_{\nu_n}. \tag{2.19}$$

Here F_{ν_n} and G_{ν_n} are Matsubara Green's functions defined for f fermions and electrons as:

$$F_{\nu_n} = -\left\langle T_\tau f_i f_i^\dagger \right\rangle_{\nu_n} = \left(i\nu_n + i\omega_K \, \mathrm{sgn}(\nu_n)\right)^{-1}, \tag{2.20}$$

$$G_{\nu_n} = \sum_k G^{(0)}_{\nu_n k} \simeq -i\pi\rho \, \mathrm{sgn}(\nu_n). \tag{2.21}$$

Here ρ is the density of states at the Fermi energy and $\omega_K = \pi\rho r_0^2$.
$G^{(0)}_{\nu_n k}$ is the free electron Green function,

$$G^{(0)}_{\nu_n k} = -\left\langle T_\tau c_i c_i^\dagger \right\rangle_{\nu_n, k} = \left(i\nu_n - \xi_k\right)^{-1}. \tag{2.22}$$

From Eq. 2.19 we have

$$-\frac{3}{4} \, r_0 J k_B T \sum_{\nu_n} F_{\nu_n} G_{\nu_n} = r_0, ; \tag{2.23}$$

and thus

$$\omega_K = D \, \exp\left(-\frac{4}{3\rho J}\right). \tag{2.24}$$

ω_K differs parametrically from the correct Kondo temperature, $k_B T_K \sim D e^{-1/(\rho J)}$, where there is no factor of 4/3 in the exponent. This is a shortcoming of the mean field approach.

The frequency dependent local susceptibility is given by

$$\begin{aligned}\frac{\chi_i(\omega_m)}{(g_s\mu_B)^2} &= \langle T_\tau\, S_i^z(\tau)\, S_i^z(\tau')\rangle_\omega = -k_BT\sum_{\nu_n} F_{\nu_n}F_{\nu_n+\omega_m} \\ &= \frac{2\omega_K}{\pi|\omega_m|\,(|\omega_m|+2\omega_K)}\left[\psi\left(\frac{1}{2}+\frac{\omega_K+|\omega_m|}{2\pi k_BT}\right)-\psi\left(\frac{1}{2}+\frac{\omega_K}{2\pi k_BT}\right)\right] \\ &\simeq \frac{1}{\pi\,(|\omega_m|+\omega_K)}, \qquad T\ll\omega_K. \end{aligned} \tag{2.25}$$

Here ψ is the Digamma function and ω_m are bosonic Matsubara frequencies. At $\omega_m = 0$, the static spin susceptibility is

$$\begin{aligned}\chi_i(0) &= \frac{(g_s\mu_B)^2}{2\pi^2k_BT}\psi'\left(\frac{1}{2}+\frac{\omega_K}{2\pi k_BT}\right) \\ &\simeq (g_s\mu_B)^2 \begin{cases}(\pi\omega_K)^{-1} & \text{if } T\ll\omega_K \\ (4k_BT)^{-1} & \text{if } T\gg\omega_K\end{cases}\end{aligned} \tag{2.26}$$

The susceptibility obtained by this mean field analysis correctly shows a saturating behaviour at low temperatures as expected for the unitarity limit of the Kondo model. The high temperature result is also in agreement with the Curie susceptibility of an isolated impurity spin. However at finite temperatures near ω_K, a $1/(T+\omega_K)$ dependence is predicted instead of the correct $(1-(T/\omega_K)^2)/\omega_K$. While this does have an effect on the temperature dependence of the nuclear relaxation rate, we will use an appropriate modification to correct the discrepancy.

Nuclear relaxation rate

The nuclear relaxation rate follows from Eq. 2.5 for which we need the transverse local susceptibility $\chi_i^{+-}(\omega)$. At low temperatures $T \ll \omega_K$,

$$\begin{aligned}\frac{\chi_i^{+-}(\omega_m)}{(g_s\mu_B)^2} &= \langle T_\tau\, S_i^+(\tau)\, S_i^-(\tau\prime)\rangle_{\omega_m} \\ &= -k_BT\sum_{\nu_n} F_{\nu_n}X_{\nu_n+\omega_m} \approx \frac{1}{\pi}\frac{1}{(|\omega_m|+\omega_{Ki})}.\end{aligned} \tag{2.27}$$

Here

$$X_{\nu_n} = -\langle T_\tau\chi_i(\tau)\chi_i(0)\rangle_{\nu_n} = (i\nu_n + i\omega_{Ki}\,\mathrm{sgn}(\nu_n))^{-1}$$

is the Green function for the Majorana fermions. The transverse susceptibility and the longitudinal susceptibility we defined in Eq. 2.25 are equal: this is correct as

long as there is no external magnetic field. An analytic continuation, $\chi_i^{+-}(\omega_m) \to \chi_i^{+-}(\omega) = (g_s\mu_B)^2/\pi(-i\hbar\omega + \omega_{Ki})$, to real frequencies leads to

$$T_{1i}^{-1} = \frac{A_d^2 k_B T}{\pi\hbar\omega_K^2} = \frac{\pi A_d^2 k_B T}{\hbar(g_s\mu_B)^4}\chi_i(0)^2. \tag{2.28}$$

Thus, a few non-interacting local spins give a linear-T relaxation rate. If the localized spins are nearby, RKKY interactions compete with the Kondo screening. To analyze the effects of this competition, we will consider below two interacting nearby spins.

2.2.2 Two impurity spins

To understand the effects of the competition between Kondo screening and inter-impurity interactions, we considered two nearby localized spins $\mathbf{S}_1, \mathbf{S}_2$ at $\mathbf{R} = \mathbf{R}_1, \mathbf{R}_2$ which interact via an exchange interaction

$$H_{\rm ex} = J_{\rm ex}(R_{12})\mathbf{S}_1 \cdot \mathbf{S}_2. \tag{2.29}$$

If the wave-functions of the localized electrons have a significant overlap, then direct exchange would be dominant. Indirect (or RKKY) exchange is more important at larger separations. Here it also becomes important to compare the relative strengths of the RKKY interaction between the impurity spins with the hyperfine interaction of either of the impurities with neighbouring nuclei. The RKKY interaction $J_{\rm RKKY}$ falls off with distance R_{12} as $J_{\rm RKKY} \sim \frac{J^2\rho}{R_{12}^2}$. This should be compared with $A_d = \frac{A_s}{l_{\rm loc}R_p^2}$, where R_p is the size of the electron puddle (localized electrons) in the plane of the heterostructure. We use the following parameters for a GaAs/AlGaAs heterostructure, $J\rho \sim 1$, $l_{\rm loc} \sim 1$nm, $R_p \sim 10$nm, $A_s = 3.8 \times 10^{-54}$Jm^3, and $m = 0.063m_e$. Then $J_{\rm RKKY} \gg A_d/N_{\rm nuc}$ is satisfied if $R_{12} \ll \sqrt{1/A_d\rho} \approx 1$mm. For the experimental system, the sample sizes are usually a few microns; thus the RKKY interaction is large compared to the interaction of the nuclei with the individual localized spins. The nuclei couple to the RKKY bound pair $\mathbf{S}_1 + \mathbf{S}_2$ rather than the spins separately. The impurity susceptibility now involves both on-site ($\chi_i^{+-}(\omega)$) and intersite ($C_{ij}^{+-}(\omega)$) correlations:

$$(g_s\mu_B)^2\langle\Big\{S_i^+(t), S_j^-(0)\Big\}\rangle_\omega = \coth\left(\frac{\hbar\omega}{2k_BT}\right)\mathrm{Im}(C_{ij}^{+-}(\omega)). \tag{2.30}$$

Therefore, using eq. 2.3, the nuclear relaxation rate can be written as

$$T_1^{-1} \propto A_d^2 \left(\mathrm{Im}\frac{\chi_1^{+-}(\omega)}{\omega} + \mathrm{Im}\frac{\chi_2^{+-}(\omega)}{\omega} \right)_{\omega\to 0} + 2A_d^2\, \mathrm{Im} \left(\frac{C_{12}^{+-}(\omega)}{\omega} \right)_{\omega\to 0}. \qquad (2.31)$$

We have already shown that $\mathrm{Im}\left(\frac{\chi_i^{+-}(\omega)}{\hbar\omega}\right)_{\omega=0} = \frac{(g_s\mu_B)^2}{\pi\,\omega_{K_i}^2}$. The inter-site correlation

$$\begin{aligned} \frac{C_{ij}^{+-}(\omega_m)}{(g_s\mu_B)^2} &= -\frac{J_{\mathrm{ex}}(R_{12})}{2} \left(-k_B T \sum_{\nu_n} F_{\nu_n} X_{\nu_n+\omega_m} \right)^2 \\ &\approx -\frac{J_{\mathrm{ex}}(R_{12})}{2} \frac{1}{\pi(|\omega_m| + \omega_K^i)} \cdot \frac{1}{\pi(|\omega_m| + \omega_K^j)}, \end{aligned} \qquad (2.32)$$

is similarly analytically continued to real frequencies ω yielding

$$\frac{1}{(g_s\mu_B)^2} \mathrm{Im} \left(\frac{C_{12}^{+-}(\omega)}{\hbar\omega} \right)_{\omega=0} = -\frac{J_{\mathrm{ex}}(R_{12})}{2\pi^2} \frac{(\omega_{K1}+\omega_{K2})}{(\omega_{K1}\omega_{K2})^2}.$$

In the last step in Eq. 2.32 we have considered the low temperature limit, $k_B T \ll \omega_K$. Thus for two impurities we have, to leading order in inter-impurity interaction,

$$T_1^{-1} = \frac{A_d^2 k_B T}{\pi\hbar} \left(\frac{1}{\omega_{K1}^2} + \frac{1}{\omega_{K2}^2} - \frac{J_{\mathrm{ex}}(R_{12})}{\pi} \frac{(\omega_{K1}+\omega_{K2})}{(\omega_{K1}\omega_{K2})^2} \right). \qquad (2.33)$$

The above expression reflects the fact that as J_{ex} increases (antiferromagnetic coupling), the uniform susceptibility of the two-impurity system decreases, thus decreasing the nuclear relaxation rate. For identical impurities ($\omega_{K1} = \omega_{K2}$),

$$T_1^{-1} = \frac{2}{\pi} \frac{A_d^2 k_B T}{\omega_K^2 \hbar} \left(1 - \frac{1}{\pi} \frac{J_{\mathrm{ex}}(R_{12})}{\omega_K} \right). \qquad (2.34)$$

It is also evident from Eq. 2.33 that when the two Kondo temperatures are very dissimilar, the competition of the Kondo and antiferromagnetic inter-impurity interaction is determined by the relative strengths of J_{ex} and the *larger* of the two Kondo temperatures.

When $J_{\mathrm{ex}}/\omega_K \geq \pi$, the nuclear relaxation rate is suppressed to zero: this is the maximum value of J_{ex}/ω_K for which the behaviour is governed by the Kondo screening of the impurity spins. At antiferromagnetic couplings $J_{\mathrm{ex}} > \pi\omega_K$, the ground state is an RKKY singlet which is unable to exchange spins with the nuclei. While our analysis is only to leading order in J_{ex}, more accurate calculations [22] based on numerical renormalization group methods have shown that this critical

point occurs at $J_{\rm ex}/k_BT_K \approx 2.2$. On the other hand, even for a large *ferromagnetic* coupling of the spins, the ground state is a Kondo singlet [22].

The main difference we have shown from the single impurity case is that nuclei in the vicinity of a double Kondo impurity system would not relax through their coupling to the impurities if the antiferromagnetic coupling of the impurities were sufficiently large to form an RKKY singlet. With a larger number of spatially disordered impurity spins, one can show that for weak interimpurity interactions, the nuclear relaxation rates have linear-T behavior with logarithmic factors arising from the random distribution of Kondo temperatures of individual impurities [23] ignore the Kondo effect to leading order. In that case, it is known that the magnetic susceptibility at low temperatures is dominated by pairs with the weakest exchange interactions [24]. This leads to a weakly increasing susceptibility $e^{C\ln^{1/2}(T_0/T)}$ (instead of zero for the double impurity case). Nevertheless, the nuclear relaxation rate is dominated by the linear-T pre factor as the exponential term is weaker than any power law.

2.2.3 Lattice of impurity spins

Nuclear relaxation in a Kondo lattice is also affected by the competition of the exchange interaction and the impurity spin screening tendency of the conduction electrons. However, as we show below, the results are qualitatively different from the two-impurity case. The main physical difference from the two-impurity case is the existence of low energy magnetic excitations in the lattice for any value of the ratio $J_{\rm ex}/\omega_K$. As a result, significant nuclear relaxation still occurs for large antiferromagnetic inter-impurity couplings unlike the two-impurity case where it vanishes.

Kondo interaction dominated behaviour: $\omega_K \gg J_{\rm ex}$

We consider first the scenario where we have a lattice of Kondo impurities with a weak exchange interaction among the neighbouring spins. At low temperatures, the ground state of such a system consists of "heavy-fermions": a narrow band of fermions with a large density of states.

Interestingly, in the absence of RKKY interactions, the formation of the heavy fermion band has no qualitative effect on the nuclear relaxation rate [20]. This is because the enhancement $1/Z_0$ in the density of states is canceled by the quasi particle weight Z_0.

We consider weak exchange interaction among the spins and treat it as a perturbation:

$$H_{RKKY} = \sum_{\langle ij \rangle} J_{\rm ex}(R_{ij}) \mathbf{S}_{\rm i} \cdot \mathbf{S}_{\rm j} = \sum_{\mathbf{q}} J_{\rm ex}(\mathbf{q}) \mathbf{S}_{\mathbf{q}} \cdot \mathbf{S}_{-\mathbf{q}}. \tag{2.35}$$

In the random phase approximation, the q dependent spin susceptibility is given by

$$\chi^{+-}_{\mathbf{q}}(\omega, T) = \frac{\chi^{+-}_{i}(\omega, T)}{1 - \frac{n_{\rm imp} J_{\rm ex}(\mathbf{q})}{(g_s \mu_B)^2} \chi^{+-}_{i}(\omega, T)}. \tag{2.36}$$

The local nature of the Kondo effect implies the impurity susceptibility χ_i has no wave-vector dependence. We assume that $J_{\rm ex}(\mathbf{q})$ has maximum value at $\mathbf{q} = \mathbf{Q}$, and the wave-vector dependence in the vicinity of the maximum is $J_{\rm ex}(\mathbf{Q} + \mathbf{q}) = J_{\rm ex}(\mathbf{Q}) - (D_s/n_{\rm imp}) a^2 q^2$, where a is the lattice constant of the Kondo array and D_s the spin wave stiffness. The susceptibility in this momentum region has the form

$$\chi^{+-}_{\mathbf{Q}+\mathbf{q}}(\omega, T) = \frac{(g_s \mu_B)^2}{\pi \left(\omega_{sf}(T) - i\hbar\omega + \frac{D_s a^2 q^2}{\pi} \right)}, \quad \text{where} \tag{2.37}$$

$$\omega_{sf}(T) = \frac{(g_s \mu_B)^2}{\pi \chi^{+-}_{i}(0, T)} - \frac{J_{\rm ex}(Q) n_{\rm imp}}{\pi}. \tag{2.38}$$

$\omega_{sf}(0) = \omega_K - J_{\rm ex}(Q) n_{\rm imp}/\pi$ is a new energy scale that represents the competition of Kondo and inter-impurity exchange interactions. As $J_{\rm ex}(Q) n_{\rm imp} \to \pi \omega_K$, the uniform, static transverse susceptibility tends to diverge signaling a magnetic phase transition. The condition $J_{\rm ex}(Q) n_{\rm imp}/\omega_K = \pi$ for transition from the Kondo phase to a (antiferro)magnetic phase is the same as the one we found for the double impurity problem.

From Eq (2.26), expanding ψ' for $k_B T \ll \omega_K$, we can get the temperature dependence for the single impurity susceptibility,

$$\chi_i^{-1}(0, T) \simeq \frac{\pi \omega_K}{(g_s \mu_B)^2} \left(1 + \frac{3\pi k_B T}{\omega_K} + \frac{4\pi^2 k_B^2 T^2}{\omega_K^2} \right).$$

The linear dependence of $\chi_i(T)$ on T is an artifact of our mean-field treatment, for it is well known from phenomenological and Bethe ansatz studies of the Kondo model that at low temperatures, $\chi(T)$ has a T^2 correction and not a linear-T correction. Therefore, we use the correct temperature dependence of χ in further calculations.

$$\chi^{+-}_{i}(0, T) = \chi_i(0, T) \simeq \chi_i(0) \left(1 - \frac{C k_B^2 T^2}{\omega_K^2} \right), \tag{2.39}$$

(C is a constant). Together with the frequency dependence of Im χ per impurity from Eq. 2.36 and Eq. 2.37, we have

$$\begin{aligned} \mathrm{Im}\left(\frac{\chi^{+-}(\omega)}{\hbar\omega}\right)_{\omega\to 0} &= \frac{(g_s\mu_B)^2}{\pi N_{\mathrm{imp}}}\sum_q \frac{1}{\left(\omega_{sf}(T)+D_s a^2 q^2\right)^2} \\ &= \frac{(g_s\mu_B)^2}{4\pi^2 D_s \omega_{sf}\left(T\right)}, \end{aligned} \tag{2.40}$$

and the nuclear relaxation rate for $k_BT \ll \omega_K$ comes out to be

$$\frac{1}{T_1} = \frac{A_d^2 k_B T}{4\pi^2 \hbar D_s \omega_{sf}(T)}. \tag{2.41}$$

The temperature dependence of $\omega_{sf}(T)$ is obtained from Eq. 2.38. For $k_BT \ll \omega_K$,

$$\omega_{sf}\left(T\right) \approx \omega_{sf}(0)\left(1+\frac{Ck_B^2T^2}{\omega_K\omega_{sf}(0)}\right). \tag{2.42}$$

This shows the crucial differences between the nuclear relaxation results for the Kondo lattice in Eq. 2.41 and the two-impurity case in Eq. 2.34. First, at the transition $J_{\mathrm{ex}}(Q)n_{\mathrm{imp}}/\omega_K = \pi$, $1/T_1$ for the Kondo lattice is large and finite, while it vanishes for the two-impurity case. Second, as $\omega_{sf}(0) \to 0$, the temperature dependence of the nuclear relaxation rate for the two-impurity system remains linear$-T$, while for the (two-dimensional) Kondo lattice it becomes $1/T$. These differences arise from the existence of long wavelength, low energy magnetic excitations in the lattice even for large $J_{\mathrm{ex}}(Q)$. Further differences between the lattice and a double impurity can be seen in the strong RKKY regime, $J_{\mathrm{ex}}(Q)n_{\mathrm{imp}}/\omega_K > \pi$.

RKKY interaction dominated behaviour: $J_{\mathbf{ex}} \gg \omega_K$

We consider the case when localised spin-spin interactions are dominant and neglect the Kondo interaction in the zeroth order. We are particularly interested in the regime close to a magnetic phase transition. The Hamiltonian describing the system would be

$$H = \sum_{k,\sigma}\xi_k c_{k\sigma}^\dagger c_{k\sigma} + \sum_{\mathbf{q}} J_{\mathrm{ex}}(q)\mathbf{S_q}\cdot\mathbf{S_{-q}} + J\sum_i \boldsymbol{\sigma}_i\cdot\mathbf{S}_i,$$

where J is to be treated now as a perturbation. $J_{\mathrm{ex}}(q)$ represents all exchange processes except indirect exchange (RKKY),

$$J_{\rm RKKY}(\mathbf{q},\omega) = J^2 \int (d^2\mathbf{k}) \frac{n_{\mathbf{k}-\mathbf{q}/2} - n_{\mathbf{k}+\mathbf{q}/2}}{\omega + \epsilon_{\mathbf{k}-\mathbf{q}/2} - \epsilon_{\mathbf{k}+\mathbf{q}/2} + i\delta}.$$

Thus we may write the effective inter-impurity exchange interaction as $J_{\rm ex}(q,\omega) = J_{\rm ex}(q) + J_{\rm RKKY}(q,\omega)$. The spin susceptibility within RPA approximation near the ordering point is

$$\begin{aligned} \chi^{+-}(q,\omega) &= \frac{\chi_i(\omega,T)}{1 - \frac{J_{\rm ex}(\mathbf{q},\omega) n_{\rm imp}}{(g_s\mu_B)^2}\chi_i(\omega,T)}, \\ \chi_i(\omega,T) &= \frac{(g_s\mu_B)^2}{4k_BT}. \end{aligned} \tag{2.43}$$

We re-express Eq. 2.43 introducing the mean-field transition temperature $T_C^{\rm mf}$ (where the denominator of Eq. 2.43 vanishes):

$$\begin{aligned} \chi^{+-}(\mathbf{Q}+\mathbf{q},\omega) &= \frac{(g_s\mu_B)^2}{4k_BT\left(1 - \frac{J_{\rm ex}(\mathbf{q},\omega)}{J_{\rm ex}(\mathbf{Q})}\frac{T_C^{\rm mf}}{T}\right)} \\ &= \frac{(g_s\mu_B)^2}{4k_BT_C^{\rm mf}\left\{\Delta - \left(1 - \frac{J_{\rm ex}(\mathbf{Q}+\mathbf{q})}{J_{\rm ex}(\mathbf{Q})}\right) - i\gamma(\mathbf{Q}+\mathbf{q},\omega)\right\}}, \end{aligned} \tag{2.44}$$

where Q is the wave vector of ordering, $\Delta = \frac{T - T_C^{\rm mf}}{T_C^{\rm mf}}$ and $\gamma(\mathbf{q},\omega)$ is the imaginary part of $\frac{J_{\rm ex}(\mathbf{q},\omega)}{J_{\rm ex}(\mathbf{Q})}$,

$$\begin{aligned} \gamma(\mathbf{q},\omega) &= -\frac{\pi J^2}{J_{\rm ex}(\mathbf{Q})} \int (d^2\mathbf{k}) \left(n_{\mathbf{k}-\mathbf{q}/2} - n_{\mathbf{k}+\mathbf{q}/2}\right) \delta\left(\hbar\omega + \epsilon_{\mathbf{k}-\mathbf{q}/2} - \epsilon_{\mathbf{k}+\mathbf{q}/2}\right) \\ &\simeq \frac{\pi(J\rho)^2\hbar\omega}{4J_{\rm ex}(\mathbf{Q})k_Fq} = \gamma(q)\omega. \end{aligned} \tag{2.45}$$

We now Taylor expand the exchange interaction near its extremum, $J_{\rm ex}(\mathbf{Q}+\mathbf{q}) = J_{\rm ex}(\mathbf{Q})(1 - \alpha^2q^2)$. We have introduced the new parameter α for simplicity; it is related to the Kondo lattice constant a and stiffness D_s introduced in Sec. 2.2.3 through $J_{\mathbf{ex}}(\mathbf{Q})\alpha^2 = (D_s/n_{\mathbf{imp}})a^2$. The expression for the transverse susceptibility then becomes

$$\chi^{+-}(\mathbf{Q}+\mathbf{q},\omega) = \frac{(g_S\mu_B)^2}{4k_BT_C^{\rm mf}\{\Delta + \alpha^2q^2 - i\gamma(\mathbf{Q}+\mathbf{q})\omega\}}. \tag{2.46}$$

Strictly speaking, a magnetic continuous phase transition is not possible in an infinite 2D system at finite temperatures. This needs to be reconciled with the fact that the susceptibility in Eq. 2.46 has a Stoner instability at a finite temperature $T_C^{\rm mf}$. Sufficiently above the mean field transition temperature $T_C^{\rm mf}$, a Curie-Weiss law would be approximately correct. However, close to the Stoner instability ($T = T_C^{\rm mf}$), there are beyond-RPA corrections to Δ. For example, in the context of a 2D itinerant electron ferromagnet, it is known [21] that for $T < T_C^{\rm mf}$, Δ decreases exponentially with temperature ($\Delta \sim e^{-C/T}$), vanishing only at $T = 0$. For a correct treatment, one should identify Δ with α^2/ξ^2, where ξ is the correlation length:

$$\chi^{+-}(\mathbf{Q}+\mathbf{q},\omega) = \frac{(g_S\mu_B)^2}{4k_BT_C^{\rm mf}\{\alpha^2/\xi^2 + \alpha^2q^2 - i\gamma(\mathbf{Q}+\mathbf{q})\omega\}}. \tag{2.47}$$

It follows from Eq. 2.44 and Eq. 2.45 that

$$\mathrm{Im}\left(\frac{\chi^{+-}(\mathbf{Q}+\mathbf{q},\omega)}{\omega}\right)_{\omega\to 0} = \frac{(g_S\mu_B)^2\gamma(\mathbf{Q}+\mathbf{q})}{4k_BT_C^{\rm mf}\alpha^2\left(\xi^{-2}+q^2\right)^2}.$$

We can now estimate the nuclear relaxation rate. For an antiferromagnetic square lattice, the ordering happens at $\mathbf{Q} = (\pi/a, \pi/a)$. Then the relaxation rate at the site of any given impurity is

$$\begin{aligned} T_1^{-1}(T) &\approx \frac{A_d^2\gamma(Q)T}{4N_{\rm imp}\hbar^2T_N^{\rm mf}}\sum_{\mathbf{q}}\frac{J_{\rm ex}^2(Q)}{(D_s/n_{\rm imp})^2a^4\left(\xi^{-2}+q^2\right)^2} \\ &= \frac{A_d^2(J\rho)^2J_{\rm ex}(Q)n_{\rm imp}^2}{64\hbar D_s^2k_FQ}\frac{T}{T_N^{\rm mf}}\frac{\xi(T)^2}{a^2}. \end{aligned} \tag{2.48}$$

The correlation length ξ has the following temperature dependence,

$$\xi(T) \simeq \begin{cases} \min\left(\alpha\sqrt{\frac{T_N^{\rm mf}}{T-T_N^{\rm mf}}}, a\right), & T > T_N^{\rm mf} \\ \max\left(\frac{\hbar v}{2\pi D_s'}\exp(\frac{2\pi D_s'}{k_BT}), L\right), & T < T_N^{\rm mf} \end{cases}, \tag{2.49}$$

where the low temperature behaviour was obtained in Ref. [25]. v is the spin wave speed, and $D_s' \approx 0.2J_{\rm ex}(\mathbf{Q})n_{\rm imp}$ is the exact spin wave stiffness at $T = 0$ for a 2D Heisenberg antiferromagnet. Eq. 2.48 differs from estimates [25] of $1/T_1$ for

Heisenberg antiferromagnets because in our case, the magnon decay is due to the scattering from conduction electrons and not due to magnon-magnon scattering. Likewise for the ferromagnetic case,

$$\begin{aligned} T_1^{-1}(T) &\approx \frac{A_d^2 T}{4N_{\rm imp}\hbar^2 T_C^{\rm mf}} \sum_{\mathbf{q}} \frac{J_{\rm ex}^2(Q)\gamma(q)}{(D_s/n_{\rm imp})^2 a^4 \left(\xi^{-2}+q^2\right)^2}. \\ &= \frac{A_d^2 \pi (J\rho)^2 J_{\rm ex}(Q) n_{\rm imp}}{128\hbar k_F a D_s^2} \frac{T}{T_C^{\rm mf}} \frac{\xi(T)^3}{a^3}. \end{aligned} \tag{2.50}$$

The temperature dependences of the correlation lengths are similar to the antiferromagnetic case,

$$\xi(T) \simeq \begin{cases} \min\left(\alpha\sqrt{\frac{T_C^{\rm mf}}{T-T_C^{\rm mf}}}, a\right), & T > T_C^{\rm mf} \\ \max\left(\sqrt{\frac{D_s'}{k_B T}} a \exp(\frac{2\pi D_s'}{k_B T}), L\right), & T < T_C^{\rm mf} \end{cases}, \tag{2.51}$$

where the low temperature behavior for the antiferromagnet was obtained in Refs. [25, 26], and for the ferromagnet from Refs. [26, 27]. $D_s' \approx 0.18 J_{\rm ex}(\mathbf{Q}) n_{\rm imp}$ is the exact spin wave stiffness at $T = 0$ for a 2D (square lattice) Heisenberg magnet. These results also differ from the usually-encountered 3D Kondo lattice systems [28], because of the qualitative difference in the behavior of $\xi(T)$ at low temperatures.

In presence of inter-impurity exchange interactions, the singular Kondo corrections ($\sim (J\rho)\ln(D/k_B T)$) to the gyromagnetic ratio of the impurity spins are modified to $(J\rho)\ln(D/\sqrt{J_{\rm ex}^2 + k_B^2 T^2})$ [29]. Consequently, the primary effect of Kondo corrections is to decrease the Stoner critical temperature $T_C^{\rm mf}$ as well as the pre-factor in the expressions for the nuclear relaxation rates but the temperature dependence of T_1^{-1} does not change significantly.

2.3 Summary

We calculated the nuclear relaxation rates T_1^{-1} for the Kondo lattice and the few disordered magnetic impurities cases and showed that they have qualitatively different low temperature behaviors: when inter-spin exchange interactions are strong compared to the Kondo energy ω_K, the temperature dependence of T_1^{-1} for the few-impurity system will follow an approximate linear$-T$ law, while for the Kondo lattice T_1^{-1} will show an exponential behaviour $e^{A/T}$ at low temperatures. In contrast, we argued that transport measurements [9] in this case may not provide a convincing

evidence for the formation of crystalline order (Kondo lattice). The exponential temperature dependence is special to two dimensions and indicates stronger spin fluctuations: a power-law behavior is expected in three dimensions on either side of the transition temperature [28]. These results also differ from a 2D Heisenberg magnet because in our case, magnon decay is mediated by conduction electrons. We hope our study will work towards encouraging the use of NMR measurements as an additional handle for studying magnetism and long-range order in low-dimensional conductors.

References

[1] A. C. Hewson, *The Kondo Problem to Heavy Fermions*, Cambridge Univ. Press, Cambridge, (1993).

[2] J. P. Franck, F.D. Manchester, D.L. Martin, *The specific heat of pure copper and of some dilute copper-iron alloys showing a minimum in the electrical resistance at low temperatures* Proc. R. Soc. London, Ser. A **263**, 494 (1961).

[3] P. Gegenwart, Q. Si and F. Steglich, *Quantum criticality in heavy-fermion metals*, Nature Phys. **4**, 186 (2008).

[4] P. Coleman and A. J. Schofield, *Quantum criticality*, Nature **433**, 226 (2005).

[5] H. v. Löhneysen, *Non-Fermi-liquid behavior in a heavy-fermion alloy at a magnetic instability* Phys. Rev. Lett. **72**, 3262 (1994).

[6] A. Schröder, G. Aeppli, R. Coldea, M. Adams, O. Stockert, H. v. Löhneysen, E. Bucher, R. Ramazashvili and P. Coleman *Onset of antiferromagnetism in heavy-fermion metals*, Nature **407**, 351 (2000).

[7] J. Custers, P. Gegenwart, H. Wilhelm, K. Neumaier, Y. Tokiwa, O. Trovarelli, C. Geibel, F. Steglich, C. Ppin and P. Coleman, *The break-up of heavy electrons at a quantum critical point*, Nature **424**, 524 (2003).

[8] N. D. Mathur, F. M. Grosche, S. R. Julian, I. R. Walker, D. M. Freye, R. K. W. Haselwimmer and G. G. Lonzarich, *Magnetically mediated superconductivity in heavy fermion compounds*, Nature **394**, 39 (1998).

[9] C. Siegert, A. Ghosh, M. Pepper, I. Farrer and D, A. Ritchie, *The possibility of an intrinsic spin lattice in high-mobility semiconductor heterostructures*, Nature Phys. **3**, 315 (2007).

[10] M. S. Bello,E. I. Levin, B. I. Shklovskii and A. L. Efros, *Density of localized states in the surface impurity band of a metal-insulator-semiconductor structure*, Sov. Phys. JETP 53, 822829 (1981).

[11] R. Grill and G. H. Döhler, *Effect of charged donor correlation and Wigner liquid formation on the transport properties of a two-dimensional electron gas in modulation $\delta-$doped heterojunctions* Phys. Rev. B **59**, 10769 (1999).

[12] H. Jeong, A. M. Chang, M. R. Melloch, *The Kondo Effect in an Artificial Quantum Dot Molecule*, Science **293**, 2221 (2001).

[13] H. Alloul, P. Mendels, H. Casalta, J. F. Marucco, and J. Arabski, *Correlations between magnetic and superconducting properties of Zn-substituted $YBa_2Cu_3O_{6+x}$*, Phys. Rev. Lett. **67**, 31403143 (1991).

[14] Y. Kohori, K. Asayama, T. Kohara, N. Sato, H. Yashima, H. Mori, T. Satoh *^{29}Si NMR study of the dense Kondo system Ce-Si*, Journal of Magnetism and Magnetic Materials, **52**, 349 (1985).

[15] D. C. Dixon *et al.*, Phys. Rev. B **56**, 4743 (1997); T. Machida *et al.*, Phys. Rev. B **65**, 233304 (2002); V. Tripathi *et al.*, Europhys. Lett. **81**, 68001 (2008).

[16] A. Narath, *Relaxation of Local-moment Nuclei in Metals*, Physica Scripta. Vol. 11, 237-243, 1975.

[17] V. Tripathi and N. R. Cooper, *Nuclear magnetic resonance probes for the Kondo scenario for the 0.7 feature in semiconductor quantum point contact devices* , J. Phys. Cond. Mat. **20**, 164215 (2008).

[18] K. Dhochak, V. Tripathi, *Kondo Lattice scenarios in Disordered Semiconductor Heterostructures* Phys. Rev. Lett. **103**, 067203 (2009).

[19] D. C. Mattis, *The Theory of Magnetism*, Harper & Row, New York(1965).

[20] G. G. Khaliullin, *Spin fluctuations and heavy fermions in the Kondo lattice*, JETP **79** (3), 1994.

[21] M. Hatatani and T. Moriya, *Ferromagnetic Spin Fluctuations in Two-Dimensional Metals*, J. Phys. Soc. Jpn. **64**, 3434 (1995).

[22] B. A. Jones, C. M. Varma and J. W. Wilkins, *Low-Temperature Properties of the Two-Impurity Kondo Hamiltonian*, Phys. Rev. Lett. **61**, 125 (1988); C.

Jayaprakash H. R. Krishnamurthy and J. W. Wilkins, *Two-Impurity Kondo Problem*, Phys. Rev. Lett. **47**, 737 (1981).

[23] E. Miranda *et al.*, Phys. Rev Lett. **78**, 290 (1997).

[24] R. Bhatt and D. Fisher, Phys. Rev. Lett. **68**, 3072 (1992).

[25] S. Chakravarty, B. I. Halperin and D. R. Nelson, *Two-dimensional quantum Heisenberg antiferromagnet at low temperatures*, Phys. Rev. B **39**, 2344 (1989).

[26] D. Arovas and A. Auerbach, *Functional integral theories of low-dimensional quantum Heisenberg models*, Phys. Rev. B **38**, 316 (1988).

[27] M. Takahashi, *Comment on Finite 2D Quantum Heisenberg Ferromagnet*, Prog. Theor. Phys. **83**, 815 (1989).

[28] T. Moriya, *Nuclear Magnetic Relaxation near the Curie Temperature*, Prog. Theor. Phys. **28**, 371 (1962).

[29] Y. C. Tsay and M. W. Klein, *Theory of the Two-Impurity Kondo Effect in the Presence of an Impurity-Impurity Exchange Interaction*, Phys. Rev. B **7**, 352 (1973).

Chapter 3

Magnetic impurities in the honeycomb Kitaev model

3.1 Introduction

Impurity effects are an essential part of our understanding of strongly correlated electron systems, both as probes for the underlying electronic state as well as due to the numerous nontrivial effects they have on the properties of the system [1]. Recently many studies have explored impurity effects as probes for the putative quantum spin liquid state in underdoped cuprate superconductors [2] and geometrically frustrated magnets [3]. The $S = 1/2$ honeycomb lattice Kitaev model [4] provides a very appealing system to study in this context as the model is integrable via several schemes of spin-fractionalization into fermions [4, 5, 6] and exhibits both gapless and gapped quantum spin liquid phases. The Kitaev model has been studied in various contexts ranging from the possibility of quantum computation with the anyons [4, 7] that the model predicts, understanding dynamics of quantum quenches in a critical region [8] to fractional charge excitations in topological insulators [9].

We study the behavior of spin-S impurities in the gapless spin liquid regime of the Kitaev model on the honeycomb lattice. The impurity coupling K scales away from an unstable fixed point $K_c \sim J/S$ irrespective of the sign of impurity coupling, similar to impurity problems in pseudogapped bosonic spin liquids [17]. The Kitaev model magnetic impurity problem is nevertheless qualitatively different for two important reasons. First, the unstable fixed point separates topologically distinct sectors in the Kitaev model, with the strong coupling sector associated with non-abelian anyons. Second, the gapless spinons in the Kitaev spin liquid mediate a

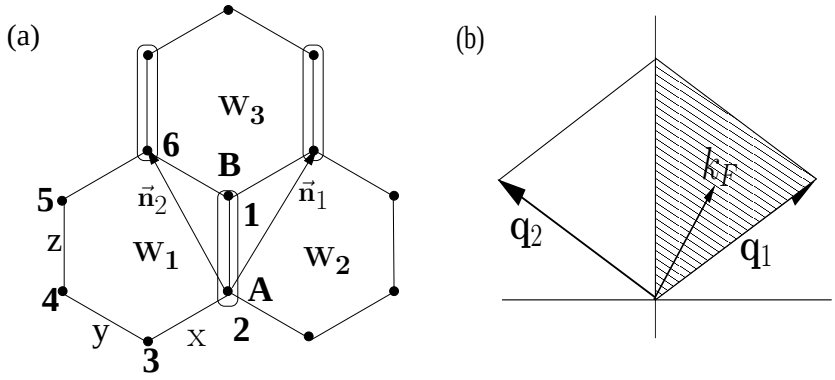

Figure 3.1: (a) Schematic of the Kitaev lattice showing the A and B sites and the x, y and z types of bonds. (b) Figure showing the reciprocal lattice vectors for the A sublattice. The Dirac point for the massless Majorana fermions is denoted by k_F and momentum summations are over the (shaded) half Brillouin zone.

non-dipolar RKKY interaction proportional to $S^2_{i\alpha}S^2_{j\beta}/R^3_{ij}$ between distant magnetic impurities provided that (a) each impurity couples to more than one lattice site on the host and (b) the impurity spin $S \neq 1/2$. The absence of long-range interaction for $S = 1/2$ impurities could give a way for local manipulation of the Kitaev system.

3.1.1 Kitaev model

The $S = 1/2$ Kitaev model [4] is a honeycomb lattice of spins with nearest neighbour interactions with a strong direction dependence. The Hamiltonian for the Kitaev model is,

$$H_0 = -J_x \sum_{x\text{-links}} \sigma^x_j \sigma^x_k - J_y \sum_{y\text{-links}} \sigma^y_j \sigma^y_k - J_z \sum_{z\text{-links}} \sigma^z_j \sigma^z_k, \tag{3.1}$$

where the three bonds at each site are labeled as x, y and z links. The model can be solved [4] by representing the spins in terms of Majorana fermions c, b^x, b^y, b^z as $\sigma^\alpha_i = ib^\alpha_i c_i$ and using the fact that there are macroscopic number of conserved quantities for the model. As was shown in ref. [4], the flux operators $W_p = \sigma^x_1\sigma^y_2\sigma^z_3\sigma^x_4\sigma^y_5\sigma^z_6$ defined for each elementary plaquette p are conserved (see Fig.3.1), with eigenvalues ± 1, and form a set of commuting observables which divides the Hilbert space into distinct sectors. Along with the flux operators, on each $\alpha-$type bond, $u^\alpha_{ij} = ib^\alpha_i b^\alpha_j$ is also conserved and these u_{ij}'s commute with each other. The representation in terms of Majorana fermions b^x_i, b^y_i, b^z_i, c_i spans a larger Fock space, and we restrict to the physical Hilbert space of the spins by choosing the gauge condition $D_i = ib^x_i b^y_i b^z_i c_i = 1$ such that $\sigma^x\sigma^y\sigma^z = i$.

Using these conserved quantities, the Hamiltonian becomes a problem of free hopping Majorana fermions on honeycomb lattice.

$$H_0 = \frac{i}{4}\sum_{jk} A_{jk} c_j c_k, \tag{3.2}$$

where

$$A_{jk} = \begin{cases} 2J_{\alpha_{jk}} u_{jk} & \text{if } j,k \text{ are neighbouring sites on an } \alpha\text{-bond,} \\ 0 & \text{otherwise.} \end{cases}$$

Also, the flux operators can be expressed as product of u_{ij} over the bonds of the plaquette. Ground state of the Kitaev model lies in the vortex free sector with all $W_p = 1$. The gauge invariant ($D = 1$) state of the system only depends on the configuration of W_p's and we can therefore fix all $u_{ij} = 1$ for studying the ground state properties. The physical state corresponding to the $u_{ij} = 1$ state is the appropriately gauge projected state $|\psi_p\rangle$ such that $D_i|\psi_p\rangle = |\psi_p\rangle$:

$$|\psi_p\rangle = \Pi_a \left(\frac{1+D_a}{2}\right) |\{u_{ij=1}\}\rangle \tag{3.3}$$

The model has two types of quasi-particle excitations: free dispersing fermions and Z_2 vortices. The excited state manifolds with finite vorticity are separated from the ground state manifolds by a gap of order J_α.

Defining the Bravais lattice with two point basis (Fig.3.1), the Hamiltonian is translationally invariant and can be diagonalized in momentum space,

$$H_0 = \frac{i}{4}\sum_{\mathbf{q}>0,\alpha} \epsilon_\alpha(\mathbf{q}) a^\dagger_{\mathbf{q},\alpha} a_{\mathbf{q},\alpha}, \tag{3.4}$$

with $\epsilon_\alpha(\mathbf{q}) = \pm|f(\mathbf{q})|$, $f(\mathbf{q}) = 2(J_x e^{ia\mathbf{q}\cdot\mathbf{n_1}} + J_y e^{ia\mathbf{q}\cdot\mathbf{n_2}} + J_z)$ and the eigen-basis,

$$\begin{aligned} a_{\mathbf{q},0} &= \tilde{c}_{\mathbf{q},A} + \tilde{c}_{\mathbf{q},B} e^{-i\tilde{\alpha}(\mathbf{q})}, \\ a_{\mathbf{q},1} &= \tilde{c}_{\mathbf{q},A} - \tilde{c}_{\mathbf{q},B} e^{-i\tilde{\alpha}(\mathbf{q})}. \end{aligned} \tag{3.5}$$

Here A/B is the site label for the two types of sites in Kitaev model, $\tilde{\alpha}(\mathbf{q})$ is the phase of $f(\mathbf{q})$ and $\tilde{c}_\mathbf{q}$ represents the Fourier transform of c_i. The lattice constant is a. As we see in Eq. 3.4, the sum over momenta is only over half of first Brillouin zone as c_i's are real fermions. The above Hamiltonian has gapless excitation for a

region of parameter space where J's satisfy the triangle inequalities $|J_x|+|J_y| \geq |J_z|$ etc. and a gapped spectrum outside this parameter regime. The gapless phase has point Fermi surface where $\epsilon(\mathbf{k}_F) = 0$ and $\epsilon(\mathbf{q})$ has linear dispersion around $\mathbf{k}_F$ (Fig.3.1). The position of the Fermi point in the Brillouin zone depends on the relative values of J_x, J_y and J_z. For simplicity, and without loss of generality, we will assume $J_x = J_y = J_z = J$ for further analysis.

The Kitaev model ground state is a quantum spin liquid with only nearest neighbor spin-spin correlations. On an $\alpha-$bond, only $\langle \sigma_i^\alpha \sigma_j^\alpha \rangle$ is non zero and other two spin correlations are zero. Four spin bond-bond correlations are long ranged with power law decay in the gapless phase of the Kitaev model.

In the gapless phase, the vortex excitations have non-abelian statistics if the gapless fermionic excitations are gapped by applying magnetic field. In the non-abelian phase, the states are topologically protected and thus could be useful for quantum computation. Although such anisotropic interactions are difficult to form in solid state systems, there have been proposals of possible formation of Kitaev model in systems with strong spin-orbit interactions [10] which could lead to anisotropic interactions. Sodium/Lithium Irridate (A_2IrO_3) in which Ir atoms form hexagonal lattice and have strong spin orbit coupling were proposed to have Kitaev like spin interactions but there is a significant Heisenberg coupling also in these materials along with Kitaev interactions. Various other methods of creating a Kitaev model in optical lattices [11], Josephson junction circuits [12] etc. have also been proposed.

3.2 Kondo effect in Kitaev model

Now we couple a spin S Kondo impurity to a Kitaev spin at an A site ($\mathbf{r} = 0$) by an exchange interaction:

$$\begin{aligned} V_K =& i\sum_\alpha K^\alpha S^\alpha b^\alpha c_A = i \sum_{\mathbf{q}\in HBZ,\alpha} \frac{K^\alpha}{\sqrt{2N}} S^\alpha b^\alpha (\tilde{c}_{\mathbf{q},A} + \tilde{c}^\dagger_{\mathbf{q},A}) \\ \equiv& \frac{1}{\sqrt{N}} \sum_{\mathbf{q}\in HBZ,\alpha,\beta} Q^\alpha S^\alpha b^\alpha (a_{\mathbf{q},\beta} + a^\dagger_{\mathbf{q},\beta}). \end{aligned} \tag{3.6}$$

The index HBZ is to remind us that the momenta $\mathbf{q}$ are summed over half of the first Brillouin zone (see Fig. 3.1).

We now do a poor man's scaling analysis for the Kondo coupling K. The idea of the Poor Man scaling [13, 14] process is as following. To study the system properties

at low temperatures, we compute the effective Hamiltonian in a reduced bandwidth for the fermionic excitations ($-D+\delta D$ to $D-\delta D$) by integrating out the excitations in the band edges (($-D$ to $-D+\delta D$) and (D to $D-\delta D$)). We perform this process successively to get a scaling law for the coupling constants in the Hamiltonian. To do the analysis for our problem, we consider the Lippmann-Schwinger expansion for the $T-$matrix element $\langle\Omega, b^\beta|K^\beta S^\beta b^\beta c_{a,A}|\Omega+(\mathbf{q},\alpha)\rangle$. We make a perturbation expansion $T = T^{(1)} + T^{(2)} + \cdots$ in increasing powers of K and follow its variation as a function of the decrease of the bandwidth $(-D, D)$. The first correction to the bare $T-$matrix comes from two *third* order terms (see Fig. 3.2). The contribution from on-site scattering (Fig.3.2a) is

$$T^{(3),a} = \langle\Omega, b^\beta|V_K G_0^+(E) V_K G_0^+(E) V_K|\Omega+(\mathbf{q},\alpha)\rangle$$

$$= \frac{Q^\beta S^\beta}{N} \sum_{(D-\delta D)\le|\epsilon_{q'}|,|\epsilon_{q''}|\le D,\tilde\alpha,\tilde\beta,\tilde\alpha'} (Q^{\tilde\beta})^2 (S^{\tilde\beta})^2 \langle b^\beta|\, b^\dagger_\beta (a_{\mathbf{q}'',\tilde\alpha'} + a^\dagger_{\mathbf{q}'',\tilde\alpha'})\, G_0^+(\epsilon)\, b_{\tilde\beta}$$
$$\times (a_{\mathbf{q}',\tilde\alpha} + a^\dagger_{\mathbf{q}',\tilde\alpha})\, G_0^+(\epsilon)\, b^\dagger_{\tilde\beta} c_{\mathbf{q},\alpha}|(\mathbf{q},\alpha)\rangle$$

$$= -\frac{Q^\beta S^\beta}{N} \sum_{\mathbf{q}',\tilde\beta} (Q^{\tilde\beta})^2 (S^{\tilde\beta})^2 \left\langle a^\dagger_{\mathbf{q}',1} a_{\mathbf{q}',1} \frac{1}{E-(H_0-\epsilon_{q',1})} + a_{\mathbf{q}',0} a^\dagger_{\mathbf{q}',0} \frac{1}{E-(H_0+\epsilon_{q',0})} \right\rangle \frac{1}{E-\epsilon_b}$$

$$\simeq -2Q^\beta S^\beta \frac{\rho(D) a^2 |\delta D|}{E-D} \cdot \frac{1}{E-J} \sum_{\tilde\beta} (Q^{\tilde\beta})^2 (S^{\tilde\beta})^2. \tag{3.7}$$

Here $\rho(D)$ is the density of states at the band edge, a is the lattice constant and $G_0(E) = (E - H_0 + i\delta)^{-1}$.

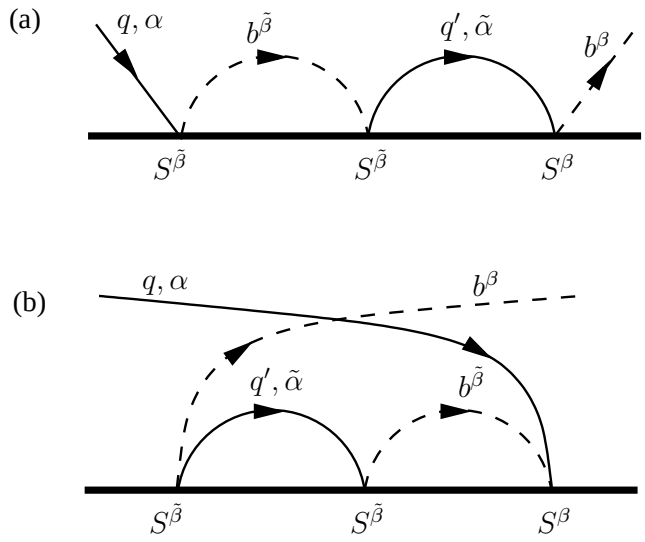

Figure 3.2: Diagrams contributing to the scaling of Kondo coupling K^{α} when the impurity couples to a single Kitaev spin.

Similarly, the contribution from Fig. 3.2(b) is

$$T^{(3),b} = \frac{Q^{\beta}S^{\beta}}{N} \sum_{(D-\delta D)\leq|\epsilon_{q'}|,|\epsilon_{q''}|\leq D,\tilde{\alpha},\tilde{\beta},\tilde{\alpha}'} (Q^{\tilde{\beta}})^2 (S^{\tilde{\beta}})^2 \, \langle \Omega, b^{\beta}| \, b_{\tilde{\beta}} c_{\mathbf{q},\alpha} b^{\dagger}_{\beta} c^{\dagger}_{\mathbf{q},\alpha}$$
$$\times \frac{1}{E-(H_0+\epsilon_b+\epsilon_{q,0})} \, b^{\dagger}_{\tilde{\beta}} (a_{\mathbf{q}'',\tilde{\alpha}'} + a^{\dagger}_{\mathbf{q}'',\tilde{\alpha}'}) \frac{1}{E-(H_0+\epsilon_b+\epsilon_{q,0})} \, (-a_{\mathbf{q}',\tilde{\alpha}} - a^{\dagger}_{\mathbf{q}',\tilde{\alpha}})|\Omega\rangle$$

$$= -\frac{Q^{\beta}S^{\beta}}{N} \sum_{\mathbf{q}',\tilde{\beta}} (Q^{\tilde{\beta}})^2 (S^{\tilde{\beta}})^2 \, \frac{1}{E-2\epsilon_b}$$
$$\times \left\langle a^{\dagger}_{\mathbf{q}',1} a_{\mathbf{q}',1} \frac{1}{E-(-\epsilon_{q',1}+\epsilon_b+\epsilon_{q,0})} + a_{\mathbf{q}',0} a^{\dagger}_{\mathbf{q}',0} \frac{1}{E-(\epsilon_{q',0}+\epsilon_b+\epsilon_{q,0})} \right\rangle$$

$$\simeq -2Q^{\beta}S^{\beta} \, \frac{\rho(D)a^2|\delta D|}{E-D-J} \cdot \frac{1}{E-2J} \sum_{\tilde{\beta}} (Q^{\tilde{\beta}})^2 (S^{\tilde{\beta}})^2. \tag{3.8}$$

Adding the two contributions (taking $E \simeq 0$),

$$T^{(3)} \simeq 2Q^{\beta}S^{\beta}\rho(D) \frac{a^2\delta D}{\epsilon_b} \sum_{\tilde{\beta}} (Q^{\tilde{\beta}})^2 (S^{\tilde{\beta}})^2 \left\{ \frac{1}{D} + \frac{1}{2(D+J)} \right\}. \tag{3.9}$$

Here we have taken $E, \epsilon_{q,\alpha} \ll D$, J and neglected them.

If either the impurity is a $S = \frac{1}{2}$ spin, or the Kondo interaction is rotationally symmetric, the above contribution renormalizes the Kondo coupling constant. However for $S \neq \frac{1}{2}$ with anisotropic coupling, new terms are generated and one needs to go to higher order diagrams to obtain the scaling of these new coupling terms. For $S = 1/2$ or for symmetric impurity coupling we thus have

$$\delta K \sim -2K^3 S(S+1)\rho(D)a^2 \frac{\delta D}{J}\left\{\frac{1}{D} + \frac{1}{2(D+J)}\right\}. \tag{3.10}$$

Just as for the Kondo effect in graphene[15], owing to the change in the density of states with bandwidth (here $\rho(\epsilon) = (1/2\pi v_F^2)|\epsilon| \equiv C|\epsilon|$), we also need to consider the change in K due to the rescaling done in order to keep the total number of states fixed. This gives a contribution $K \to K(D'/D)^r, \quad (D' = D - |\delta D|)$. In addition, as we shall scale the bandwidth D to smaller values, the second term in braces in Eq. 3.10 may be dropped. Thus

$$\begin{aligned}\delta K &\simeq -2K^3 S(S+1)\rho(D)a^2 \frac{\delta D}{DJ} + K\frac{\delta D}{D} \\ &= -K\frac{\delta D}{D}\left(2K^2 a^2 CDS(S+1)/J - 1\right).\end{aligned} \tag{3.11}$$

Thus, as we decrease the bandwidth by integrating out the high energy excitations, the effective coupling K has an unstable fixed point at $K_c = \sqrt{J/[2a^2\rho(D)S(S+1)]}$; or in other words, $K_c \sim \sqrt{J/S^2a^2CD} \sim J/S$. Here we used $D \lesssim J$ and $C \sim 1/(Ja)^2$. Clearly for $K > K_c$, the coupling flows to infinity independent of the nature of coupling (ferromagnetic or antiferromagnetic), while for $K < K_c$, the coupling flows to zero. For anisotropic Kondo coupling we can show

$$\delta K_{z,\pm} \sim -K_{z,\pm}\frac{\delta D}{D}\left[2a^2\rho(D)S(S+1)\frac{K_z^2 + K_+K_-}{J} - 1\right]. \tag{3.12}$$

The two-parameter Kondo flow is therefore given by

$$\frac{\delta K_z}{\delta K_\pm} = \frac{K_z}{K_\pm} \Rightarrow \frac{K_z}{K_\pm} = \text{const.} \tag{3.13}$$

A comparison of Kondo effect and RKKY interaction in graphene [15, 16], a bosonic spin bath [17] and the Kitaev model are shown in Table 3.1.

Similarly we can analyze the flow of the Kondo coupling constant when the impurity spin is at the centre of a Kitaev lattice hexagon. The spin couples to the

	Graphene	Z_2 bosonic spin bath with pseudogap density of states $\rho(\epsilon) = C\|\epsilon\|$.	Kitaev, honeycomb lattice
Kondo scaling	Unstable intermediate coupling fixed pt. only for AFM coupling. Only AFM flows to strong coupling above unstable fixed pt.	Flow direction is independent of the sign of magnetic impurity coupling. Unstable intermediate coupling fixed pt. for both FM and AFM.	Scaling same as Z_2 bosonic spin bath case. However a topological transition is associated with the unstable fixed point.
RKKY	$S_{i\alpha}S_{j\alpha}/R_{ij}^3$	$S_{i\alpha}S_{j\alpha}/R_{ij}^3$	$S_{i\alpha}^2 S_{j\beta}^2/R_{ij}^3$

Table 3.1: Comparison of Kondo effect and RKKY interaction in graphene, a Z_2 bosonic spin bath with a pseudogap density of states and the Kitaev model on the honeycomb lattice.

Kitaev spins at the vertices of hexagon as

$$V_K = i \sum_{j\in\text{hexagon},\alpha} K_j^\alpha S^\alpha b_j^\alpha c_j = \sum_{\mathbf{q}\in HBZ,j,\alpha} \frac{iK_j^\alpha S^\alpha b_j^\alpha}{\sqrt{2N}} (\mathrm{e}^{i\mathbf{q}\cdot\mathbf{r}_j}\tilde{c}_{\mathbf{q},\lambda_j} + \mathrm{e}^{-i\mathbf{q}\cdot\mathbf{r}_j}\tilde{c}^\dagger_{\mathbf{q},\lambda_j})$$

$$= \frac{1}{\sqrt{N}} \sum_{\alpha,j,\mathbf{q}\in HBZ} Q_j^\alpha\, S^\alpha\, b_j^\alpha \Big\{ \mathrm{e}^{i\lambda_j\tilde{\alpha}(\mathbf{q})}\mathrm{e}^{i\mathbf{q}\cdot\mathbf{r}_j}(a_{\mathbf{q},0} + (-1)^{\lambda_j} a_{\mathbf{q},1}) + \mathrm{e}^{-i\lambda_j\tilde{\alpha}(\mathbf{q})}\mathrm{e}^{-i\mathbf{q}\cdot\mathbf{r}_j}(a^\dagger_{\mathbf{q},0} + (-1)^{\lambda_j} a^\dagger_{\mathbf{q},1}) \Big\}. \tag{3.14}$$

$\lambda_j = 0$ or 1 specifies the sublattice A or B to which j belongs.

We look at the scaling of scattering term of the type $Q_i^\alpha S^\alpha b_i^\alpha c_{\mathbf{q},0}\mathrm{e}^{i\mathbf{q}\cdot\mathbf{r}_i}$. Two of the terms contributing to this matrix element are same as the terms calculated above for the case of an impurity at the site of Kitaev lattice. These give

$$T_{1i}^{(3)} \simeq 2Q_i^\beta S^\beta \mathrm{e}^{i\mathbf{q}\cdot\mathbf{r}_i} \sum_{\tilde{\beta}} (Q_i^{\tilde{\beta}})^2 (S^{\tilde{\beta}})^2 \rho(D) a^2 \frac{\delta D}{JD}.$$

The new terms contributing to the matrix element are those coming from Fig. 3.3. The contribution from the top diagram in Fig. 3.3 is

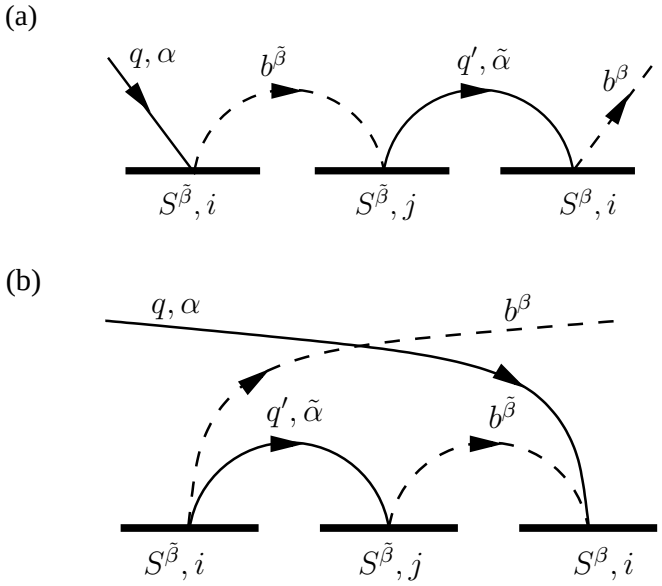

Figure 3.3: Third order contributions to the $T-$matrix arising from site off-diagonal scattering.

$$
\begin{aligned}
T_{2a}^{(3)} = \frac{Q^{\beta}S^{\beta}\mathrm{e}^{i\mathbf{q}\cdot\mathbf{r}_i}}{N}\sum_{\mathbf{q}',\tilde{\beta},j}(Q^{\tilde{\beta}})^2(S^{\tilde{\beta}})^2(Q^{\tilde{\beta}})^2(S^{\tilde{\beta}})^2\langle\Omega,b^{\beta}|\, b^{\dagger}_{\beta,i,\mathrm{A}} \\
\times\left(\mathrm{e}^{i\mathbf{q}'\cdot\mathbf{r}_i}(a_{\mathbf{q}',0}+a_{\mathbf{q}',1})+\mathrm{e}^{-i\mathbf{q}'\cdot\mathbf{r}_i}(a^{\dagger}_{\mathbf{q}',0}+a^{\dagger}_{\mathbf{q}',1})\right)\, G_0^{+}(\epsilon)\; b_{\tilde{\beta},j,\mathrm{B}} \\
\times\left(\mathrm{e}^{i\tilde{\alpha}(\mathbf{q}')}\mathrm{e}^{i\mathbf{q}'\cdot\mathbf{r}_j}(a_{\mathbf{q}',0}-a_{\mathbf{q}',1})+\mathrm{e}^{-i\tilde{\alpha}(\mathbf{q}')}\mathrm{e}^{-i\mathbf{q}'\cdot\mathbf{r}_j}(a^{\dagger}_{\mathbf{q}',0}-a^{\dagger}_{\mathbf{q}',1})\right) \\
\times\; G_0^{+}(\epsilon)\, b^{\dagger}_{\tilde{\beta},i,\mathrm{A}}c_{\mathbf{q},\alpha}\mathrm{e}^{i\mathbf{q}\cdot\mathbf{r}_i}|\Omega+(\mathbf{q},\alpha)\rangle
\end{aligned}
$$

$$
\begin{aligned}
= -\frac{Q^{\beta}S^{\beta}\mathrm{e}^{i\mathbf{q}\cdot\mathbf{r}_i}}{N}\,\frac{1}{E-\epsilon_b}\sum_{\mathbf{q}',\tilde{\beta},j}(Q^{\tilde{\beta}})^2(S^{\tilde{\beta}})^2\left\langle\mathrm{e}^{-i\mathbf{q}'\cdot(\mathbf{r}_i-\mathbf{r}_j)}\mathrm{e}^{i\tilde{\alpha}(\mathbf{q}')}a^{\dagger}_{\mathbf{q}',1}a_{\mathbf{q}',1}\right. \\
\left.\frac{1}{E-(H_0-\epsilon_{q',1})}-\mathrm{e}^{i\mathbf{q}'\cdot(\mathbf{r}_i-\mathbf{r}_j)}\mathrm{e}^{-i\tilde{\alpha}(\mathbf{q}')}a_{\mathbf{q}',0}a^{\dagger}_{\mathbf{q}',0}\frac{1}{E-(H_0+\epsilon_{q',0})}\right\rangle
\end{aligned}
$$

$$
\begin{aligned}
= -Q^{\beta}S^{\beta}\mathrm{e}^{i\mathbf{q}\cdot\mathbf{r}_i}\,\frac{1}{E-\epsilon_b}\sum_{\tilde{\beta},q',j}(Q^{\tilde{\beta}})^2(S^{\tilde{\beta}})^2 \\
\left\langle\mathrm{e}^{-i\mathbf{q}'\cdot(\mathbf{r}_i-\mathbf{r}_j)}\mathrm{e}^{i\tilde{\alpha}(\mathbf{q}')}a^{\dagger}_{\mathbf{q}',1}a_{\mathbf{q}',1}\,\frac{1}{E-|f(\mathbf{q}')|}-\mathrm{e}^{i\mathbf{q}'\cdot(\mathbf{r}_i-\mathbf{r}_j)}\mathrm{e}^{-i\tilde{\alpha}(\mathbf{q}')}a_{\mathbf{q}',0}a^{\dagger}_{\mathbf{q}',0}\,\frac{1}{E-|f(\mathbf{q}')|}\right\rangle
\end{aligned}
$$

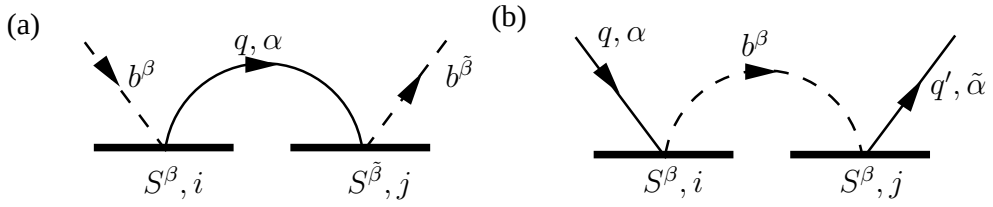

Figure 3.4: New vertices generated from site off-diagonal scattering.

Thus,

$$T_{2a}^{(3)} = 2iQ_i^\beta S^\beta \mathrm{e}^{i\mathbf{q}\cdot\mathbf{r}_i} \frac{1}{E-J}\frac{1}{E-D} \sum_{\mathbf{q}'\in HBZ,\tilde\beta,j} Q_i^{\tilde\beta} Q_j^{\tilde\beta} (S^{\tilde\beta})^2 \sin(\mathbf{q}'\cdot(\mathbf{r}_i-\mathbf{r}_j)-\tilde\alpha(\mathbf{q}')).$$

Similarly calculating the contribution from the bottom diagram in Fig. 3.3,

$$T_{2b}^{(3)} = 2iQ_i^\beta S^\beta \mathrm{e}^{i\mathbf{q}\cdot\mathbf{r}_i} \frac{1}{E-2J}\frac{1}{E-J-D} \sum_{\mathbf{q}'\in HBZ,\tilde\beta,j} Q_i^{\tilde\beta} Q_j^{\tilde\beta} (S_{\tilde\beta})^2 \sin(\mathbf{q}'\cdot(\mathbf{r}_i-\mathbf{r}_j)-\tilde\alpha(\mathbf{q}')).$$

Adding all the contributions,

$$\begin{aligned} T_i^{(3)} = & -2Q_i^\beta S^\beta e^{i\mathbf{q}\cdot\mathbf{r}_i}\rho(D)a^2\frac{|\delta D|}{JD}\sum_{\tilde\beta}(S^{\tilde\beta})^2 \\ & \times\left((Q_i^{\tilde\beta})^2 - i\sum_{\mathbf{q}'=D/v_F,j\in i} Q_i^{\tilde\beta}Q_j^{\tilde\beta}\sin(\mathbf{q}'\cdot(\mathbf{r}_i-\mathbf{r}_j)-\tilde\alpha(\mathbf{q}'))\right). \end{aligned} \tag{3.15}$$

There are also new terms of second order in K that are generated. These terms are as shown in figures (3.4). The term corresponding to figure (3.4a) is $\sim K^\beta K^{\tilde\beta} S^\beta S^{\tilde\beta} b_i^\beta b_j^{\tilde\beta}$. When projected to the vortex free ground state, it becomes $\sim (K^\beta)^2 (S^\beta)^2$ generating anisotropic potential for the impurity spin. The second term (3.4b) is $\sim (K^\beta)^2\,(S^\beta)^2 c_i c_j/J$ which contributes to the long range interaction between impurity spins.

3.2.1 Stability of strong coupling point

Our poor Man's scaling analysis is only valid for small Kondo couplings as the perturbation theory breaks down much before the critical value of the coupling. Our analysis shows that the coupling flows to larger values for coupling above the critical coupling K_c. we can not predict whether it flows to ∞ or whether there is some other fixed point beyond K_c. To have an idea of the stability of the strong coupling fixed point, we study the model close to this point and see if it is a stable fixed point.

In the strong coupling limit, K is the largest energy scale and the impurity spins forms a singlet/triplet with the Kitaev spin at origin. We analyze whether this composite decouples from the rest of the Kitaev model and we are left with a Kitaev model with one spin missing or does it couple strongly to the rest of the Kitaev model.

We consider the Hamiltonian such that the Kondo term and the Kitaev model with one spin missing (H_{K-}) form the unperturbed Hamiltonian and Kitaev coupling to the site at origin is the perturbation.

$$H_0 = K\mathbf{S}\cdot\sigma_0 + H_{K-} \tag{3.16}$$

$$V = J(\sigma_0^x\sigma_1^x + \sigma_0^y\sigma_2^y + \sigma_0^z\sigma_3^z) \tag{3.17}$$

For antiferromagnetic Kondo coupling ($K > 0$), the ground state consists of a Kondo singlet of S and σ_0 and the Kitaev model with one spin missing. The perturbation term causes transitions from singlet to triplet states of the Kondo singlet. We use effective Hamiltonian scheme [18] to include the effects of the perturbation terms within the projected ground state subspace.

$$H_{\text{eff}} = \mathrm{e}^{iQ}H\mathrm{e}^{-iQ}, \tag{3.18}$$

where Q is chosen such that the terms which take us out of the reduced Hilbert space are canceled order by order. This gives the reduced Hamiltonian as

$$H_{\text{eff}} = H_0 + H_1 + H_2 + O(V^3), \tag{3.19}$$

$$\langle\alpha|H_1|\beta\rangle = \langle\alpha|V|\beta\rangle, \tag{3.20}$$

$$\langle\alpha|H_2|\beta\rangle = \frac{1}{2}\sum_{\gamma\neq\alpha,\beta}\langle\alpha|V|\gamma\rangle\langle\gamma|V|\beta\rangle\left(\frac{1}{E_\alpha - E_\gamma} + \frac{1}{E_\beta - E_\gamma}\right), \tag{3.21}$$

where α, β belong to the ground state manifold and γ belongs to excited state man-

ifold. The eigenstates of the Kondo term are singlet $|s\rangle$ and triplet states $|t,(0,\pm1)\rangle$

$$|s\rangle = \frac{1}{\sqrt{2}}\left(|\uparrow,\Downarrow\rangle - |\downarrow,\Uparrow\rangle\right) \tag{3.22}$$

$$|t,1\rangle = |\uparrow,\Uparrow\rangle \tag{3.23}$$

$$|t,0\rangle = \frac{1}{\sqrt{2}}\left(|\uparrow,\Downarrow\rangle + |\downarrow,\Uparrow\rangle\right) \tag{3.24}$$

$$|t,-1\rangle = |\downarrow,\Downarrow\rangle \tag{3.25}$$

Here $\uparrow$ refers to the Kitaev spin and $\Uparrow$ refers to the impurity spin state.

Anti-ferromagnetic coupling

For the antiferromagnetic Kondo coupling case, ground state is the singlet state. As $\langle s|V|s\rangle = 0$, $H_1 = 0$ and

$$\langle s,K_-|H_2|s,K'_-\rangle = \frac{1}{2}\sum_{t,K''_-}\langle s,K_-|V|t,K''_-\rangle\langle t,K''_-|V|s,K'_-\rangle\left(\frac{1}{E_0-E_t}+\frac{1}{E'_0-E_t}\right), \tag{3.26}$$

Here, K_- denotes the eigenstates of the Kitaev model with the spin at origin missing. Since change in energy of the Kitaev state is $\sim J \ll K$, we ignore their contribution in the energy denominators of the perturbation term. Then H_2 becomes

$$\begin{aligned}
\langle s,K_-|H_2|s,K'_-\rangle &\simeq \frac{J^2}{E_0-E_t}\sum_{t,K''_-,\alpha,\beta}\langle s|\sigma_0^\alpha|t\rangle\langle t|\sigma_0^\beta|s\rangle\langle K_-|\sigma_\alpha^\alpha|K''_-\rangle\langle K''_-|\sigma_\beta^\beta|K'_-\rangle \\
&\simeq -\frac{J^2}{K}\sum_{\alpha,\beta}\langle s|\sigma_0^\alpha(\mathbf{1}-|s\rangle\langle s|)\sigma_0^\beta|s\rangle\langle K_-|\sigma_\alpha^\alpha\sigma_\beta^\beta|K'_-\rangle \\
&= -\frac{3J^2}{K}\sum_{\alpha,\beta}\langle K_-|\sigma_\alpha^\alpha\sigma_\beta^\beta|K'_-\rangle
\end{aligned}$$

$$H_2 \simeq -\frac{3J^2}{K}\sum_{\alpha,\beta}\sigma_\alpha^\alpha\sigma_\beta^\beta \tag{3.27}$$

Here, in σ_α^α, the subscript α refers to a neighour site of origin in $\alpha-$bond direction

Thus, in the anti-ferromagnetic coupling case, the Kondo singlet decouples from the rest of the Kitaev model and a small interaction ($J^2/K \ll J$) is generated between the three neighbor sites of origin in the second order perturbation. The strong coupling fixed point is thus a stable fixed point and is equivalent to Kitaev model with one spin missing.

Ferromagnetic case

In the ferromagnetic Kondo coupling case, the triplet states form the ground state manifold. We can do degenerate perturbation theory to get the effective Hamiltonian.

$$\langle t', K'_-|H_1|t, K_-\rangle = J\langle t', K'_-|V|t, K_-\rangle \tag{3.28}$$

$$= \sum_\alpha \langle t'|\sigma_0^\alpha|t\rangle\langle K'_-|\sigma_\alpha^\alpha|K_-\rangle \tag{3.29}$$

If we calculate the matrix elements of $\langle t'|\sigma_0^\alpha|t\rangle$, these matrices are just the spin-1 matrices:

$$\sigma_0^x = \begin{pmatrix} 0 & \frac{1}{\sqrt{2}} & 0 \\ \frac{1}{\sqrt{2}} & 0 & \frac{1}{\sqrt{2}} \\ 0 & \frac{1}{\sqrt{2}} & 0 \end{pmatrix},$$

$$\sigma_0^y = \begin{pmatrix} 0 & -\frac{i}{\sqrt{2}} & 0 \\ \frac{i}{\sqrt{2}} & 0 & -\frac{i}{\sqrt{2}} \\ 0 & \frac{i}{\sqrt{2}} & 0 \end{pmatrix},$$

$$\sigma_0^z = \begin{pmatrix} 1 & 0 & 0 \\ 0 & 0 & 0 \\ 0 & 0 & -1 \end{pmatrix}$$

and the Hamiltonian in the reduced subspace becomes

$$H_1 = JS_0^\alpha \sigma_\alpha^\alpha. \tag{3.30}$$

where $\mathbf{S}_0$ represents the spin-1 at the origin.

Thus for the ferromagnetic impurity coupling, the new terms which couple the triplet and the rest of the Kitaev model are similar to the original Kitaev coupling

and of the same strength. The model becomes a Kitaev like model with the spin at origin being a spin-1. Thus the Kondo triplet does not decouple from the rest of the Kitaev model in strong coupling limit. The new model need to be studied in further detail to understand the behaviour of ferromagnetic strong coupling fixed point.

3.2.2 Topological transition

A remarkable property of the Kondo effect in Kitaev model is that the unstable fixed point is associated with a topological transition from the zero flux state to a finite flux state. The strong antiferromagnetic coupling limit amounts to studying the Kitaev model with a missing site or cutting the three bonds linking this site to the neighbors. Kitaev has shown [4] that such states with an odd number of cuts are associated with a finite flux, and also that these vortices are associated with unpaired Majorana fermions and have non-abelian statistics under exchange. It has also been shown numerically for the gapless phase [19] that the ground state of the Kitaev model with one spin missing has a finite flux pinned to the defect site. We argued the existence of a localized zero energy Majorana mode from degeneracy of the ground state in presence of impurity spin and elucidated on the nature of this zero mode.

For the Hamiltonian $H = H_0 + V_K$, the three plaquettes W_1, W_2 and W_3 (Fig. 3.5) that touch the impurity site are no longer associated with conserved flux operators, while the flux operators that do not include the origin remain conserved. The three plaquette operator $W_0 = W_1W_2W_3$ is still conserved and $W_0 = 1$ in the ground state of the unperturbed Kitaev model. We define the composite operators $\tau^x = W_2W_3S^x$, $\tau^y = W_3W_1S^y$ and $\tau^z = W_1W_2S^z$ (S^α are the Pauli spin matrices corresponding to the impurity) which are also conserved in presence of the impurity coupling. The τ^α's do not commute with each other and instead obey the $SU(2)$ algebra, $[\tau^\alpha, \tau^\beta] = 2i\epsilon_{\alpha\beta\gamma}\tau^\gamma$. This $SU(2)$ symmetry, which is exact for all couplings is realized in the spin-1/2 representation $\left((\tau^\alpha)^2 = 1\right)$. Thus all eigenstates, including the ground state are doubly degenerate (corresponding to $\tau^z = \pm 1$).

In strong (antiferromagnetic) coupling limit $J_K \to \infty$, the low energy states will be the ones in which the spin at the origin forms a singlet $|0\rangle$ with the impurity spin, $|\psi\rangle = |\psi K^-\rangle \otimes |0\rangle$. $|\psi K^-\rangle$ stands for the low energy states of the Kitaev model with the spin at the origin removed. To see the action of the $SU(2)$ symmetry generators on these states, we note that they can be written as $\tau^\alpha = \tilde{W}^\alpha \otimes \sigma_0^\alpha \otimes S^\alpha$ and $\tilde{W}^\alpha$ do not involve the components of the spin at the origin, σ_0^α. We then have $\tau^\alpha|\psi\rangle =$

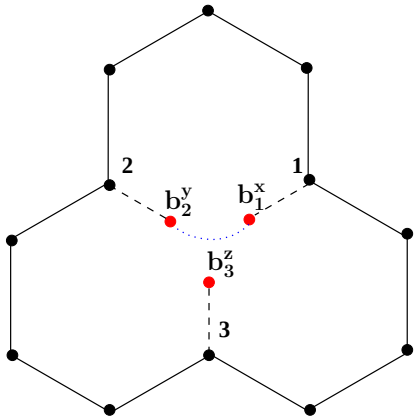

Figure 3.5: Schematic of the three unpaired b–Majorana fermions formed as a result of cutting the links to the Kitaev spin at the origin. Any two of the three can be given an expectation value (dotted bond).

$-(\tilde{W}^\alpha|\psi K^-\rangle) \otimes |0\rangle$. Thus, in the strong coupling limit, the symmetry generators act non-trivially only in the Kitaev model sector. This implies that the low energy states of the Kitaev model with one spin removed are all doubly degenerate, with the double degeneracy emerging from the Kitaev sector. This implies there is a zero-energy mode in the single particle spectrum. The two degenerate states correspond to the zero mode being occupied or unoccupied.

Let us examine the structure of the zero mode. Removing a Kitaev spin creates three unpaired $b-$Majorana fermions at the neighboring sites, say, b_3^z, b_1^x and b_2^y (Fig. 3.5). Now $ib_1^x b_2^y$ is conserved and commutes with all the conserved flux operators W_i but not with the two other combinations $ib_2^y b_3^z$ and $ib_3^z b_1^x$. So, we can choose a gauge where the expectation value of $ib_1^x b_2^y$ is equal to $+1$ such that these two b modes drop out of the problem and we equivalently have one unpaired $b-$Majorana fermion. The unpaired b_3^z Majorana has dimension $\sqrt{2}$ and therefore, there must be an unpaired Majorana mode in the c sector (again of dimension $\sqrt{2}$) so that together these two give the full (doubly degenerate) zero energy mode. Also, while the b_3^z mode is sharply localized, the wave function of the c mode can be spread out in the lattice. Existence of a zero energy $c-$Majorana mode has also been shown explicitly by considering the Kitaev model with one site missing [20].

3.3 RKKY interactions

In the absence of impurities, in the ground state manifold (vortex free state), we have only nearest neighbour two-spin correlations in the Kitaev model [5]. This is because each Kitaev spin is a bilinear of a massless c Majorana fermion and a massive b Majorana fermion, and the b Majorana fermions have only short range correlations. For instance, for an $\alpha-$type bond between neighbours i and j, $i\langle b_i^\alpha b_j^\beta\rangle = \delta_{\alpha\beta}$. We now add impurities with each one locally coupled to Kitaev spins. Distant impurities can interact only if they are coupled via the massless Majorana fermions. By contracting b Majorana fermions locally by second order perturbation in the Kondo coupling, and using the identities $(b_i^\alpha)^2 = 1$, and $i\langle b_i^\alpha b_j^\beta\rangle = \delta_{\alpha\beta}$, we generate vertices of the type $(K^\alpha S^\alpha)^2 c_i c_j/J$, where i and j are not farther than nearest neighbour (are on a bond). Since $c_i^2 = 1$, these vertices will contain massless Majorana fermions only when i and j belong to *different* sites. This effectively means that two distant impurities coupled to a single Kitaev site each *cannot* interact. However when the impurities interact with more than one neighbouring Kitaev spins, we see that a long range interaction of the spins is possible. As an example, we analyze the interaction when the two impurities are at the centers of distant hexagons. The interaction term is

$$V_K = i \sum_{j\in \text{hex1},\alpha} K^\alpha S_1^\alpha b_j^\alpha c_j + i \sum_{j\in \text{hex2},\alpha} K^\alpha S_2^\alpha b_j^\alpha c_j. \tag{3.31}$$

The effective interaction generated involving $c-$type Majorana fermions at two neighbouring sites ($i \in A$, $j \in B$) is given by (see Fig. 3.4)

$$\begin{aligned} V_{\text{eff}} &= \sum_\nu \langle \Omega_b|V|\nu\rangle \frac{1}{E_0 - E_\nu} \langle \nu|V|\Omega_b\rangle \\ &\approx \frac{2}{J} \sum_{a,<ij>_\alpha} (K^{\alpha_{ij}})^2 (S_a^{\alpha_{ij}})^2 c_i c_j. \end{aligned}$$

Here α_{ij} refers to the $z-$component when neighbouring sites i and j are along a $z-$bond, etc. Now the interaction between the two impurity spins is given by the second order term in V_{eff} (or, equivalently, fourth order in K). These terms are of the type

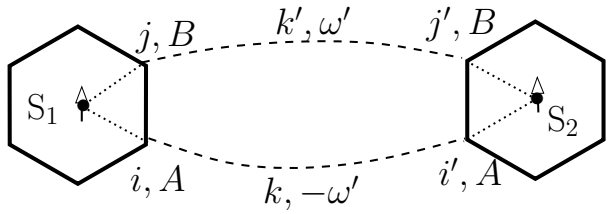

Figure 3.6: A typical long-distance impurity interaction mediated by a pair of propagating c Majorana fermions emanating from the ends of a Kitaev bond.

$$\begin{aligned}
&\frac{1}{J^2}\langle (K^{\alpha_{ij}})^2 (S_1^{\alpha_{ij}})^2 (K^{\beta_{i'j'}})^2 (S_2^{\beta_{i'j'}})^2 c_i c_j c_{i'} c_{j'}\rangle \\
=&\frac{1}{4J^2N^2}(K^{\alpha_{ij}})^2 (S_1^{\alpha_{ij}})^2 (K^{\beta_{i'j'}})^2 (S_2^{\beta_{i'j'}})^2 \sum_{\{\mathbf{k},\mathbf{k}',\mathbf{q},\mathbf{q}'\}\in HBZ} \langle (c_{\mathbf{k},A}\, \mathrm{e}^{i\mathbf{k}\cdot\mathbf{r}_i} + c^\dagger_{\mathbf{k},A}\, \mathrm{e}^{-i\mathbf{k}\cdot\mathbf{r}_i}) \\
&\times (c_{\mathbf{k}',B}\, \mathrm{e}^{i\mathbf{k}'\cdot\mathbf{r}_j} + c^\dagger_{\mathbf{k}',B}\, \mathrm{e}^{-i\mathbf{k}'\cdot\mathbf{r}_j})(c_{\mathbf{q},A}\, \mathrm{e}^{i\mathbf{q}\cdot\mathbf{r}_{i'}} + c^\dagger_{\mathbf{q},A}\, \mathrm{e}^{-i\mathbf{q}\cdot\mathbf{r}_{i'}})(c_{\mathbf{q}',B}\, \mathrm{e}^{i\mathbf{q}'\cdot\mathbf{r}_{j'}} + c^\dagger_{\mathbf{q}',B}\, \mathrm{e}^{-i\mathbf{q}'\cdot\mathbf{r}_{j'}})\rangle.
\end{aligned}$$

Writing $c_{\mathbf{k}}$'s in terms of $a_{\mathbf{k}}$'s and considering the $i \leftrightarrow i'$, $j \leftrightarrow j'$ (Fig. 3.6) case, and denoting $\Gamma^{\alpha,\beta} = \frac{1}{J^2}(K^{\alpha_{ij}})^2 (S_1^{\alpha_{ij}})^2 (K^{\beta_{i'j'}})^2 (S_2^{\beta_{i'j'}})^2$, (from now we use $\alpha \equiv \alpha_{ij}$ and $\beta \equiv \beta_{i'j'}$) the contribution from above term is

$$\begin{aligned}
J^{\alpha\beta}_{12(a)} \sim& -\frac{\Gamma^{\alpha,\beta}}{N^2} \sum_{\{\mathbf{k},\mathbf{k}'\}\in HBZ,\omega'} \left[\frac{\sin(\mathbf{k}\cdot(\mathbf{r}_i - \mathbf{r}_{i'}))}{-i\omega' - \epsilon_{k,0}} + \frac{\sin(\mathbf{k}\cdot(\mathbf{r}_i - \mathbf{r}_{i'}))}{-i\omega' - \epsilon_{k,1}}\right] \\
&\times \left[\frac{\sin(\mathbf{k}'\cdot(\mathbf{r}_j - \mathbf{r}_{j'}))}{i\omega' - \epsilon_{k',0}} + \frac{\sin(\mathbf{k}'\cdot(\mathbf{r}_j - \mathbf{r}_{j'}))}{i\omega' - \epsilon_{k',1}}\right] \\
=& -\frac{\Gamma^{\alpha,\beta}}{2N^2} \sum_{\{\mathbf{k},\mathbf{k}'\}\in HBZ} \sin(\mathbf{k}\cdot(\mathbf{r}_i - \mathbf{r}_{i'}))\sin(\mathbf{k}'\cdot(\mathbf{r}_j - \mathbf{r}_{j'})) \\
&\times \left[\frac{\tanh(\frac{|\epsilon_k|}{2T}) + \tanh(\frac{|\epsilon_{k'}|}{2T})}{|\epsilon_k| + |\epsilon_{k'}|} + \frac{\tanh(\frac{|\epsilon_k|}{2T}) - \tanh(\frac{|\epsilon_{k'}|}{2T})}{|\epsilon_k| - |\epsilon_{k'}|}\right],
\end{aligned}$$

where ω' are fermionic Matsubara frequencies. In the $T \to 0$ limit, the second term becomes zero. Near the Fermi point, we have $|\epsilon_{\mathbf{k}_F+\mathbf{q}}| \simeq v_F q$. Converting the k and k' sums to integrals over q and q', we have

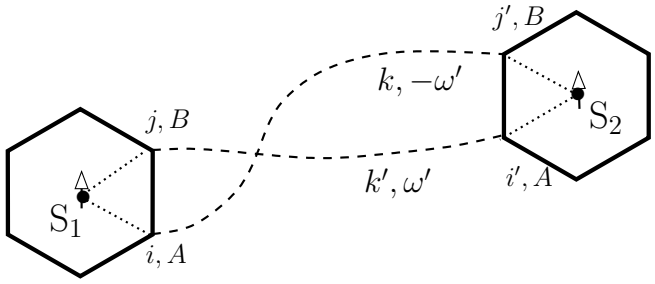

Figure 3.7: Another contribution to long range impurity interaction from the same pair of bonds as Fig. 3.6.

$$J^{\alpha\beta}_{12(a)} \sim -\frac{2\Gamma^{\alpha,\beta}}{v_F N^2}\sum_{\mathbf{q},\mathbf{q}'}\sin((\mathbf{k}_F+\mathbf{q})\cdot\mathbf{R}_{12})\sin((\mathbf{k}_F+\mathbf{q}')\cdot\mathbf{R}_{12})\frac{\tanh(\frac{v_F k_F}{2T})}{q+q'}$$

$$= -\frac{8\Gamma^{\alpha,\beta}a^4}{v_F(2\pi)^4}\int dq\, dq' qq' J_0(qR_{12})J_0(q'R_{12})\sin^2\phi\frac{1}{q+q'}$$

$$\simeq -\frac{8}{v_F}\frac{\Gamma^{\alpha,\beta}a^4}{(2\pi)^4}\frac{\pi}{R_{12}^3}\sin^2\phi\int_0^\infty d\tilde{q}\int_0^\infty d\tilde{q}'\sqrt{\tilde{q}\tilde{q}'}\cos(\tilde{q}-\frac{\pi}{4})\,\cos(\tilde{q}'-\frac{\pi}{4})\frac{1}{\tilde{q}+\tilde{q}'}.$$

Here $\phi = \mathbf{k}_F\cdot\mathbf{R}_{12}$ and we used the asymptotic limit of the Bessel functions. Thus the contribution of above term to the long range interaction goes as

$$J^{ij,i'j'}_{12(a)} \sim -(K^\alpha)^2(S_1^\alpha)^2(K^\beta)^2(S_2^\beta)^2\ \frac{a^4[1-\cos(2\mathbf{k}_F\cdot\mathbf{R}_{12})]}{4v_F J^2\pi^3 R_{12}^3}.$$

Similarly the term corresponding to $i\leftrightarrow j'$, $j\leftrightarrow i'$ (Fig.3.7) makes the following

contribution to the long range interaction:

$$
\begin{aligned}
J^{\alpha\beta}_{12(b)} \sim & \\
& -\frac{\Gamma^{\alpha,\beta}}{N^2}\sum_{\{\mathbf{k},\mathbf{k}'\}\in HBZ,\omega}\left\{\frac{-2i\sin(\mathbf{k}\cdot(\mathbf{r}_i-\mathbf{r}'_j)-\tilde{\alpha}(\mathbf{k}))}{-i\omega'-\epsilon_{k,0}}+\frac{-2i\sin(\mathbf{k}\cdot(\mathbf{r}_i-\mathbf{r}'_j)-\tilde{\alpha}(\mathbf{k}))}{-i\omega'-\epsilon_{k,1}}\right\}\cdot \\
& \qquad\cdot\left\{\frac{-2i\sin(\mathbf{k}'.(\mathbf{r}_j-\mathbf{r}'_i)+\tilde{\alpha}(\mathbf{k}'))}{i\omega'-\epsilon_{k',0}}-\frac{-2i\sin(\mathbf{k}'.(\mathbf{r}_j-\mathbf{r}'_i)+\tilde{\alpha}(\mathbf{k}'))}{i\omega'-\epsilon_{k',1}}\right\} \\
& \simeq -\frac{2\Gamma^{\alpha,\beta}}{v_F N^2}\sum_{\mathbf{q},\mathbf{q}'}\sin((\mathbf{k}_F+\mathbf{q}).R_{12}-\tilde{\alpha}(\mathbf{k}_F))\ \sin((\mathbf{k}_F+\mathbf{q}').R_{12}+\tilde{\alpha}(\mathbf{k}_F))\ \frac{1}{q+q'} \\
& \simeq -\frac{8\Gamma^{\alpha,\beta}a^4}{v_F(2\pi)^4}\int d\mathbf{q}d\mathbf{q}'\ \frac{\sin(qR_{12}\cos\theta+\phi+\tilde{\alpha}(\mathbf{k}_F))\ \sin(q'R_{12}\cos\theta'+\phi-\tilde{\alpha}(\mathbf{k}_F))}{q+q'}
\end{aligned}
$$

which gives

$$
J^{ij,i'j'}_{12(b)} \sim -(K^\alpha)^2(S^\alpha_1)^2(K^\beta)^2(S^\beta_2)^2\times\frac{a^4}{4v_F J^2\pi^3}\frac{(\cos(2\tilde{\alpha}(\mathbf{k}_F))-\cos(2\mathbf{k}_F\cdot\mathbf{R}_{12}))}{R^3_{12}},
$$

where $\tilde{\alpha}(\mathbf{k}_F)$ is the phase of $f(\mathbf{k}_F)$. Adding the two terms, we get the contribution to the long range interaction coming from the pair of bonds ij and $i'j'$:

$$
J^{ij,i'j'}_{12} \sim -(K^\alpha)^2(S^\alpha_1)^2(K^\beta)^2(S^\beta_2)^2\frac{a^4}{4v_F J^2\pi^3}\frac{1+\cos(2\tilde{\alpha}(\mathbf{k}_F))-2\cos(2\mathbf{k}_F\cdot\mathbf{R}_{12})}{R^3_{12}}. \tag{3.32}
$$

This is the long range interaction between impurity spins each coupled to a bond. The power law correlation reflects the bond-bond (four spin) correlations in the Kitaev model ground state which are long ranged while two-spin correlations are only nearest neighbour. We find that if for spin-1/2 impurities, $(S^\alpha)^2 = 1/4$ and no long-ranged interaction is generated. If the impurities couple to the full hexagon, we can sum these bond contributions to get full answer. If the Kondo coupling is isotropic and all types of Kitaev bonds (x, y, z) are involved, the resulting sums $\sum_{\text{bond pairs}}(S^{\alpha_{ij}}_1)^2(S^{\beta_{i'j'}}_2)^2$ will yield a constant $S_1(S_1+1)S_2(S_2+1)$, which will make the long range interaction vanish in this this approximation. One may then need to obtain any long range interaction taking care of the small differences in the separation between the different pairs of bonds.

The inter impurity interactions have an interesting non-dipolar nature ($(S^\alpha_1)^2(S^\beta_2)^2$) unlike the usual dipolar ($\mathbf{S_1}\cdot\mathbf{S_2}$) RKKY interaction in metals. The $1/R^3$ behaviour

in two-dimensions is characteristic of the linearly vanishing density of states at Fermi energy, as is the case for graphene also.

This study of impurity effects shows that the Kitaev model is quite robust to external magnetic disorder. If Kondo coupling is small, the impurity coupling flows to zero and does not affect the system significantly. Also if the impurity spins are spin-half or they are coupled to only one Kitaev spin each, there are no significant interactions generated between the spins and thus collective behaviour of impurity spins is less likely to affect the Kitaev model state.

3.4 Summary

To summarize, we studied the effect of impurity quantum spins coupled to the ground state manifold of Kitaev model in its gapless spin-liquid state. We found an unusual Kondo effect with an unstable fixed point demarcating a topological transition between zero flux and finite flux sectors. When more than one impurity is present, we showed that under certain circumstances, massless spinons in the Kitaev model mediate a higher order (non-dipolar) RKKY interaction between distant impurity spins. Topological transition and non-dipolar impurity interactions make the Kitaev Kondo effect qualitatively different from the Kondo effect in some bosonic spin liquids that also have an unstable fixed point.

In the strong Kondo coupling limit we showed that a non-zero flux is created with an unpaired $b-$Majorana fermion localized in its vicinity and a delocalized $c-$counterpart. Localized $b-$Majorana fermion at the finite flux defect is reminiscent of the localized Majorana fermions at the cores of half vortices in $p-$wave superconductors [21]. One difference, as pointed out by Kitaev, is that in $p-$wave superconductors, the currents associated with the fluxes are charged (and thus interact with impurity potentials). Besides, the individual charges acquire abelian phases of their own. Another difference is that in the Kitaev model, the full (doubly degenerate) zero mode is made of a b and a c Majorana fermion while in the superconductor, two vortex core Majorana fermions make a zero mode. $p-$wave paired ground states in the Kitaev model and its vortex excitations have also been studied in Ref. [22]. There are already numerous proposals in the literature how a Kitaev model could be realized [11, 10, 12], and we are hopeful that eventually these novel impurity effects may also be experimentally studied.

References

[1] H. Alloul, J. Bobroff, M. Gabay and P. J. Hirschfeld, *Defects in correlated metals and superconductors*, Rev. Mod. Phys. **81**, 45 (2009).

[2] G. Khaliullin, R. Kilian, S. Krivenko, P. Fulde, *Impurity-induced moments in underdoped cuprates*, Phys. Rev B **56**, 11882 (1997).

[3] A. Sen, K. Damle, R. Moessner, *Fractional Spin Textures in the Frustrated Magnet* $SrCr_{9p}Ga_{12-9p}O_{19}$, Phys. Rev. Lett. **106**, 127203 (2011).

[4] A. Yu. Kitaev, *Anyons in an exactly solved model and beyond*, Ann. Phys. (Berlin) **321**, 2 (2006).

[5] G. Baskaran, S. Mandal, and R. Shankar, *Exact Results for Spin Dynamics and Fractionalization in the Kitaev Model*, Phys. Rev. Lett. **98**, 247201 (2007).

[6] X.-Y. Feng, G. M. Zhang, and T. Xiang, *Topological Characterization of Quantum Phase Transitions in a Spin-1/2 Model*, Phys. Rev. Lett. **98**, 087204 (2007).

[7] S. Dusuel, K. P. Schmidt, and J. Vidal, *Creation and Manipulation of Anyons in the Kitaev Model*, Phys. Rev. Lett. **100**, 177204 (2008).

[8] K. Sengupta, D. Sen, and S. Mondal, *Exact Results for Quench Dynamics and Defect Production in a Two-Dimensional Model*, Phys. Rev. Lett. **100**, 077204 (2008).

[9] D. H. Lee, G. M. Zhang, and T. Xiang, *Edge Solitons of Topological Insulators and Fractionalized Quasiparticles in Two Dimensions*, Phys. Rev. Lett. **99**, 196805 (2007).

[10] G. Jackeli, and G. Khaliullin, *Mott Insulators in the Strong Spin-Orbit Coupling Limit: From Heisenberg to a Quantum Compass and Kitaev Models*, Phys. Rev. Lett. **102**, 017205 (2009).

[11] L.-M. DuanE. Demler, and M. D. Lukin, *Controlling Spin Exchange Interactions of Ultracold Atoms in Optical Lattices*, Phys. Rev. Lett. **91**, 090402 (2003).

[12] J. Q. You, X.-F. Shi, X. Hu, and F. Nori, *Quantum emulation of a spin system with topologically protected ground states using superconducting quantum circuits*, Phys. Rev. B **81**, 014505 (2010).

[13] P. W. Anderson, *A poor man's derivation of scaling laws for the Kondo problem*, J. Phys. C: Solid State Phys. **3** 2436 (1970)

[14] A. Hewson, *The Kondo Problem to Heavy Fermions*, Cambridge University Press, Cambridge, 1992.

[15] D. Withoff and E. Fradkin, *Phase transitions in gapless Fermi systems with magnetic impurities*, Phys. Rev. Lett. **64**, 1835 (1990).

[16] S. Saremi, *RKKY in half-filled bipartite lattices: Graphene as an example*, Phys. Rev. B **76**, 184430 (2007).

[17] S. Florens, L. Fritz, M. Vojta, *Kondo Effect in Bosonic Spin Liquids*, Phys. Rev. Lett. **96**, 036601 (2006).

[18] H. Primas. *Generalized perturbation theory in operator form*, Rev. Mod. Phys. **35**, 710 (1963); Arnab Sen, *Frustrated Antiferromagnets with Easy Axis Anisotropy*, Ph.D. Thesis, Tata Institute of Fundamental Research, Mumbai, 2009.

[19] A.J. Willans, J. T. Chalker, R. Moessner, *Disorder in a Quantum Spin Liquid: Flux Binding and Local Moment Formation*, Phys. Rev. Lett. **104**, 237203 (2010).

[20] G. Santhosh, V. Sreenath, A. Lakshminarayan and R. Narayanan, *Localized zero-energy modes in the Kitaev model with vacancy disorder*, Phys. Rev. B **85**, 054204 (2012).

[21] D. A. Ivanov, *Non-Abelian Statistics of Half-Quantum Vortices in p-Wave Superconductors*, Phys. Rev. Lett. **86**, 268 (2001).

[22] Y. Yu , *An exactly soluble model with tunable p-wave paired fermion ground states*, Europhys. Lett., **84**, 57002 (2008).

[23] H. Alloul, *Susceptibility and Electron-Spin Relaxation of Fe in Cu below T_K: A NMR Study of ^{63}Cu Satellites*, Phys. Rev. Lett. **35**, 460 (1975).

Chapter 4

Charge transport in magnetic semiconductor heterostructures

4.1 Introduction

Magnetic semiconductors usually consist of a semiconductor host doped with magnetic atoms (about $0.1 - 1\%$). (III,Mn)V (*e.g.* (Ga/In,Mn)As, (Ga,Mn)P/N) is a common class of these materials which have been studied extensively [1]. In such materials, if the Mn concentration is not too high, Mn substitutes Ga acting as an acceptor, so doping GaAs with Mn yields both local magnetic moments and free holes. Semiconductor materials have the great advantage that their properties can be controlled via various means like gate voltages, light, doping etc which make them useful for various electronic technological processes. Combining magnetism with semiconducting properties thus has potential usability for spintronic applications which exploit the spin of the charge carriers to manipulate the charge transport [2]. For these purposes, it is desirable to get magnetism in these systems at room temperatures. Magnetic transitions of the order of 150K have been achieved in these materials. Higher transition temperatures have been difficult to achieve due to limited solubility of Mn/other magnetic atoms in these semiconductor compounds and it is an active area of research. The mechanism of ferromagnetism in these dilute magnetic semiconductors (DMS) has not been understood very well [3]. The microscopic interaction governing the ferromagnetism (FM) could be of Zener/Ruderman-Kittel-Kasuya-Yosida (RKKY) type or double-exchange type. The Zener/RKKY model is applicable when the effective coupling between local magnetic moments and the spins of charge carriers is smaller than the carrier bandwidth [5, 1]. This model is

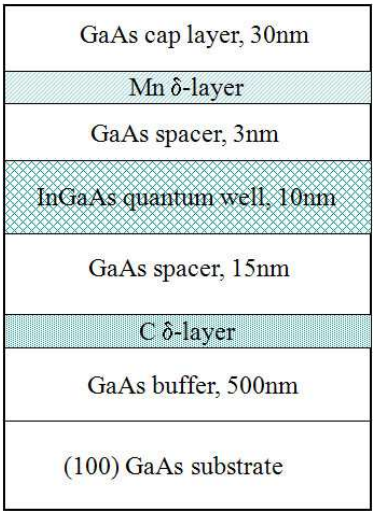

Figure 4.1: Schematic layout of the heterostructure δ-doped by Mn.

more likely at higher concentration of Mn atoms such that the impurity band states are extended on the length scale of inter-Mn distances. Other picture of ferromagnetism is based on interacting bound polaron scenario [1, 4] which is dominant when number of holes (charge carriers) is small. Here, the localized hole polarizes the Mn atoms in its vicinity and these magnetic polarons interact via the hopping of holes giving rise to ferromagnetism at low temperatures and this is regarded as a double exchange mechanism. The current opinion is that both mechanisms of FM can take place in bulk DMSs. Conditions for realization of either mechanism strongly depend not only on the concentration of magnetic metal ions, but also on the character of their distribution in the Semiconductor host.

In bulk DMS materials, carrier mobilities are usually small due to large scattering from the dopants and these systems are usually close to metal-insulator transition. Another major direction of work in this field has been magnetic semiconductor heterostructures, (fig. 4.1). These structures have planar two dimensional geometries and can thus be easily incorporated in to existing microelectronic devices. In these systems, the Mn atoms are doped in the form of a $\delta-$layer spatially away from the quantum well where charge transport takes place. This gives higher charge mobilities to these systems as well as incorporates the effects of the ferromagnetism. Also, exploring these systems could provide insights into understanding the microscopic mechanism of ferromagnetism in these semiconductors.

Two mechanisms for the FM ordering in these two-dimensional (2D) GaAs/InGaAs/GaAs

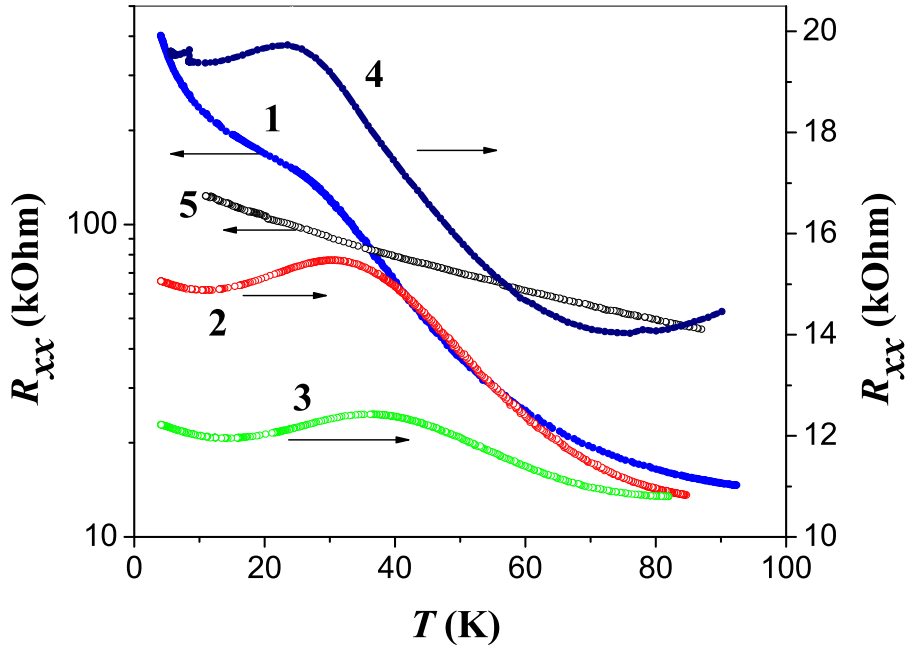

Figure 4.2: Resistance data for Mn δ-doped heterostructures (1, 2, 3, and 4) for different carrier and doping densities (see Table 4.1) and a carbon δ-doped heterostructure (5). Note the absence of any resistance anomaly in the carbon δ-doped sample, while the Mn δ-doped samples exhibit an anomaly (hump or shoulder), which is likely due to magnetic ordering.

heterostructures δ-doped by Mn have been proposed in the current literature [8, 9]. The first model [8] attributes FM ordering to indirect interaction of Mn atoms by means of holes in a 2D conducting channel. The efficiency of this mechanism is based on the large mean free path of 2D carriers due to their remoteness from the Mn layer. In the second model, FM ordering arises within the Mn layer, possibly mediated by the holes in the layer, like in usual DMS structures [9].

One of the most relevant questions is the effect of FM ordering on the temperature dependence of resistivity, in particular, the relation of the FM ordering to the resistance anomaly (a peak or shoulder) near T_C [5]. Several theories have been proposed [10, 11, 12, 13, 14, 15] for explaining the resistivity in bulk DMSs but there are not many works on these effects in 2D semiconductor heterostructures. In addition to magnetism, disorder plays a significant role in DMS transport properties [16].

We studied the effects of spatial disorder of dopant concentration in the Mn δ-layer on the electronic properties of the 2D hole gas and showed that at low carrier densities, competition of disorder and nonlinear screening results in formation of

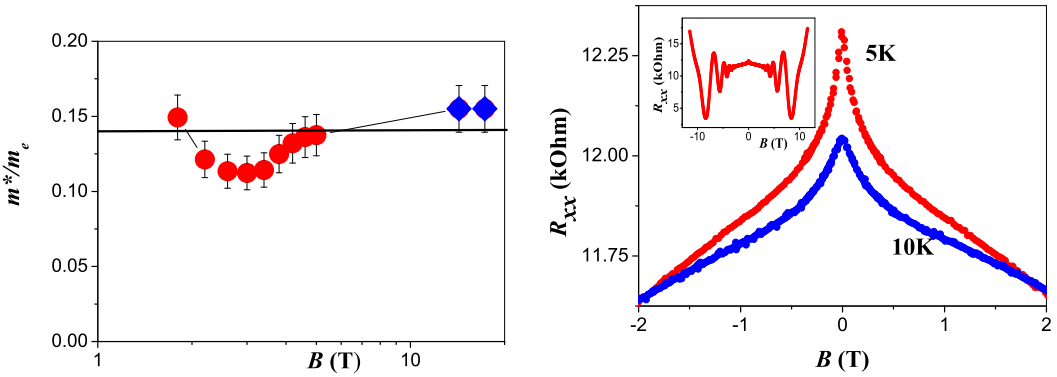

Figure 4.3: (a) Effective mass dependence on magnetic field for Sample 2 (red circles) measured by ShdH oscillations and for Sample 4 (blue diamonds) measured by cyclotron resonance. Solid black line corresponds to $m^*/m_e = 0.14$. (b) Magnetic field dependence of the resistance of Sample 3 at different temperatures. The inset shows Shubnikov–de Haas (ShdH) oscillations indicating metallicity.

"metallic" droplets separated by insulating regions in hole gas in quantum well. We make estimates for droplet sizes and inter-droplet distance, energy level spacing in these droplet structures and the potential barrier separating neighboring droplets. Using these as parameters in a simple model for resistivity which incorporates the effect of ferromagnetism on inter-droplet tunneling, we obtained a quantitative explanation of the temperature dependence of resistivity in the DMS ferromagnetic heterostructures.

A schematic layout of the studied structures is shown in Fig. 4.1. The structures consist of an $In_xGa_{1-x}As$ quantum well (QW) inside a GaAs matrix with a Mn δ-layer separated from the QW by a GaAs spacer of width 3 nm. The QW thickness W is about 10 nm and the In fraction is $x \approx 0.2$. A carbon δ-layer ($\approx 2 \times 10^{12}\text{cm}^{-2}$) is introduced at a distance 10–15 nm below the QW just at the top of the buffer layer to compensate the hole depletion of the QW by the (undoped) buffer layer. The mobility and other electrical and structural parameters of the studied structures are shown in Table 4.1.

Existence of well pronounced Shubnikov–de Haas (ShdH) oscillations in Samples 2 and 3 tells us that these two samples are on the metallic side of the percolation transition. In Fig. 4.3(b), we show magnetic field dependence of the resistance at two temperatures. The inset shows ShdH oscillations previously discussed in Ref. [6]. In contrast to Samples 2 and 3, Sample 1 is quite insulating, with $R(5K)/R(70K) \approx 30$. The resistance $R(T)$ exhibits an Arrhenius behavior (activation energy ≈ 110 K for

Sample	Mn content, monolayers ($cm^{-2} \times 10^{14}$)	In content x	Quantum well depth $-V_0$, meV	$V_{fluc}(z=0, R_c)$ at 77 K, meV	Overlap probability of the hole wavefunction with Mn layer (77 K)	Hole mobility μ_p (77 K), $cm^2/V{\cdot}s$	Hole density p (77 K), $cm^{-2} \times 10^{12}$	Overlap probability of the hole wavefunction with Mn layer (5 K)	Hole mobility μ_p (5 K), $cm^2/V{\cdot}s$	Hole density p (5 K), $cm^{-2} \times 10^{12}$
1	1.2 (6.0)	0.18	85	260	0.15×10^{-2}	1350	1.8	0.15×10^{-3}	180	0.3
2	0.5 (3.0)	0.21	100	170	0.51×10^{-2}	1860	2.0	0.52×10^{-3}	2950	0.71
3	0.4 (2.5)	0.23	115	160	0.39×10^{-2}	1930	1.8	0.63×10^{-3}	3240	0.79
4	0.35 (2.0)	0.17	70	145	0.72×10^{-2}	2370	1.4	0.9×10^{-3}	3400	0.46
5	0	0.18	85	–	–	1600	0.5	–	–	–

Table 4.1: Parameters characterizing the samples under study. Samples 1–4 are δ-doped by Mn. Sample 5 is δ-doped by carbon instead of Mn. All the samples have a carbon layer too as shown in Fig. 4.1. We also show the model estimates for the fluctuation potential V_{fluc} at the quantum well edge facing the Mn dopant layer, and overlap probability of the hole wavefunction with a 1 nm thick region centered at the δ-layer of Mn situated 3 nm away from the quantum well. Here, R_c is the screening length. At each In content, the quantum well depth was estimated using the known experimental results, according to which the valence band discontinuity is about 1/3 of the band gap discontinuity [18].

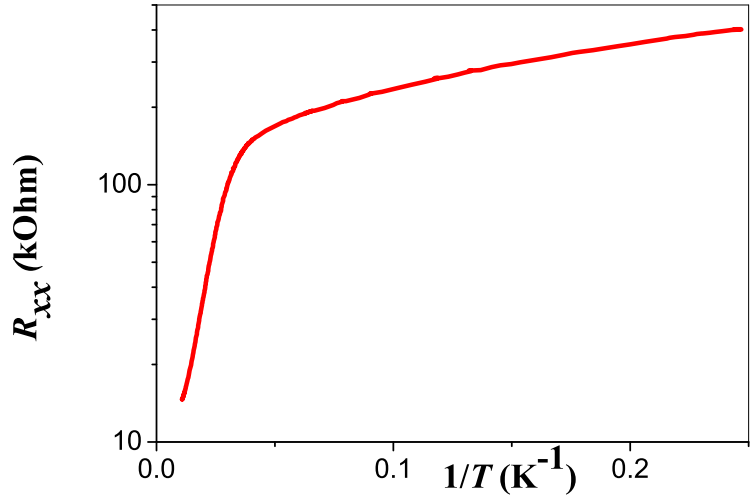

Figure 4.4: Plot of $\log R(T)$ vs T for Sample 1 demonstrating an Arrhenius behavior for temperatures higher than about 30 K and a hopping behavior at low temperatures.

$T \gtrsim 30$ K) with crossover to variable hopping regime at temperatures less than 30 K (see Fig. 4.4). Sample 4 with a smaller carrier density compared to Samples 2 and 3 is closer to the percolation transition having high enough values of $R(5K) = 19.7$ kOhm and $R(5K)/R(70K) \approx 1.5$. We found that the temperature dependence of the resistivity can be fitted to the Arrhenius law (activation energy ≈ 20 K for $T \gtrsim 30$ K). Charge transport is two-dimensional in these systems which is confirmed by ShdH oscillations for Samples 2 and 3, which are observed only when the magnetic field is perpendicular to the sample plane (inset of Fig. 4.3(b)). Manifestations of the quantum Hall effect (QHE) were observed even in the most insulating Sample 1 (Ref. [6]), which establishes its 2D nature.

Evidence of ferromagnetic (FM) correlations playing a crucial role comes from observation of a hump or shoulder in the temperature dependence of resistivity as shown in Fig. 4.2. The fact that this feature is observed for all samples doped by Mn but is absent for Sample 5 doped by C instead of Mn shows that it has a magnetic origin. Direct evidence of FM ordering for Samples 1 and 4 was through the observation of hysteresis loop in the magnetization curve [7, 19, 20]. The observation of anomalous Hall effect (AHE) in all mentioned samples [6, 7, 17] is yet another evidence. Results of the AHE measurements are presented in Fig. 4.5 for samples 1, 2 and 4. It is commonly accepted that the "anomalous" hump or shoulder of this temperature dependent resistance can be used as a measure of the Curie temperature

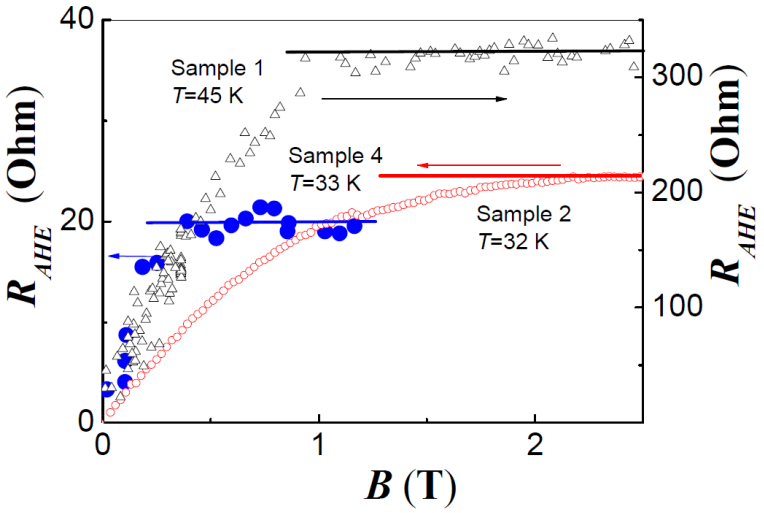

Figure 4.5: Magnetic field dependence of the AHE for Samples 1, 2 and 4. Temperature of the measurements and sample numbers are shown near the curve. For insulating samples (1 and 4) the temperature of measurement is greater than the peak temperature, while for the metallic Sample 2, they are close. For insulating samples, AHE curves can be seen to saturate, while for metallic samples, saturation is not reached or will be reached at higher fields.

[1, 5, 12]. There are differing opinions on whether the anomaly in $R(T)$ or dR/dT should be accepted as T_C [21]. While it is justified for the case of bulk metals to associate the temperature at which the anomaly occurs with T_C, we find below that in the 2D case, the situation is quite different.

4.2 Model of nanoscale inhomogeneities

We consider the effects of the Coulomb potential due to charged Mn atoms on the state of the charge carriers in the quantum well. For the purpose of analysis, we can consider the following system, which captures the main physics. The two-dimensional hole gas (2DHG) is formed within the InGaAs quantum well and additional holes for the 2DHG are provided by Mn acceptors distributed in the δ-layer with density n_d, which is spatially separated from the quantum well by a GaAs spacer of thickness λ. We thus have two interacting subsystems - the δ-layer, where the Mn atoms are a source of holes as well as of magnetism owing to their spins, and the quantum well, where the behavior of the holes is affected by the charge

and spin of Mn atoms. In addition, the holes in the 2DHG are known to affect the distribution of magnetization in the δ-layer. This will be particularly true for the more metallic samples [8].

The parameters characterizing the samples under study are listed in Table 4.1. The table shows the total Mn content in the δ-layer, the quantum well depth V_0 in the absence of fluctuations, the hole densities p, and mobilities μ_p in the 2DHG layer at two different temperatures on either side of the resistance anomaly.

At low carrier density, it has been shown [22, 23, 24, 25, 26] that the interplay of disorder (due to random potentials of the charged Mn atoms) and nonlinear screening by the holes can lead to inhomogeneities in the carrier density. The physical picture of droplet formation and metal-insulator transition is as follows. Charge fluctuations of the ionized Mn acceptors create a fluctuating potential for the hole gas in the quantum well. Holes begin filling the deepest energy levels in the potential profile. Introduction of holes also affects the size of the potential fluctuation because of screening. We assume a Gaussian white noise distribution for the charge density $\rho(\mathbf{r}, z) = en(\mathbf{r})\delta(z + \lambda)$ of the Mn atoms in the δ-layer (z axis is directed perpendicular to the δ-layer, $z = 0$ corresponds to the GaAs/InGaAs interface). For points $\mathbf{r}$, $\mathbf{r}'$ lying in the δ-layer we have,

$$\langle n(\mathbf{r})n(\mathbf{r}')\rangle - \langle n^2\rangle = n'_a\delta(\mathbf{r} - \mathbf{r}'), \tag{4.1}$$

where n'_a is the total density of ionized Mn atoms in the δ-layer: $n'_a = n^-_a + n^+_a$. n^-_a is the density of negatively charged Mn atoms (acceptors) and n^+_a is the density of positively charged (donor) Mn atoms which could happen if the Mn atom goes into an interstitial position. In the further calculations, for simplicity and consistency, we take a typical value of n'_a and assume that $n'_a = 0.1n_d$ (n_d is the total Mn density), which is in agreement with the effective ionization of about 0.1 observed in $Ga_{1-y}Mn_yAs$ samples [1, 3].

From Eq. (4.1), it is easy to see that the variance of the fluctuation charge density in a circular region of size R is $\langle\delta n^2(R)\rangle = n'_a/(\pi R^2)$. The random distribution of charges creates a fluctuating potential ϕ at the interface. In the presence of holes in 2DHG, potential fluctuations are screened beyond a length scale R_c where the fluctuation charge density $\sqrt{\langle\delta n^2(R_c)\rangle} = \sqrt{n'_a/\pi}/R_c$ becomes less than the hole density p. The variance of the potential fluctuations at the interface is then given

by [25]

$$\langle \delta\phi^2 \rangle = \frac{n_a' e^2}{8\pi\kappa^2\epsilon_0^2} \left\{ \ln\left[\frac{4d^2}{\lambda(2d-\lambda)}\right] - 2\ln\left[\left(\frac{\lambda^2+R_c^2}{(2d-\lambda)^2+R_c^2}\right)^{\frac{1}{4}} + \left(\frac{(2d-\lambda)^2+R_c^2}{\lambda^2+R_c^2}\right)^{\frac{1}{4}}\right]\right\}. \tag{4.2}$$

Here, $\kappa = 12.9$ is the permittivity of GaAs and $R_c = \sqrt{n_a'/\pi}/p$ is the characteristic screening length described above. Parameter d is a length scale, beyond which the potential fluctuations get screened even in the absence of holes in the quantum well. Often there is a metallic gate on the sample, in which case d is equal to the distance from the quantum well to the gate.

In cases where the inequality $2d \gg R_c, \lambda$ is met, potential fluctuations can be expressed in a much simpler form,

$$\langle \delta\phi^2 \rangle \approx \frac{n_a' e^2}{16\pi\kappa^2\epsilon_0^2} \ln\left[1 + \left(\frac{R_c}{\lambda}\right)^2\right]. \tag{4.3}$$

Holes in the quantum well are centered at a distance z_0 (measured from the interface closest to the Mn layer) in the direction perpendicular to the interface. To obtain z_0, we solve the Schrödinger equation in the quantum well taking into account the (z-dependent) fluctuating potential,

$$\left[-\frac{\hbar^2}{2m^*}\frac{d^2}{dz^2} + V(z)\right]\psi_n = E_n\psi_n. \tag{4.4}$$

Here $V(z)$ is the quantum well potential together with the fluctuations (see Fig. 4.6). $n = 1, 2, 3\ldots$ refers to the subband index. For holes, we use the approximation of the parabolic dispersion with the effective mass $m^* = 0.14m_e$ as measured from cyclotron resonance for these structures (Fig. 4.3). We approximate $V(z)$ as follows. For $z < 0$, $V(z) = \alpha(|z+\lambda| - \lambda)$, $\alpha = ep/\kappa\epsilon_0$. For $z > W$, we have $V(z) = 0$, where W is the quantum well thickness. For $0 < z < W$, we have $V(z) = V_{QW}(z) - e\sqrt{\langle\delta\phi^2(R_c, z)\rangle}$, where $V_{QW}(z) = -V_0 + \alpha z$. For the present devices, we have taken $W = 10$ nm, $\lambda = 3$ nm and the values of V_0 are as shown in Table 4.1. We also assume that the spatially varying fluctuation potential does not affect the valence band position away from the quantum well. The condition for existence of a subband is $E_n < 0$. Table 4.1 shows the overlap probability $\int_{\delta z} dz|\psi_1(z)|^2$,

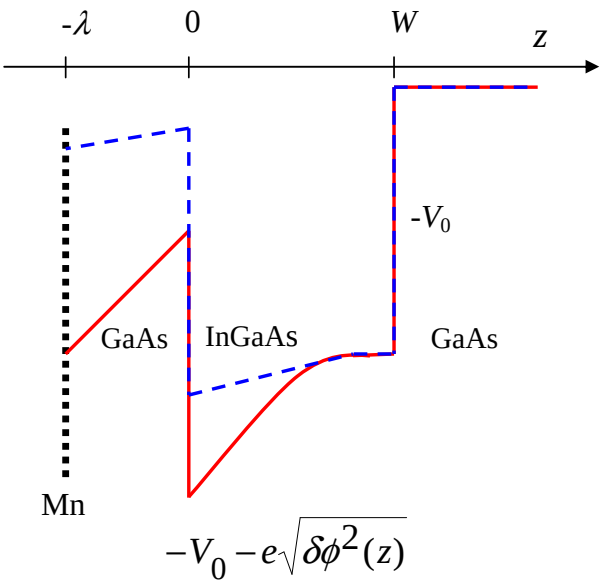

Figure 4.6: Schematic of the quantum well potential (shown inverted). Dashed (blue) line represents the quantum well potential in the absence of fluctuations and the solid (red) line shows the potential well with an attractive fluctuation potential. The dotted line indicates the Mn dopants at a distance λ from the left face of the quantum well. The quantum well of thickness W is defined in the InGaAs layer sandwiched between GaAs regions.

of the hole wavefunction with the Mn layer, where δz is a 1 nm thick region centered at the δ-layer.

We also find that the hole wavefunction in the GaAs region decreases away from the quantum well with a localization length ξ_z having a value ranging from 1 nm to 2 nm. This is comparable to the localization length estimated in Ref. [8]. We will henceforth use $\lambda + z_0$ as the distance of the hole gas from the δ-layer for the purpose of calculating the potential fluctuations. For a given subband n, we determine $z_{0,n}$ as $z_{0,n} = \int dz\, z|\psi_n(z)|^2$. Tables 4.2 and 4.3 show the values of E_n and $z_{0,n}$ for the first two subbands. For simplicity, we will denote $e\sqrt{\langle\delta\phi^2(d+z_{0,n}, \lambda+z_{0,n}, R)\rangle}$ by $V_{\rm fluc}(z_{0,n}, R)$. The values of the fluctuation potential are also shown in Table 4.1.

Now, we describe how at low enough densities, holes in the 2DHG can get organized into charge droplets. Let $R_{p,n}$ be the size of a droplet. The potential fluctuations associated with this length scale are given by $V_{\rm fluc}(z_{0,n}, R_{p,n})$. Suppose that

the holes fill this potential well up to a wavevector $k_{\max}$. From the virial theorem,

$$\frac{\hbar^2 k_{\max,n}^2}{2m^*} = \frac{1}{2} V_{\text{fluc}}(z_{0,n}, R_{p,n}), \tag{4.5}$$

where the factor of 1/2 is for a linear-in-$R_{p,n}$ confining potential, which is approximately the case here. Number of occupied states in the droplet is approximately $(k_{\max} R_p)^2/2$, which can be equated with the fluctuation charge $N_h = \pi R_p^2 \times \sqrt{n_a'/\pi}/R_p = \sqrt{\pi n_a'} R_p$, if only the lowest subband is occupied. We will discuss below the case where more than one subband is occupied. If only the lowest subband is occupied and $2d \gg R_c, \lambda$, Eq. (4.5) yields a very simple solution for the droplet size

$$R_{p,1} \approx \sqrt{2a_B(\lambda + z_{0,1})}. \tag{4.6}$$

Eq. (4.6) is valid when $\lambda + z_0$ is much greater than a_B. The Bohr radius corresponding to these parameters is $a_B \approx 5.3$ nm. In our case $\lambda + z_0 \approx a_B$, and this approximation does not give the correct values. We solve for R_p numerically using Eqs. (4.5) and (4.7). Droplet size R_p and the number of holes per droplet are only weakly dependent on p.

Now, we consider the case where two subbands are occupied. Energy of the highest occupied state measured from the bottom of the lowest subbands ($n = 1$) is of the order of (we will obtain a better estimate below)

$$E_{\max,1} = \frac{\hbar^2 k_{\max,1}}{2m^*} = \frac{\hbar^2 \sqrt{\pi n_a'}}{m^* R_{p,1}}. \tag{4.7}$$

From this estimate of $E_{\max,1}$ and the energies E_1 and E_2, we can see that the second subband is also partially occupied for Sample 1. Filling of the two subbands is not independent and following two conditions need to be satisfied in addition to the relations in Eq. (4.5). First, the chemical potential of the droplets corresponding to the two subbands should be the same (see Fig. 4.7)

$$E_{\max,1} - E_{\max,2} = \frac{\hbar^2}{2m^*}(k_{\max,1}^2 - k_{\max,2}^2) = E_2 - E_1. \tag{4.8}$$

Second, the total number of bound holes is now distributed over the two bands. This effectively results in the transfer of some of the higher energy holes in the lower subband to lower energy empty states in the upper subband. This would lead to a decrease of the droplet size corresponding to the lower subband, and a finite droplet

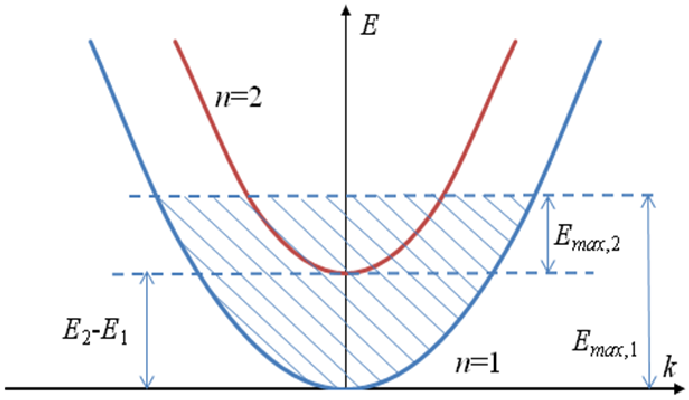

Figure 4.7: A schematic picture of the dispersion curves $E(k)$ (at small k) corresponding to the two lowest subbands $n = 1$ and $n = 2$. E_1 and E_2 are the fluctuation potentials corresponding to $z_{0,1}$ and $z_{0,2}$ respectively, and $R = R_c$. The shaded region represents filled states. The two subbands have a common chemical potential.

size in the upper subband. The transfer of charge from the lower subband to the upper subband naturally makes the concentration of charge in the droplet higher since the charge carriers can occupy two bands in the same region.

We need to now satisfy the following condition

$$\sqrt{\pi n_a'} R_{p,1} = \frac{(k_{\max,1} R_{p,1})^2}{2} + \frac{(k_{\max,2} R_{p,2})^2}{2}. \tag{4.9}$$

Eqs. (4.8), (4.9), and (4.5) form a system of coupled nonlinear equations that may be solved for $E_{\max,n}$ and $R_{p,n}$. Tables 4.2 and 4.3 show the calculated values of $E_{\max,1}$, $R_{p,1}$, and $R_{p,2}$.

Now we analyze the conditions for a metal-insulator crossover. Localization length, which characterizes the spread of the hole wavefunction outside the droplets is

$$\xi = \frac{\hbar}{\sqrt{2m^*(|E_1| - |V_{QW}(z_0)| - |E_{\max,1}|)}}. \tag{4.10}$$

A percolation transition to a more conducting regime is expected when the droplets begin to overlap. The droplets are said to "overlap" once the interdroplet tunneling becomes significant; in other words, the localization length ξ of holes in the droplets becomes comparable to the separation D_1 between the surfaces of neighbor-

Sample	R_c (nm)	$z_{0,1}$(nm)	E_1(meV)	$z_{0,2}$(nm	E_2(meV)	$R_{p,1}$(nm)	$R_{p,2}$(nm)	$E_{\max,1}$(meV)	D_1(nm)	D_2(nm)	ξ(nm)
1	24.28	1.79	-203	3.62	-80	8.96	0	83	11.58	–	1.82
2	15.45	1.57	-142	0.78	-33	8.79	0	60	5.72	–	3.50
3	15.67	1.71	-147	2.30	-40	8.90	0	54	5.82	–	3.70
4	18.02	1.71	-106	1.34	-17	8.90	0	48	7.53	–	3.46

Table 4.2: Calculated values (at 77 K) of the screening length R_c, droplet sizes $R_{p,n}$, droplet separations D_n corresponding to $R_{p,n}$, penetration depths $z_{0,n}$, energy levels E_n, the maximum energy, $E_{\max,1}$, of occupied states measured from the bottom of the potential well for the lowest subbands ($n = 1$) and the localization length ξ. The calculations are for an effective $n'_a = 0.1n_a$. Note that in the last three samples, the separation of the droplets is comparable with the localization length, implying proximity to the "metallic" phase.

Sample	R_c (nm)	$z_{0,1}$(nm)	E_1(meV)	$z_{0,2}$(nm)	E_2(meV)	$R_{p,1}$(nm)	$R_{p,2}$(nm)	$E_{\max,1}$(meV)	D_1(nm)	D_2(nm)	ξ(nm)
1	145.7	2.99	-275	5.37	-204	9.8	0.6	76	55.59	73.59	1.45
2	43.52	2.64	-206	5.16	-128	9.57	0	55	21.68	–	1.93
3	35.71	2.58	-198	5.10	-119	9.51	0	51	17.83	–	2.13
4	54.85	2.93	-155	5.36	-91	9.77	0	41	26.75	–	2.11

Table 4.3: Calculated values at 5K for the same quantities as described in Table 4.2 for an effective $n'_a = 0.1n_a$. Note that all the samples are found to be well-insulating at this temperature. The interdroplet distance D_1 is very sensitive to the hole density p, and since p increases rapidly with temperature, the ratio D_1/ξ can become comparable to unity at relatively low temperatures enabling a transition to the "metallic" phase.

ing droplets ($D_1/\xi \sim 1$). To obtain the separation of the droplets, we note that the total number of holes in a droplet with both bands considered is $N_h = \sqrt{\pi n_a'} R_{p,1}$. These holes are "drained" from an area of size R such that $N_h = \pi R^2 p$. We thus get the size of the catchment area of a droplet, $R = \sqrt{R_{p,1} R_c}$. The distance D_1 between the surfaces of neighboring droplets is then $D_1 = 2(\sqrt{R_{p,1} R_c} - R_{p,1})$. Assuming that the potential well corresponding to second subband is also centered at the well corresponding to first subband, we find the distance between the droplets corresponding specifically to holes in the second subband, $D_2 = 2(\sqrt{R_{p,1} R_c} - R_{p,2})$.

From Tables 4.2 and 4.3, we see that the droplet size is fairly constant for different temperatures and hole densities. Sample 1 is insulating at all temperatures. The behavior of the remaining samples differs significantly for $T = 77$ K and $T = 5$ K. For these samples at 77 K, the interdroplet separation is comparable to the localization length ξ which means that they are more "metallic". Note that the interdroplet distance is larger for Sample 4, which gives rise to an Arrhenius-type behavior in a wide enough temperature range. At $T = 5$ K, the interdroplet separation far exceeds ξ so that all the samples are in the insulating regime. That does not agree with experimental results because Samples 2 and 3 exhibit a quasimetallic behavior even at $T = 5$ K. This could result from the strong dependence of D_1 on the sample parameters (the carrier density, for example) at low temperatures. Thus, the droplet picture following from our calculations being quite reasonable at $T = 77$ K, may give overestimated values of the interdroplet distances at $T = 5$ K. Since D_1 is very sensitive to the carrier density p, and p changes rapidly with temperature, the insulator to metal crossover will take place in Samples 2-4 as the temperature is increased from 5 K. We also find that in contrast to the usual situation encountered in GaAs heterostructures, where the contribution of all but the lowest subbands can be neglected, in Sample 1, the second subband is also occupied.

The energy level spacing, Δ, of a droplet can be found by noting that addition of a hole to a droplet increases $R_{p,1}$ by an amount $1/\sqrt{\pi n_a'}$. The difference of the values of $E_{\max,1}$ of the droplets of size $R_{p,1} + 1/\sqrt{\pi n_a'}$ and $R_{p,1}$ respectively gives us the level spacing at the chemical potential. The level spacing is of the order of 30 K, which falls within the range of the measured activation energies for resistivity. As one approaches the metal-insulator crossover, the potential barrier separating neighboring droplets (see Eq. (4.10)) decreases. Holes near the Fermi level in the potential wells can be thermally excited above the potential barrier to energies above the percolation threshold; this is an alternate mechanism for transport as against the usual inter-droplet tunneling followed by Coulomb blockade.

Using the reduced dopant density n_a' does not affect the droplet sizes significantly but it does reduce R_c by a factor $\sqrt{n_a'/n_a}$, thus bringing the system closer to the metallic percolation transition. Sample 1, which has higher dopant density, thus is more insulating as the potential fluctuations are large. Since we are looking at the charge distribution at the moment, we have ignored magnetism. Magnetism, and its effect on transport will be considered in the next section.

4.3 Resistivity

The droplet picture developed in the previous section can be used to understand the experimentally observed temperature dependence of the resistivity of the insulating samples. We will study the resistivity of Samples 1 and 4 where the holes are well-localized in a droplet phase. In addition to localization effects, we will also need to take into account the effect of ferromagnetic correlations.

In absence of magnetism, as in many disordered insulators, the temperature dependence of resistivity is expected to be of variable-range hopping type at very low temperatures and of Arrhenius type at higher temperatures. In the Arrhenius regime, one could either have nearest-neighbor tunneling together with an activation energy of the order of the mean droplet level spacing, Δ, or the classical thermal excitation over the barrier separating neighboring droplets. Our resistivity measurements will not distinguish the two mechanisms and we will denote the Arrhenius energy fitting the data by E_A; and $E_A = \Delta$ for the tunneling mechanism, which was estimated in the previous section. We analyze the behavior of resistivity across the mean-field Curie temperature T_C, below which the ferromagnetic correlations increase rapidly. There is no continuous transition to a ferromagnetic state in two dimensions at a finite temperature and T_C is a characteristic energy scale of the order of the exchange interaction associated with the ferromagnetism. Since the resistivity peak is in the vicinity of 30 K, we are in the Arrhenius regime. This was experimentally observed for Samples 1 and 4.

In absence of magnetism, the resistivity would behave as $\rho(T) \sim e^{E_A/T}$. When the droplets are magnetically polarized, there is an additional energy cost associated with introducing an extra charge into a given droplet if the spin orientation of the electrons in the droplet differs from that of the extra charge. Suppose the droplets are individually polarized (with different orientations) and let θ_{ij} be the angle between the magnetizations of droplets at sites i and j. When a hole tunnels between these two droplets, the extra energy cost $\Delta_{ij}^{\mathrm{mag}}$ at the destination droplet

depends on the relative orientations of the magnetizations

$$\Delta_{ij}^{\mathrm{mag}} = J(1 - \cos\theta_{ij}). \tag{4.11}$$

If magnetic order in the droplet is induced by the Mn layer, then J is related to local magnetization in the Mn layer. If magnetic order is mainly determined by the interaction of holes in the quantum well then J is related to the exchange interaction in the droplets. Our analysis is not dependent on the mechanism of ferromagnetism since J and T_C are phenomenological parameters. The temperature dependence of resistivity is governed by the total energy $E_A + \Delta_{ij}^{\mathrm{mag}}$ associated with introducing an extra charge carrier into the droplet j from a neighboring droplet i

$$\rho(T) \approx Ae^{E_A/T + J(1-\langle\cos\theta_{ij}\rangle)/T}, \tag{4.12}$$

where we have approximated $\langle e^{-\cos\theta_{ij}/T}\rangle \approx e^{-\langle\cos\theta_{ij}\rangle/T}$. For a two-dimensional ferromagnet, $\langle\cos\theta_{ij}\rangle = e^{-D_1/\xi_M(T)}$, where [27, 28, 29]

$$\xi_M(T) = \begin{cases} a/\sqrt{1 - T_C/T}, & T \gg T_C \\ a\exp[\pi T_C/2T], & T \ll T_C \end{cases}. \tag{4.13}$$

Here $a \sim 1/\sqrt{n_d}$ is a length scale of the order of inter-atomic separation of the Mn dopants (n_d id the total Mn density). T_C is the Curie temperature, below which the ferromagnetic correlations increase rapidly. If ferromagnetism is intrinsic to the Mn layer, then due to disorder, we expect the local ferromagnetic interaction J to be larger than the global transition temperature T_C. For a homogeneous distribution of Mn atoms, $J \sim T_C$ for the same mechanism of ferromagnetism. If ferromagnetism is due to indirect exchange mediated by the holes, then T_C falls with interdroplet tunneling probability and is smaller than J in general.

Fig. 4.8(a) shows the calculated resistivity as a function of temperature. While we assumed a T_C of 30 K, the peak in the resistivity appears at a significantly lower temperature. This is a characteristic feature of the 2D DMS heterostructures in contrast with bulk DMS where the peak appears near the critical temperature T_0 which for Heisenberg ferromagnets is not very different from the Curie temperature T_C. In the bulk case, while the peak does not also coincide with T_0, it is nevertheless possible to obtain the critical temperature based on resistivity measurements [1]. The key physical difference is that the magnetic correlation length for bulk DMS diverges upon approaching T_0 from higher temperatures, whereas in 2D, the mag-

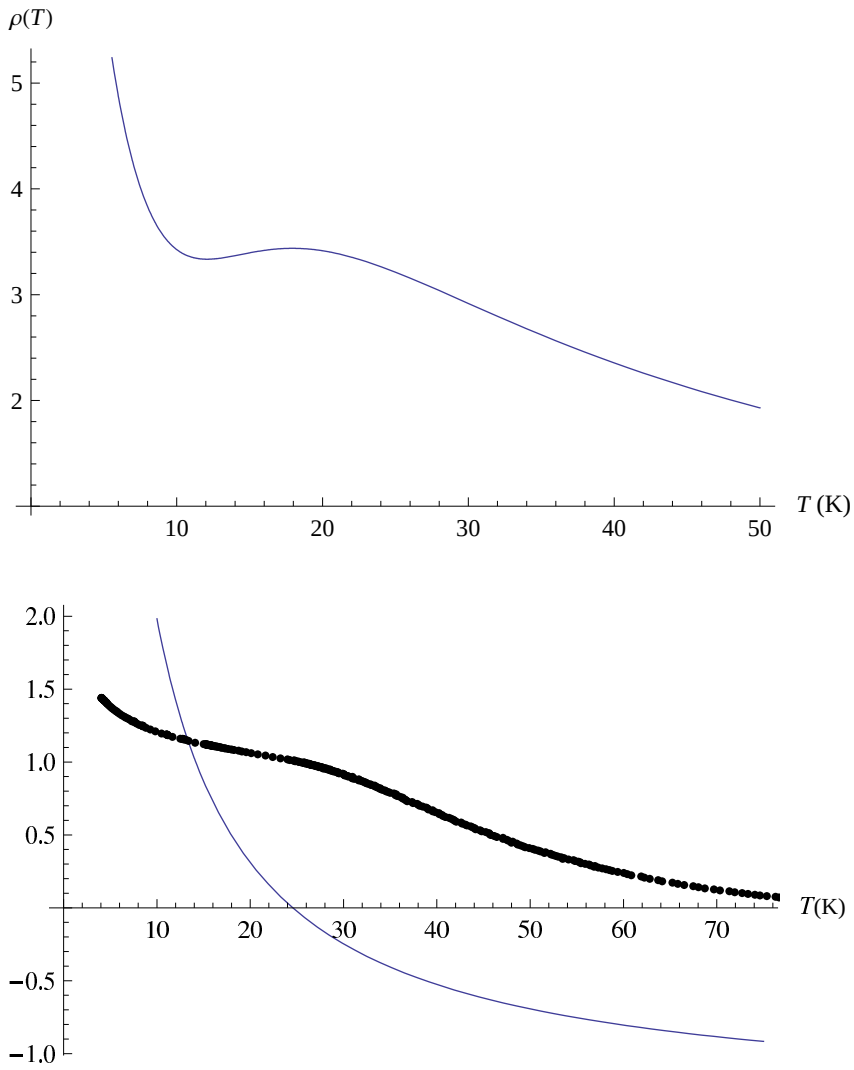

Figure 4.8: (a) Calculated resistivity (in arbitrary units) as a function of temperature. Parameters from Sample 1 were used for the plots. We assumed a degree of ionization of 0.1, ferromagnetic transition temperature $T_C = 30$ K, exchange integral $J = 70$K. The peak in the resistivity occurs at a temperature lower than T_C. (b) Plot of $\log(\xi_M/D_1)$ showing the variation of magnetic correlation length ξ_M for Sample 1 as a function of temperature (solid line). The dots show $\log[\rho(T)/\rho(77K)]$ for the same sample. The anomaly in the resistivity $\rho(T)$ occurs in the vicinity of the temperature where $\xi_M/D_1 \sim 1$.

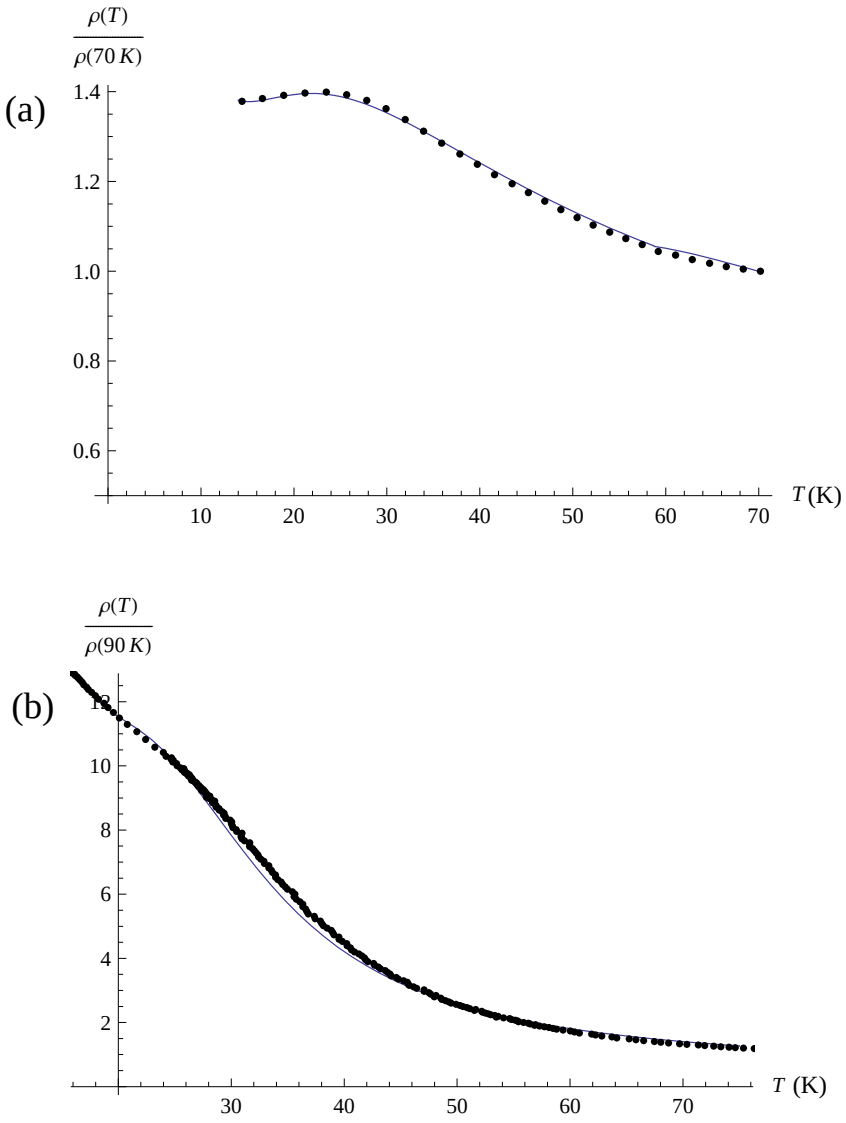

Figure 4.9: Observed temperature dependence of resistance for (a) Sample 4, in units of the resistance at 70 K, and (b) Sample 1, in units of the resistance at 90 K (points), and theoretical fits (solid lines). Sample 4 is near the percolation threshold and Sample 1 is well-insulating. The fits were made using Eq. (4.12). Parameters such as the activation energy E_A and the droplet separation D_1 were chosen close to the values obtained from the droplet model. The magnetic parameters J and T_C were then varied to obtain the above fits. In both cases, the best fit value of T_C is significantly larger than the temperature, at which the resistance anomaly (hump or shoulder) is observed. At lower temperatures, the resistivity becomes variable-range hopping type (not taken into account in our model). For Sample 4 in panel (a), the values used for the fit are $D_1 = 2$ nm, $E_A = 9$ K, $J = 39$ K, and $T_C = 30$ K; for Sample 1 in panel (b), the parameters are $D_1 = 9.4$ nm, $E_A = 51$ K, $J = 56$ K, and $T_C = 49$ K.

netic correlation length remains finite except at $T = 0$ (see Eq. (4.13)) due to the absence of true long-range ferromagnetic order at finite temperatures. The peak is related to the temperature when the magnetic correlation length in the Mn layer becomes comparable to the interdroplet separation. Temperature corresponding to this peak is determined by the specific values of parameters of the sample and not only by T_C. Fig. 4.8(b) shows that the shoulder in the resistivity of Sample 1 occurs near the temperature where $\xi_M/D_1 \sim 1$.

In Fig. 4.9, we show the observed resistance and a fit based on our model (Eq. (4.12)) for Samples 1 and 4. Parameters such as activation energy E_A and droplet separation D_1 were chosen close to values obtained from the droplet model. Magnetic parameters J and T_C were then varied to obtain the above fits. While making the fits, we made following observations. Position of the peak or shoulder is sensitive to T_C and D_1, while J and E_A determine the sharpness of the resistance anomaly. If D_1 is reduced, then $\langle \cos\theta_{ij} \rangle = e^{-D_1/\xi_M(T)}$ changes from 0 to 1 at a higher temperature, which shifts the resistance anomaly to a higher temperature. Increasing T_C also shifts the anomaly to a higher temperature. We found that values of D_1 and E_A chosen near the calculated values generally gave good fits.

The resistivity anomaly can be understood qualitatively from our droplet picture in following way. We assume that the ferromagnetism is intrinsic to Mn-layer and the droplet polarization follows the local Mn magnetization. T_C corresponds to the temperature below which magnetic correlation length (ξ_M) start increasing rapidly in Mn layer. But since the droplet separation is much larger than Mn separation, onset of ferromagnetism in Mn layer does not affect transport significantly at temperatures near T_C. At lower temperature, when ξ_M becomes comparable to droplet separation D_1, inter-droplet tunneling probability increases rapidly which gives a decrease in the resistivity. This gives a dip in the resistivity which results in the peak/shoulder feature. As the temperature further decreases, the magnetic part saturates and the activated behaviour starts dominating which at further lower temperatures becomes variable range hopping. In metallic samples, as the droplet separation is lower, the peak lies closer to T_C. These results clearly show that, unlike the bulk magnetic semiconductors, the peak position should not be used as an estimate for T_C of the Mn layer in these heterostructures, specially for non-metallic samples. Our analysis is also supported by the anomalous Hall effect measurements in these samples (Fig 4.5) which show saturation at temperatures much above the peak temperature [17]. This shows that there is significant ferromagnetism in Mn layer much before the peak appearance in resistivity. The values of fitted parameters

are shown in figure 4.9

4.4 Summary

We studied the effect of disorder, Coulomb interaction and ferromagnetism on the transport properties of 2D heterostructures δ-doped by Mn. Observation of Shubnikov–de Haas oscillations for fields perpendicular to the 2D direction of the quantum well confirmed the two-dimensionality of these samples. Resistivity measurements as well as previously measured magnetic hysteresis [7, 19, 20] and anomalous Hall effect [6, 17] established magnetic ordering at low temperatures. We studied the two most insulating samples using our droplet model.

We showed that at low carrier densities, interplay of disorder in the spatial distribution of dopant Mn atoms and screening effects by holes in the 2D quantum well leads to electronic phase separation in the quantum well. For this phase, we obtained typical sizes of the hole droplets, their mean separation, and their energy levels. Unlike conventional nonmagnetic GaAs/AlGaAs heterostructures, a two-subband model was used here as the carrier density was much larger in these heterostructures. We introduced a simple nearest-neighbor hopping model for the resistivity of this droplet phase taking into account discreteness of energy levels in the droplets and the effect of ferromagnetic correlations between spins of neighboring droplets. Values of the parameters in the resistivity model were obtained from droplet model where possible. Ferromagnetic parameters such as Curie temperature were varied to fit the observed data. A good agreement with the experiments was obtained.

An important understanding that emerged from our study is that a resistance anomaly is possible in 2D even if there is no magnetic transition. The second finding concerns the relation between position of the peak or shoulder in the resistivity data and the Curie temperature. Unlike 3D DMS systems where such resistance features are found in the vicinity of the critical temperature T_0 (which is not very different from the Curie temperature T_C for Heisenberg ferromagnets), we showed that in 2D DMS heterostructures, the peak or shoulder-like feature does not directly give the Curie temperature, and furthermore, the Curie temperature can be substantially larger than the temperature at which such features are observed. This statement is supported by the AHE results presented in Fig.4.5. It is seen that for insulating Samples 1 and 4, the AHE saturates at temperatures well above the peak temperature which means that T_C is higher than the peak temperature. Physically,

this is because the resistivity changes once the magnetic correlation length becomes comparable to the inter-droplet separation. Clearly, the difference between Curie temperature and the position of the resistivity peak will be stronger for more insulating samples. However if our approach is adapted to insulating 3D DMS systems, we would expect, like other works, a resistivity anomaly in the vicinity of the critical temperature as the correlation length diverges at T_C.

References

[1] T. Jungwirth, J. Sinova, J. Mašek, J. Kučera, and A. H. MacDonald, *Theory of ferromagnetic (III,Mn)V semiconductors*, Rev. Mod. Phys. **78**, 809 (2006).

[2] I. Žutić, J. Fabian, and S. Das Sarma, *Spintronics: Fundamentals and applications*, Rev. Mod. Phys. **76**, 323 (2004).

[3] K. Sato, L. Bergqvist, J. Kudrnovský, P. H. Dederichs, O. Eriksson, I. Turek, B. Sanyal, G. Bouzerar, H. Katayama-Yoshida, V. A. Dinh, T. Fukushima, H. Kizaki, and R. Zeller, *First-principles theory of dilute magnetic semiconductors*, Rev. Mod. Phys. **82**, 1633 (2010).

[4] A. Kaminski and S. Das Sarma, *Polaron Percolation in Diluted Magnetic Semiconductors*, Phys. Rev. Lett. **88**, 247202 (2002).

[5] F. Matsukura, H. Ohno, A. Shen, and Y. Sugawara, *Transport properties and origin of ferromagnetism in (Ga,Mn)As*, Phys. Rev. B **57**, 2037R (1998).

[6] B. A. Aronzon, M. A. Pankov, V. V. Rylkov, E.Z. Meilikhov, A. S. Lagutin, E. M. Pashaev, M. A. Chuev, V. V. Kvardakov, I. A. Likhachev, O. V. Vihrova, A. V. Lashkul, E. Lähderanta, A.S. Vedeneev, and P. Kervalishvili, *Ferromagnetism of low-dimensional Mn-doped III-V semiconductor structures in the vicinity of the insulator-metal transition*, J. Appl. Phys. **107**, 023905 (2010).

[7] B. A. Aronzon, V. A. Kul'bachinskii, P. V. Gurin, A. B. Davydov, V. V. Ryl'kov, A. B. Granovskii, O. V. Vikhrova, Y. A. Danilov, B.N. Zvonkov, Y. Horikoshi, and K. Onomitsu, *Anomalous hall effect in Mn δ-doped $GaAs/In_{0.17}Ga_{0.83}As/GaAs$ quantum wells with high hole mobility*, Pis'ma Zh. Eksp. Teor. Fiz. **85**, 32 (2007) [JETP Lett. **85**, 27 (2007)].

[8] E. Z. Meilikhov and R. M. Farzetdinova, *Ferromagnetism of semiconducting structures with the indirect interaction of magnetic impurities through a quasi-*

two-dimensional conduction channel, Pis'ma Zh. Eksp. Teor. Fiz. **87**, 568 (2008) [JETP Lett. **87**, 482 (2008)].

[9] V. N. Men'shov, V. V. Tugushev, S. Caprara, P. M. Echenique and E. V. Chulkov, *Spin ordering in semiconductor heterostructures with ferromagnetic $\delta-$layers* Phys. Rev. B **80**,035315 (2009).

[10] C. P. Moca, B. L. Sheu, N. Samarth, P. Schiffer, B. Janko, and G. Zarand, *Scaling Theory of Magnetoresistance and Carrier Localization in $Ga_{1-x}Mn_xAs$*, Phys. Rev. Lett. **102**, 137203 (2009).

[11] C. Timm, M. E. Raikh, and Felix von Oppen, *Disorder-Induced Resistive Anomaly Near Ferromagnetic Phase Transitions*, Phys. Rev. Lett. **94**, 036602 (2005).

[12] F. Matsukura, M. Sawicki, T. Dietl, D. Chiba, and H. Ohno, *Magnetotransport properties of metallic (Ga,Mn)As films with compressive and tensile strain*, Physica E **21**, 1032 (2004).

[13] T. Dietl, *Interplay between Carrier Localization and Magnetism in Diluted Magnetic and Ferromagnetic Semiconductors*, J. Phys. Soc. Jpn. **77**, 031005 (2008).

[14] E. H. Hwang and S. Das Sarma, *Transport properties of diluted magnetic semiconductors: Dynamical mean-field theory and Boltzmann theory*, Phys. Rev. B **72**, 035210 (2005).

[15] P. Majumdar and P. B. Littlewood, *Dependence of magnetoresistivity on charge-carrier density in metallic ferromagnets and doped magnetic semiconductors*, Nature **395**, 479 (1998).

[16] C. Timm, *Disorder effects in diluted magnetic semiconductors*, J. Phys.: Condens. Matter **15**, R1865 (2003).

[17] B. A. Aronzon, M. V. Kovalchuk, E. M. Pashaev, M. A. Chuev, V. V. Kvardakov, I. A. Subbotin, V. V. Rylkov, M. A. Pankov, I. A. Likhachev, B. N. Zvonkov, Y. A. Danilov, O. V. Vihrova, A. V. Lashkul, and R. Laiho, *Structural and transport properties of $GaAs/\delta - Mn/GaAs/In_xGa_{1x}As/GaAs$ quantum wells* J. Phys.: Condens. Matter **20**, 145207 (2008).

[18] D. J. Arent, K. Deneffe, C. Van Hoof, J. De Boeck, and G. Borghs, *Strain effects and band offsets in GaAs/InGaAs strained layered quantum structures*, J. Appl. Phys. **66**, 1739 (1989).

[19] B. Aronzon, A. Lagutin, V. Rylkov, M. Pankov, A. Lashkul, and R. Laiho, *Disorder effects in $GaAs/In_xGa_{1x}As/GaAs$ quantum well delta doped with Mn*, Phys. Stat. Sol. (c) **5**, 814 (2008).

[20] B.A. Aronzon, A. S. Lagutin, V. V. Ryl'kov, V. V. Tugushev, V. N. Men'shov, A. V. Lashkul, R. Laiho, O. V. Vikhrova, Yu A. Danilov, and B. N. Zvonkov, *Magnetic properties of $GaAs/\delta Mn/GaAs/In_xGa_{1x}As/GaAs$ quantum wells* Pis'ma Zh. Eksp. Teor. Fiz. **87**, 192 (2008) [JETP Lett. **87**, 164(2008)].

[21] V. Novák, K. Olejník, J. Wunderlich, M. Cukr, K. Výborný, A. W. Rushforth, K.W. Edmonds, R. P. Campion, B. L. Gallagher, Jairo Sinova, and T. Jungwirth, *Curie Point Singularity in the Temperature Derivative of Resistivity in (Ga,Mn)As*, Phys. Rev. Lett. **101**, 077201 (2008).

[22] V. A. Gergel' and R. A. Suris, *Fluctuations of the surface potential in metal-insulator-conductor structures*, Zh. Eksp. Teor. Fiz. **75**, 191 (1978) [Sov. Phys. JETP **48**, 95 (1978)].

[23] J. A. Nixon and J. H. Davies, *Potential fluctuations in heterostructure devices*, Phys. Rev. B **41**, 7929 (1990).

[24] M. M. Fogler, *Nonlinear screening and percolative transition in a two-dimensional electron liquid*, Phys. Rev. B **69**, 121409(R) (2004); *Electrostatics of two-dimensional structures: Exact solutions and approximate methods* **69**, 245321 (2004).

[25] V. Tripathi and M. P. Kennett, *Magnetotransport in disordered delta-doped heterostructures*, Phys. Rev. B **74**, 195334 (2006).

[26] F. G. Pikus and A. L. Efros, *Large-scale potential fluctuations in plane layers with impurities* , Zh. Eksp. Teor. Fiz. **96**, 985 (1989) [Sov. Phys. JETP **69**, 558 (1989)].

[27] D. P. Arovas and A. Auerbach, *Functional integral theories of low-dimensional quantum Heisenberg models*, Phys. Rev. B **38**, 316 (1988).

[28] M. Takahashi, *Comment on Finite 2D Quantum Heisenberg Ferromagnet*, Prog. Theor. Phys. **83**, 815 (1990).

[29] D. A. Yablonskiy, *Tyablikov approximation in the theory of low-dimensional quantum Heisenberg ferromagnets and antiferromagnets*, Phys. Rev. B **44**, 4467 (1991).

Chapter 5

Conclusion

In this thesis, we studied disordered two dimensional quantum systems. In our study of Kondo lattice scenarios in $\delta-$doped semiconductor heterostructures, we analyzed nuclear magnetic resonance (NMR) method as a tool to probe the electronic state of a two-dimensional electron gas (2DEG) in a quantum well. In these systems, the Si $\delta-$layer produces a fluctuation potential profile for the 2DEG which can lead to bound states for the electrons. These localized electrons act as local magnetic moments (for odd number of bound electrons in a potential well), scattering the conduction electrons in the quantum well which gives a prototype Kondo system. Conduction electrons also mediate magnetic RKKY interaction between the local moments which competes with the Kondo screening and can be tuned by changing the carrier density in the quantum well. Depending on the arrangement of ionized Si atoms, the local moments in 2DEG could either form an ordered lattice or be in a disordered state. Distinguishing these two scenarios is not easy by standard transport measurements. We showed that the temperature dependence of nuclear relaxation rates (T_1^{-1}) has distinguishable features for different possible electronic states in the quantum well. In the spatially ordered state of local moments, T_1^{-1} shows an exponential increase at low temperatures in RKKY dominated regime which is clearly distinguishable from the disordered state which has small nuclear relaxation rate. NMR could thus be used to confirm the formation of an artificial Kondo lattice in semiconductor heterostructures. NMR can also distinguish between the Kondo coupling dominated regime and the RKKY regime.

Next, we studied effects of external magnetic impurities in Kitaev spin-1/2 honeycomb lattice model. The model has very anisotropic spin interactions and is exactly solvable with a spin liquid ground state with both gapped and gapless regimes.

Exact solvability of the model make it relatively simpler to explore disorder effects. We coupled a spin-S impurity to a Kitaev spin in the gapless phase of the model and looked for a possible Kondo effect due to screening of impurity spin by the gapless excitations. We analyzed scaling behaviour of the coupling constant using Poor Man's scaling approach. The impurity coupling scaling has an unstable fixed point K_C irrespective of the sign of impurity coupling. Coupling constant flows to infinity for $K > K_C$ while for $K < K_C$, it flows to zero. Another interesting feature of the Kondo effect in Kitaev model is that the unstable fixed point separates topologically distinct sectors of the Kitaev model and the strong coupling phase has finite flux with a zero energy Majorana mode at its center. We also studied the nature of interaction between two distant magnetic impurities mediated by the gapless Majorana fermionic excitations. The inter-impurity interaction has an interesting feature that it is a non-dipolar RKKY interaction proportional to $S_\alpha^2 S_\beta^2/r^3$ provided that (i) each impurity couples to more than one lattice site (bonds) on the host and (ii) the impurity spin S is not a spin-1/2.

In our study of charge transport in $\delta-$doped magnetic semiconductor heterostructures, we analyzed the influence of magnetism and disorder in Mn $\delta-$layer on the resistivity of two-dimensional hole gas (2DHG) in the quantum well. Disorder potential from ionized Mn atoms and non-linear screening of the potential by the holes in 2DHG leads to formation of charge droplets in the quantum well at low carrier densities. Charge transport then takes place by carriers hopping between the droplets and shows Arrhenius behaviour. Measured resistivity for these systems shows a peak/shoulder anomaly in its temperature dependence. We estimated sizes of the droplets, their separation and energy level separation in the droplets etc. We then incorporated effects of ferromagnetic correlations in the hopping probability and showed that resistivity anomaly can be qualitatively explained by our model. The resistance anomaly appears when magnetic correlation length in Mn layer becomes comparable to droplet separation such that droplets spins also become aligned which increases the hole tunneling probability and gives a dip in the resistivity. This temperature can be significantly different from the mean field Curie temperature for ferromagnetism in Mn layer (unlike bulk 3D systems) specially for systems in insulating regime and the peak position should not be used as a measure of the Curie temperature in these 2D ferromagnetic semiconductor structures.